AD 647645

Bulletin 36
Part 4
(of 7 Parts)

THE SHOCK AND VIBRATION BULLETIN

JANUARY 1967

A Publication of
THE SHOCK AND VIBRATION
INFORMATION CENTER
Naval Research Laboratory, Washington, D.C.

Office of
The Director of Defense
Research and Engineering

DISTRIBUTION OF THIS DOCUMENT IS UNLIMITED

ARCHIVE COPY

BLANK PAGES
IN THIS
DOCUMENT
WERE NOT
FILMED

Bulletin 36
Part 4
(of 7 Parts)

THE SHOCK AND VIBRATION BULLETIN

JANUARY 1967

A Publication of
THE SHOCK AND VIBRATION
INFORMATION CENTER
Naval Research Laboratory, Washington, D.C.

The 36th Symposium on Shock and Vibration was held in Los Angeles, California, on 18-20 October 1966. The U.S. Air Force was host.

Office of
The Director of Defense
Research and Engineering

SYMPOSIUM MANAGEMENT

The Shock and Vibration Information Center

William W. Mutch, Director

Henry C. Pusey, Coordinator

Rudolph H. Volin, Coordinator

Jean B. Goldbecker, Editor

Katherine G. Jahnel, Administrative Secretary

36th Program Committee

William R. Forlifer, NASA Goddard Space Flight Center

Edward H. Schell, Air Force Flight Dynamics Laboratory

George Stathopoulos, Naval Ordnance Laboratory

James M. Taylor, U.S. Army Missile Command

Air Force Liaison

Los Angeles Scientific and Technical Liaison Office, Research and Technology Division, Air Force Systems Command

Lt. Col. Kenneth W. Cook

Arthur E. Kimberly

Bulletin Production

Graphic Arts Branch, Technical Information Division, Naval Research Laboratory

CONTENTS

PART 4

Damping

MECHANISMS AND SCALING OF DAMPING IN A PRACTICAL STRUCTURAL JOINT . . . 1
Brantley R. Hanks and David G. Stephens, NASA Langley Research Center, Hampton, Virginia

DAMPING OF STRUCTURES BY VISCOELASTIC LINKS 9
David I. G. Jones, Air Force Materials Laboratory, Wright-Patterson Air Force Base, Ohio, and Ahid D. Nashif, University of Dayton, Dayton, Ohio

ELASTOMERS FOR DAMPING OVER WIDE TEMPERATURE RANGES 25
F. S. Owens, Air Force Materials Laboratory, Wright-Patterson Air Force Base, Ohio

A NEW METHOD FOR DETERMINING DAMPING PROPERTIES OF VISCOELASTIC MATERIALS 37
Ahid D. Nashif, University of Dayton, Dayton, Ohio

EFFECT OF TUNED VISCOELASTIC DAMPERS ON RESPONSE OF MULTI-SPAN STRUCTURES 49
David I. G. Jones and George H. Bruns, Air Force Materials Laboratory, Wright-Patterson Air Force Base, Ohio

A METHOD FOR IDENTIFYING AND EVALUATING LINEAR DAMPING MODELS IN BEAM VIBRATIONS 65
M. W. Wambsganss, Jr., B. L. Boers, and G. S. Rosenberg, Argonne National Laboratory, Argonne, Illinois

EFFECT OF AIR DAMPING ON STRUCTURAL FATIGUE FAILURE 75
John R. Fagan, Radio Corporation of America, Princeton, New Jersey

DEVELOPMENT OF DAMPED MACHINERY FOUNDATIONS 81
W. Blasingame and E. V. Thomas, Navy Marine Engineering Laboratory, Annapolis, Maryland, and R. A. DiTaranto, Pennsylvania Military Colleges, Chester, Pennsylvania

DYNAMIC MECHANICAL STUDIES OF A COMPOSITE MATERIAL 95
M. G. Sharma, M. Critchfield, and W. F. St. Lawrence, The Pennsylvania State University, University Park, Pennsylvania

PAPERS APPEARING IN PART 1
Part 1 - Confidential
(Titles Unclassified)

DYNAMIC DESIGN ANALYSIS METHOD PREDICTION VERSUS TEST MEASUREMENT OF SHIPBORNE EQUIPMENT RESPONSE
R. O. Belsheim and A. F. Dick, Naval Research Laboratory, Washington, D.C.

COMPARISON OF SHOCK MOTIONS INDUCED BY AIR BLAST AND UNDERWATER EXPLOSIONS
Robert E. Fuss and Kenneth T. Cornelius, David Taylor Model Basin, Washington, D.C.

ANALYSIS OF 21B WEAPONS SKID FOR VERTICAL SHOCK
John W. McNabb, Northern Ohio University, Ada, Ohio

NERVA NUCLEAR REACTOR VIBRATION ANALYSIS AND TEST PROGRAM WITH EMPHASIS ON NONLINEAR RESPONSES
R. D. Burack, D. F. Miller, and A. F. Maguire, Westinghouse Electric Corporation, Pittsburgh, Pennsylvania

RECENT SOVIET RESEARCH IN SHOCK, VIBRATION, AND NONLINEAR MECHANICS
David B. Singer, Aerospace Corporation, San Bernardino, California

PAPERS APPEARING IN PART 2

Opening Session

THE CHALLENGE OF THE SECOND HALF OF THE DECADE
R. G. Loewy, University of Rochester, Rochester, New York

SHOCK AND VIBRATION - A PERSPECTIVE
Alan Powell, David Taylor Model Basin, Washington, D.C.

Shock

YIELDING EFFECTS ON SHOCK SPECTRA
William R. Mentzer Jr., Bowles Engineering Corporation, Silver Spring, Maryland, and Patrick F. Cunniff, University of Maryland, College Park, Maryland

SHOCK SPECTRA OF PRACTICAL SHAKER SHOCK PULSES
John R. Fagan and Anthony S. Baran, Radio Corporation of America, Princeton, New Jersey

TRANSDUCER SHOCK STUDY
Arthur D. Carlson and Robert J. McGrattan, General Dynamics, Electric Boat Division, Groton, Connecticut

DIRECT MEASUREMENT OF 5"/54 GUN SETBACK ACCELERATION
Peter S. Hughes and Luigi A. Vagnoni, Naval Ordnance Laboratory, Silver Spring, Maryland

SIMULATION OF HEAT SHIELD PYROTECHNIC SHOCK IMPEDANCE
Norris J. Huffington, Jr., and Robert J. Goldman, The Martin Company, Baltimore, Maryland

PYROTECHNIC SHOCK TESTING OF A FULL-SCALE REENTRY VEHICLE
W. R. Britton and G. K. Jones, The Martin Company, Baltimore, Maryland

SHOCK TESTING WITH SOLID-PROPELLANT-POWERED GUNS
Larry O. Seamons, Sandia Corporation, Albuquerque, New Mexico

APPLICATION OF POLYURETHANE FOAM TO SHOCK ISOLATION OF LARGE SILO-BASED MISSILES
W. A. Volz, Westinghouse Electric Corporation, Sunnyvale, California

NEW APPROACH FOR EVALUATING TRANSIENT ENVIRONMENTAL TESTING OF SPACECRAFT
James T. Howlett and John P. Raney, NASA Langley Research Center, Hampton, Virginia

SPECIFICATION OF SHOCK TESTS - PANEL SESSION

PAPERS APPEARING IN PART 3

Vibration Testing

USE OF FORCE AND ACCELERATION MEASUREMENTS IN SPECIFYING AND MONITORING LABORATORY VIBRATION TESTS
G. W. Painter, Lockheed-California Company, Burbank, California

FEASIBILITY OF FORCE-CONTROLLED SPACECRAFT VIBRATION TESTING USING NOTCHED RANDOM TEST SPECTRA
Joseph A. Heinrichs, The Martin Company, Baltimore, Maryland

COMPARISON OF MARINER ASSEMBLY-LEVEL AND SPACECRAFT-LEVEL VIBRATION TESTS
Peter A. Franken and Terry D. Scharton, Bolt Beranek and Newman Inc., Van Nuys, California, and Thomas H. Mack, Jet Propulsion Laboratory, Pasadena, California

ACOUSTICALLY INDUCED VIBRATION TESTING OF SPACECRAFT COMPONENTS
Richard W. Peverley, General Electric Company, Houston, Texas

REPRODUCTION OF COMPLEX AND RANDOM WAVEFORMS AT VARIOUS POINTS ON A TEST ITEM
John V. Otts and Norman F. Hunter, Jr., Sandia Corporation, Albuquerque, New Mexico

MULTIPLE SHAKER GROUND VIBRATION TEST SYSTEM DESIGNED FOR XB-70A
R. G. North and J. R. Stevenson, North American Aviation, Inc., Los Angeles, California

THE HOW OF HELICOPTER VIBRATION TESTING
Ronald F. McCann, The Boeing Company, Morton, Pennsylvania

RESONANCE TESTING OF A LIFTING BODY REENTRY VEHICLE
G. Sardella and C. L. Riggen, The Martin Company, Baltimore, Maryland

SHOCK AND VIBRATION TESTING USING FOUR-SHAKER SYSTEM
Dean F. Redford, Thiokol Chemical Corporation, Brigham City, Utah

DESIGN TECHNIQUES FOR HORIZONTAL DRIVERS
Fred C. Tolleth, North American Aviation, Inc., Autonetics Division, Anaheim, California

FLIGHT LEVEL VIBRATION TESTING OF A LIFTING BODY REENTRY VEHICLE
R. McCaa and M. Matrullo, The Martin Company, Baltimore, Maryland

HYDRAULIC EXCITER COMBINED ENVIRONMENT TESTS
Edwin J. Skolka, NASA Goddard Space Flight Center, Greenbelt, Maryland

AVERAGING FUNDAMENTAL VIBRATION CONTROL SIGNALS: A THEORETICAL STUDY
W. W. Shurtleff, Sandia Corporation, Albuquerque, New Mexico

CONTROL TECHNIQUES FOR MULTI-SHAKER VIBRATION SYSTEMS
Richard A. Arone, Wyle Laboratories, Huntsville, Alabama, and Paul A. Brock, Sine Engineering Company, Granada Hills, California

PAPERS APPEARING IN PART 5

Analysis and Prediction

METHOD FOR IMPROVING A DYNAMIC MODEL USING EXPERIMENTAL TRANSIENT RESPONSE DATA
Ching-u Ip, Eli P. Howard, and Richard J. Sylvester, Aerospace Corporation, San Bernardino, California

DIGITAL ANALYSIS OF FATIGUE DAMAGE TO A MULTI-MODAL SYSTEM SUBJECTED TO LOGARITHMICALLY SWEPT SINUSOIDAL VIBRATION SPECTRA
Seymour Fogelson, The Marquardt Corporation, Van Nuys, California

ANALYSIS OF VIBRATION DISTRIBUTIONS IN COMPLEX STRUCTURES
Eric E. Ungar, Bolt Beranek and Newman Inc., Cambridge, Massachusetts, and Terry D. Scharton, Bolt Beranek and Newman Inc., Van Nuys, California

DYNAMIC ANALYSIS OF CONTINUUM BODIES BY THE DIRECT STIFFNESS METHOD
W. E. Baker, Rocketdyne, Division of North American Aviation, McGregor, Texas, and J. M. Daly, Arde Engineering Company, Asheville, North Carolina

MIN-MAX RESPONSE PROBLEMS OF DYNAMIC SYSTEMS AND COMPUTATIONAL SOLUTION TECHNIQUES
Eugene Sevin and Walter Pilkey, IIT Research Institute, Chicago, Illinois

STRAIN RESPONSE OF SIMPLY SUPPORTED BEAMS TO POINT AND ACOUSTIC LOADING
Tony L. Parrott and Joseph A. Drischler, NASA Langley Research Center, Langley Station, Hampton, Virginia

PREDICTION OF FLIGHT VIBRATION LEVELS FOR THE SCOUT LAUNCH VEHICLE
Robert B. Bost, LTV Aerospace Corporation, LTV Astronautics Division, Dallas, Texas

RESPONSE OF STRUCTURAL COMPONENTS OF A LAUNCH VEHICLE TO IN-FLIGHT ACOUSTIC AND AERODYNAMIC ENVIRONMENTS
Khushi L. Chandiramani and Richard H. Lyon, Bolt Beranek and Newman Inc., Cambridge, Massachusetts

DYNAMIC VIBRATIONS OF THICK-WALLED ELASTIC ANISOTROPIC CYLINDERS AND SPHERES WITH INTERNAL DAMPING
Gabriel Cinelli, Argonne National Laboratory, Argonne, Illinois

EFFECT OF ASYMMETRICAL TRAPEZOIDAL PULSE ON SINGLE-DEGREE-OF-FREEDOM SYSTEMS
H. Saunders, General Electric Company, Philadelphia, Pennsylvania

PAPERS APPEARING IN PART 6

Data Analysis and Instrumentation

EFFECT OF DIGITIZING DETAIL ON SHOCK AND FOURIER SPECTRUM COMPUTATION OF FIELD DATA
M. Gertel and R. Holland, Allied Research Associates, Inc., Concord, Massachusetts

AUTOMATED DIGITAL SHOCK DATA REDUCTION SYSTEM
Walter B. Murfin, Sandia Corporation, Albuquerque, New Mexico

AUTOMATED ANALOG METHOD OF SHOCK ANALYSIS
F. X. Prendergast, Bell Telephone Laboratories, Whippany, New Jersey

VIBRATION DATA REDUCTION TECHNIQUES AS APPLIED TO SATURN S-II VEHICLE
Joseph D. Weatherstone, North American Aviation, Downey, California

DIGITAL ANALYSIS OF SATURN ENVIRONMENTAL TEST RESPONSE DATA
Daniel J. Bozich, Wyle Laboratories, Huntsville, Alabama

USE OF A LOW-FREQUENCY SPECTRUM ANALYZER
S. E. Lee and R. G. Tuckerman, David Taylor Model Basin, Washington, D.C.

DETECTION OF LOOSE PARTS AND FREE OBJECTS IN SEALED CONTAINERS
M. W. Schulz, General Electric Research and Development Center, Schenectady, New York

COMBINED ENVIRONMENT TESTING OF SHIPBOARD ELECTRONIC EQUIPMENT AND UTILIZATION OF REGRESSION ANALYSIS
F. Robinson, Navy Electronics Laboratory, San Diego, California

ANALYSIS OF RANDOM VIBRATION WITH AID OF OPTICAL SYSTEMS
Ching-u Ip, Aerospace Corporation, San Bernardino, California

COMPUTER PROGRAM FOR DYNAMIC DESIGN ANALYSIS METHOD
John H. Avila, David Taylor Model Basin, Washington, D.C.

COMPUTER PROGRAM FOR GENERAL SHIP VIBRATION CALCULATIONS
Francis M. Henderson, David Taylor Model Basin, Washington, D.C.

MATHEMATICAL MODEL AND COMPUTER PROGRAM FOR TRANSIENT SHOCK ANALYSIS
Anthony C. Melodia, David Taylor Model Basin, Washington, D.C.

TRANSPORTATION ENVIRONMENTAL MEASUREMENT AND RECORDING SYSTEM
Frank J. Holley, NASA Goddard Space Flight Center, Greenbelt, Maryland

DEVELOPMENT OF VELOCITY SHOCK RECORDER FOR MEASUREMENT OF SHIPPING ENVIRONMENTS
Matthew A. Venetos, U.S. Army Natick Laboratories, Natick, Massachusetts

ABSOLUTE CALIBRATION OF VIBRATION GENERATORS WITH TIME-SHARING COMPUTER AS INTEGRAL PART OF SYSTEM
B. F. Payne, National Bureau of Standards, Washington, D.C.

EXPERIMENTAL TECHNIQUES FOR OBSERVING MOTION OF EXTENDIBLE ANTENNA BOOMS
Donald J. Hershfeld, NASA Goddard Space Flight Center, Greenbelt, Maryland

DEVELOPMENT OF LOW-COST FORCE TRANSDUCER
Marlyn W. Sterk, Sandia Corporation, Albuquerque, New Mexico, and
James A. Ellison, California Institute of Technology, Pasadena, California

AUTOMATIC CALIBRATION AND ENVIRONMENTAL MEASUREMENT SYSTEM FOR LAUNCH PHASE SIMULATOR
Harry D. Cyphers and Frank J. Holley, NASA Goddard Space Flight Center, Greenbelt, Maryland

MICROMINIATURE INSTRUMENTATION AMPLIFIERS
W. V. Bratkowski and P. F. Pittman, Westinghouse Research and Development Center, Pittsburgh, Pennsylvania

INVESTIGATION OF PULSE X-RAY TECHNIQUES FOR STUDY OF SHOCK-WAVE-INDUCED EFFECTS IN SOIL
Warren J. Baker, Frank J. Janza, and Eric H. Wang, Civil Engineering Research Facility, University of New Mexico, Albuquerque, New Mexico

PAPERS APPEARING IN PART 7

Structural Reliability

ESTIMATE OF EFFECT OF SPACECRAFT VIBRATION QUALIFICATION TESTING ON RELIABILITY
Clyde V. Stahle, Jr., The Martin Company, Baltimore, Maryland

S-IC RELIABILITY PROGRAM FROM STRUCTURAL LIFE VIEWPOINT
Roy L. Rich and James A Roberts, The Boeing Company, New Orleans, Louisiana

STRUCTURAL RELIABILITY - PANEL SESSION

Design Data and Methods

DYNAMIC ANALYSIS OF ATS-B SPACECRAFT
Saul M. Kaplan and Victor Terkun, Hughes Aircraft Company, El Segundo, California

SPACECRAFT DESIGN FOR ATLAS TORSIONAL SHOCK TRANSIENT
Sol Davis, Fairchild Hiller, Republic Aviation Division, Farmingdale, Long Island, New York

COMPARISON OF PREDICTED AND MEASURED LAUNCH LOADS FOR SNAP 10A
Everett A. Robb and A. P. Gelman, Atomics International, Canoga Park, California

GROUND-WIND-INDUCED OSCILLATIONS OF GEMINI-TITAN AIR VEHICLE AND ITS ERECTOR
John E. Tomassoni and William H. Lambert, The Martin Company, Baltimore, Maryland

NOISE LEVEL MEASUREMENTS FOR IMPROVED DELTA, ATLAS/AGENA-D, AND TAT/AGENA-D LAUNCH VEHICLES
Lloyd A. Williams and William B. Tereniak, NASA Goddard Space Flight Center, Greenbelt, Maryland

THE "VACUUM SPRING"
K. D. Robertson, U.S. Army Materials Research Agency, Watertown, Massachusetts

SELF-ADAPTIVE VIBRATION BALANCING DEVICE FOR HELICOPTERS
W. Euan Hooper, The Boeing Company, Morton, Pennsylvania

SHOCK RESPONSE OF ELECTRONIC EQUIPMENT CABINETS BY NORMAL MODE METHOD
T. K. Hasselman and C. M. Hwang, TRW Systems, Redondo Beach, California

DAMPED VIBRATIONS OF ELASTICALLY SUPPORTED RIGID BODY WITH COUPLING BETWEEN TRANSLATION AND ROTATION
Francis H. Collopy, ITEK Corporation, Lexington, Massachusetts

MISSILE HANDLING ANALYSIS
C. R. Brown and Alex J. Avis, Westinghouse Electric Corporation, Sunnyvale, California

DAMPING

MECHANISMS AND SCALING OF DAMPING IN A PRACTICAL STRUCTURAL JOINT

Brantley R. Hanks and David G. Stephens
NASA Langley Research Center
Hampton, Virginia

An investigation was conducted to determine the effect of geometric scale on the damping in a practical beam-joint assembly. A cantilever configuration was utilized wherein the beam was bolted between two angle brackets at the support. Four geometrically similar assemblies, covering a scale range of approximately 20 to 1, were tested. Free decay of the fundamental mode was measured over a range of joint clamping pressures and beam tip amplitudes. Also, damping changes resulting from the addition of liquid lubricants and viscoelastic films to the joint interfaces were investigated. Data indicate that an increase in model size results in a decrease in damping attributed to the structural joint. Furthermore, joint damping is shown to be slightly dependent on vibration amplitude and to vary as an inverse function of joint clamping pressure. Joint damping may be substantially increased by the addition of liquid lubricants or viscoelastic films at the joint interfaces.

B. R. Hanks

INTRODUCTION

Dynamic models are often used to study the vibratory response of complex systems when full-scale testing is precluded by system size and/or cost. The usefulness of model tests is dependent on a knowledge of the proper scaling relationships required to extrapolate model data to the full-scale systems. A considerable amount of information has been obtained on the scaling relationships for frequencies and mode shapes. However, the variation of damping with model size or scale is largely unknown and often either neglected or considered to be the same in both model and prototype. The development of proper scaling relationships for damping requires a knowledge of each of the damping mechanisms in the system, such as material hysteresis [1,2], air damping [3,4], and joint damping [5-7]. In space systems, scaling relationships for joint damping are of particular importance since the major source of energy dissipation in such systems [8] is usually attributed to structural interfaces or joints.

The purpose of this paper is to present the results of an experimental investigation of the nature and scaling of damping in a structural joint. The joint damping of four cantilever systems, covering a geometric scale range of 20 to 1, was examined. Data are presented to show the effects of vibration amplitude, joint clamping pressure, and model scale, as well as that of interface lubricants and films, on the magnitude of the damping in structural joints.

APPARATUS AND TEST PROCEDURE

The apparatus used in this investigation, shown in Figs. 1 and 2, consisted of four

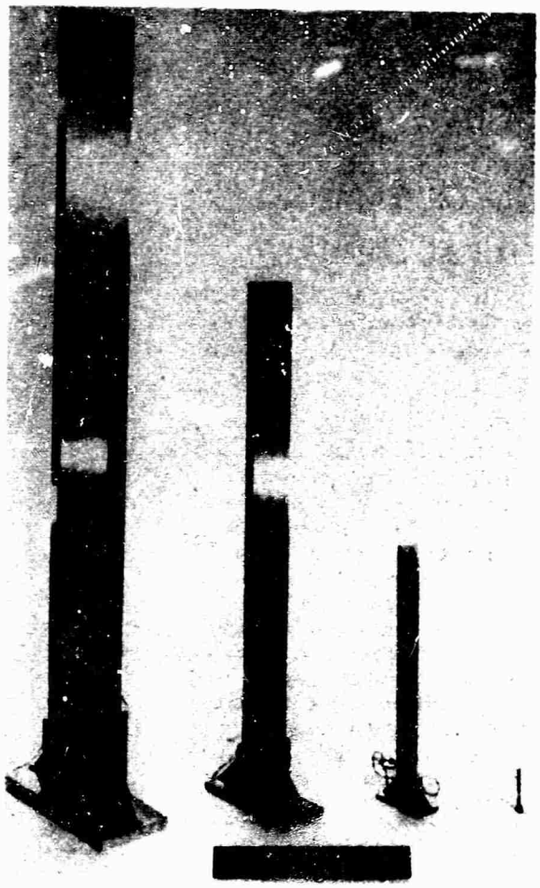

Fig. 1 - Joint damping models, showing relative sizes

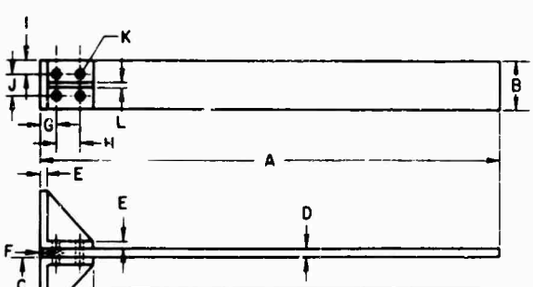

SYMBOL	DIMENSION, INCHES	SYMBOL	DIMENSION, INCHES
A	60.1 λ	G	2.19 λ
B	6.00 λ	H	3.13 λ
C	7.00 λ	I	1.69 λ
D	1.00 λ	J	2.63 λ
E	0.83 λ	K	1.13 λ
F	0.10 λ	L	0.63 λ

SCALE FACTOR λ : 1, .667, .333, .053

Fig. 2 - Dimensions of joint damping models

geometrically scaled beams bolted between correspondingly scaled angle brackets. The angle brackets were, in turn, clamped to a massive concrete and steel supporting block giving a cantilever beam configuration. The four models had scale factors λ of 1, 0.667, 0.333, and 0.053 with the beams ranging from 5 ft down to 3.2 in. in overall length. The beams and angle brackets were made of 6061 aluminum alloy with all surfaces finished to 63 μin. rms. Each angle bracket was machined from a single piece of aluminum and had a web welded to the center to provide rigidity.

Three joint interface conditions (dry, oil-coated, and viscoelastic-film-filled) were studied in an effort to find a method for improving the inherent damping of both small- and large-scale systems. The dry and oil-coated joint tests were performed on all four models, whereas the effect of viscoelastic films was studied on the 0.667 assembly. In studying the effect of joint lubrication, the interfaces were coated with a thin layer of oil before assembly. Three oils having viscosities of 158, 525, and 1400 cp were used. The effect of viscoelastic film inserts was studied using three film materials: 0.5 mil Teflon, 1 mil Mylar, and 1 mil polypropylene. The films were cut to the shape of the joint interface and placed in position during model assembly.

The test procedure was essentially the same in all cases. The total damping of the systems was measured at atmospheric pressure for a range of joint clamping pressures (by varying bolt tightening torque) and beam tip amplitudes. For a particular clamping pressure, the beam was deflected manually and released to osciliate in the first cantilever vibration mode. Oscillations of the beam were sensed by an electrical resistance strain gage attached to one side of the beam as shown in Fig. 1. The strain gage was coupled, through an amplifier, to an electronic dampometer, a device for determining the frequency and damping of a vibrating system. Basically, the dampometer counted the number of cycles as the amplitude decayed between preset limits. The logarithmic decrement δ was then calculated from the equation

$$\delta = \frac{1}{N} \log_e \frac{y_n}{y_{n+N}} , \qquad (1)$$

where N was the number of cycles counted, y_n was the amplitude at which counting started, and y_{n+N} was the amplitude at which counting ceased. In all tests the ratio of start to stop amplitude was maintained at 10/7 so that

$$\delta = \frac{1}{N} \log_e \frac{10}{7} .$$

Since the damping was measured over a band (y_n, y_{n+N}) of the decay envelope, the logarithmic decrement was specified at the average amplitude of this band. Measurements were made at several amplitude levels for each bolt torque by varying the triggering voltage of the dampometer. In all tests, sufficient initial deflection was given to the beam to allow transients to die out before the dampometer triggering amplitude was reached. Each test was repeated at least five times and the average value of the data was used in analysis.

Joint clamping pressures were calculated from the bolt tightening torques using the formula [9]

$$F = \frac{T}{0.2D}, \tag{2}$$

where F is the clamping load per bolt, T is the torque, and D is the bolt diameter. With conversion to average clamping pressure produced on the joint by the four bolts, the formula becomes

$$P = \frac{20T}{DA}, \tag{3}$$

where P is the average clamping pressure and A is the joint interface area. No allowance was made for variation of clamping pressure across the interface.

MATERIAL DAMPING CONSIDERATION

The determination of the magnitude of joint damping in a complex system involves the separation of the total damping into its various components. One contribution to the total damping is that of material or hysteretic damping within the material comprising the system. Experimental separation and measurement of this material damping is difficult in complex systems such as the one under study. However, an analytical expression developed by Zener [1] has been verified for aluminum in experimental work by Granick and Stern [2]. Material damping in a cantilever beam was shown to be closely approximated by the equation

$$\delta_m = \frac{\pi \alpha^2 ET}{c}\left[\frac{\omega\gamma}{1+\omega^2\gamma^2}\right], \tag{4}$$

where

δ_m = logarithmic decrement for material damping;

α = thermal coefficient of linear expansion, 1/°R;

E = modulus of elasticity, psi;

T = absolute temperature, °R;

c = specific heat per unit volume, BTU/in.^{3}-°R; and

ω = circular frequency of vibration, rad/sec.

For a flat beam of uniform thickness, material damping can be approximated by

$$\gamma = \frac{t^2 c}{\pi^2 K}, \tag{5}$$

where

t = beam thickness, in.; and

K = thermal conductivity, BTU/sec-°R-in.

The material damping as predicted by this equation for the four beams tested in this joint damping study is shown as a function of frequency in Fig. 3a on the left. The magnitude of the material damping at the fundamental resonant frequency is denoted for each beam by a circle. These resonant damping values are replotted as a function of scale factor in Fig. 3b. For the systems under study, material damping as predicted by the Zener equation is essentially inversely proportional to scale.

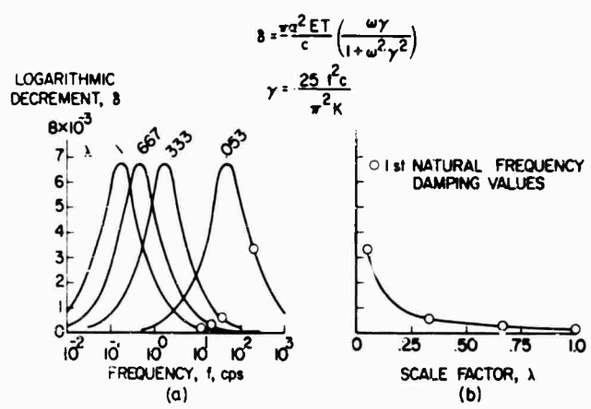

Fig. 3 - Material damping as predicted by Zener theory: (a) as function of frequency, and (b) at fundamental resonant frequency as function of scale factor

PRESENTATION AND DISCUSSION OF RESULTS

The test program consisted of an isolation and examination of the damping for the variables: vibratory amplitude, joint clamping

pressure, model scale, and interface condition (i.e., dry, lubricated, or film insert). The dependency of the damping on each of these variables is illustrated by representative data in the following sections.

Dry Interface

Effect of Vibration Amplitude — The damping measured for the 0.667-scale model, which is typical of the four assemblies, is shown in Fig. 4. The total damping in terms of the log decrement δ is presented as a function of the ratio of vibration displacement amplitude to beam thickness y/t for five values of joint clamping pressure. The total damping increases linearly with an increase in amplitude. Since the total damping represents not only losses in the joints but also internal hysteresis and air damping, the question arises as to whether the joint damping per se is amplitude dependent. Several factors suggest that the joint damping is amplitude dependent. First, Refs. 2 and 3, respectively, indicate that both the hysteretic and air-damping losses are amplitude independent for the range of amplitudes covered by these tests. Secondly, the slope of the faired lines in Fig. 4 is observed to change with a change in clamping pressure (a variable affecting joint damping only) with all other factors being held constant.

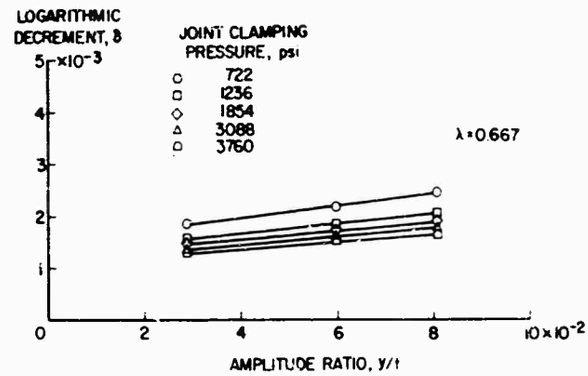

Fig. 4 - Variation of total damping with beam tip vibration amplitude

Effect of Joint Clamping Pressure — The damping for each of the models is presented as a function of joint clamping pressure in Fig. 5. These curves are cross plots of the damping-amplitude curves such as the previous example, Fig. 4. The total damping decreases rapidly as the clamping pressure is increased in low range;

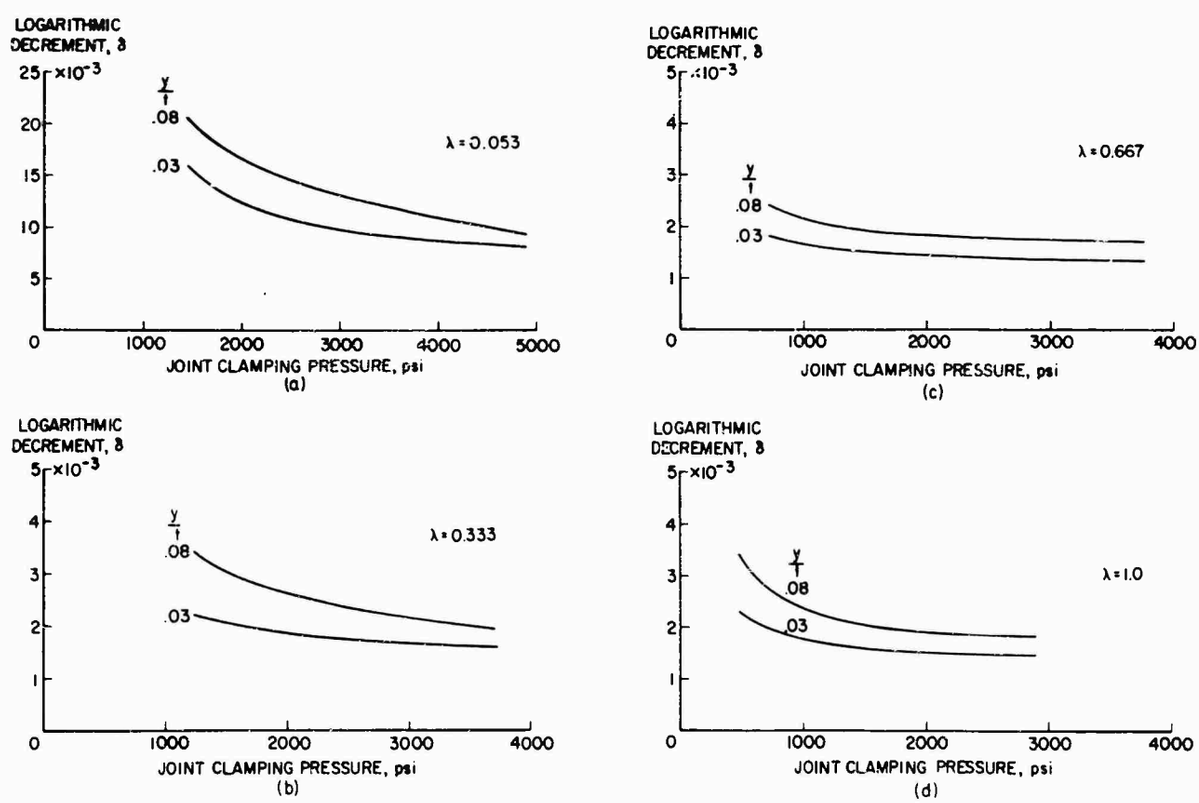

Fig. 5 - Variation of total damping with joint clamping pressure: (a) scale factor = 0.053; (b) scale factor = 0.333; (c) scale factor = 0.667; and (d) scale factor = 1.0

however, it levels out or approaches a constant value at relatively high clamping pressures. It will be assumed henceforth that the joint damping at high stress levels is negligible compared to the other or tare damping (the damping due to the surrounding air and internal hysteresis) in the system. Thus, the magnitude of the joint damping at a particular pressure and amplitude is considered to be the difference between the measured value and the respective high clamping stress asymptote.

Effect of Scale — The variation of total damping with scale factor is shown in Fig. 6 for two values of the joint clamping pressure. All of the data between the amplitude limits y/t of 0.03 to 0.08 fall within the indicated band. These data demonstrate that total damping increases with decreasing scale factor, resulting in substantially higher damping for the smaller models. The trends of these curves are very similar to the variation of material damping with scale factor as predicted by Zener, which is repeated for comparison purposes.

The damping attributed to the joint, obtained by subtracting the respective high stress asymptote (Fig. 5) from the curves of total damping (Fig. 6), is presented as a function of scale factor in Fig. 7. The joint damping is also seen to be inversely proportional to the scale factor. Examination of the curve reveals that the joint damping values for the 0.333- and 0.053-scale models are several times higher than those of the larger models. These curves indicate that caution should be used in extrapolating to full-scale systems damping data obtained in tests of small models. The common practice of assuming that the damping of the prototype is the same as in the model could lead to gross overestimates of the damping in the full-scale systems.

Treated Interfaces

Effect of Oil — In an effort to alter the joint damping, the effect of interface lubricants was examined. Typical results are shown in Fig. 8 where the total damping for the 0.667-scale

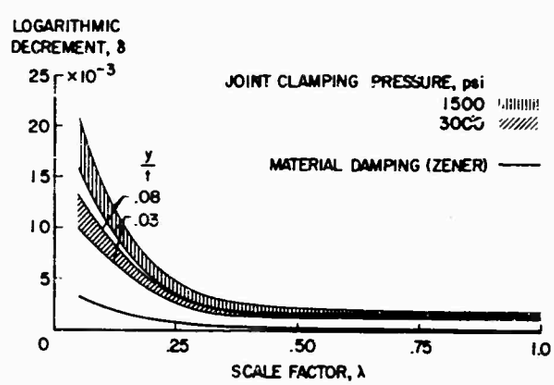

Fig. 6 - Variation of total damping with scale factor

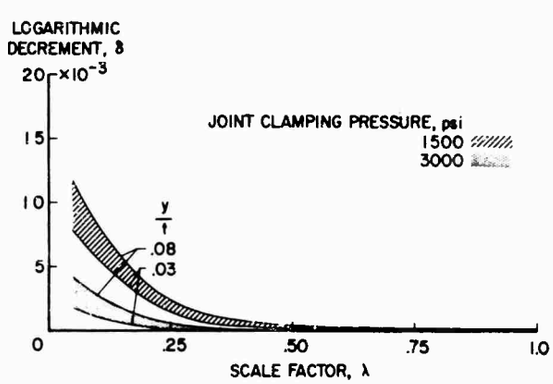

Fig. 7 - Variation of joint damping with scale factor

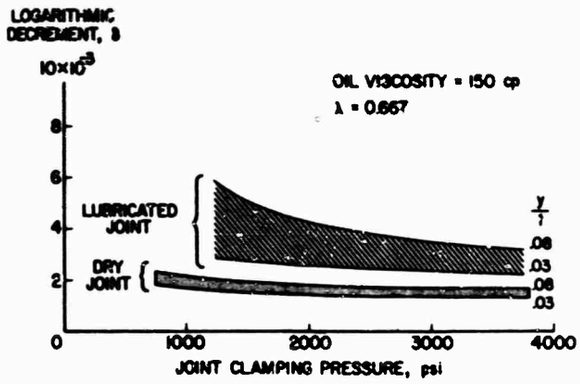

Fig. 8 - Variation of total damping with joint clamping pressure for lubricated and dry joint conditions

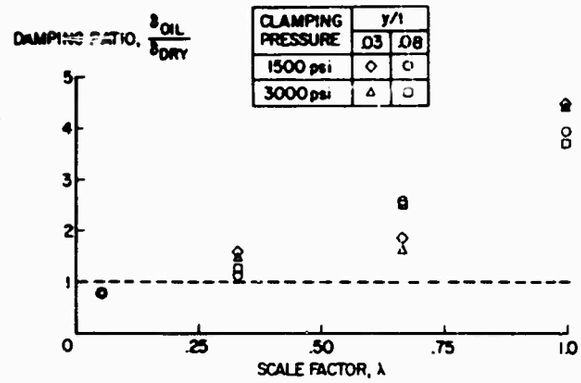

Fig. 9 - Joint lubrication effectiveness summarized for all models

model, with 150-cp oil added to the joint interfaces, is presented as a function of joint clamping pressure. For comparison purposes the "dry" data (Fig. 5) are repeated.

The dependency of the damping on clamping pressure is essentially the same in both the lubricated and the dry cases. However, the magnitude of the damping recorded for the lubricated joint is considerably higher. A similar phenomenon was reported in Ref. 10 where the damping of a cantilever beam was substantially increased by the addition of grease at the root although the exact mechanism was not fully discussed.

The dependency of the damping on amplitude, as indicated by the width of the band in Fig. 8, is higher for the lubricated case. This was noted for all models, except the 0.333-scale model for which there was little difference in amplitude dependency between the dry and lubricated joints. Although data are not presented, the dependency of the damping on amplitude was again found to be linear. Also, tests conducted with the 525- and 1400-cp oils revealed no appreciable difference when compared with the damping in the joint lubricated with the 150-cp oil.

The relative effect of oil on damping for all four models is summarized in Fig. 9, where the ratio of total damping with oil to that without oil is plotted as a function of scale factor. A lubricant is shown to increase the damping in all but the smallest model, where the addition of oil slightly decreased the damping.

Effect of Viscoelastic Films — The effect of adding viscoelastic films to the joint interfaces of the 0.667-scale model is illustrated in Fig. 10. In this figure, the range of total damping obtained with each of the three film materials is shown together with those obtained in

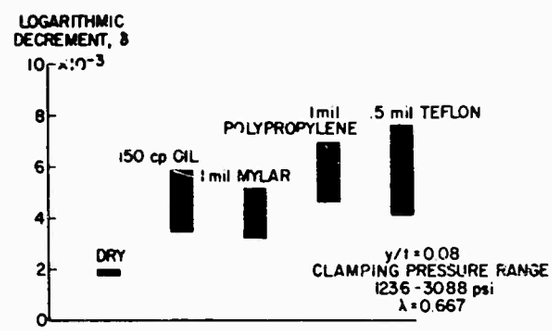

Fig. 10 - Total damping ranges obtained for various joint conditions

the dry and lubricated joint cases in bar graph form. The film materials are shown to increase the damping substantially, although they are not significantly more effective than oil in this respect.

CONCLUSIONS

An investigation was conducted to determine the effect of geometric scale on the damping in the joint of a practical beam-joint assembly. In addition, a brief study was made of the effect on joint damping of adding oil and viscoelastic films to the joint interfaces. Within the range of variables considered in these studies, the following conclusions were noted:

1. The damping attributed to the structural joint increases essentially linearly with vibration amplitude for any given joint clamping pressure.

2. Total damping decreases with increasing joint clamping pressure for low clamping

pressures but becomes essentially invariant at high pressures.

3. Both the total damping of the assembly and the joint damping increase considerably with a decrease in geometric scale.

4. The addition of oil to joint interfaces can, depending on model size, increase damping over that of the dry joint case. Thin viscoelastic films inserted between joint interfaces are also effective in increasing damping, but not significantly more so than oil.

REFERENCES

1. C. M. Zener, Elasticity and Anelasticity of Metals. University of Chicago Press, Chicago, 1948

2. Neal Granick and Jesse E. Stern, "Material Damping of Aluminum by a Resonant-Dwell Technique," NASA TN D-2893, Aug. 1965

3. W. E. Baker and F. J. Allen, "The Damping of Transverse Vibrations of Thin Beams in Air," Ballistics Res. Lab. Rept. 1033, Oct. 1957

4. David G. Stephens and Maurice A. Scavullo, "Investigation of Air Damping of Circular and Rectangular Plates, a Cylinder, and a Sphere," NASA TN D-1865, April 1965

5. Eric E. Ungar, "Energy Dissipation at Structural Joints; Mechanisms and Magnitudes," Bolt Beranek and Newman, Inc., Contract AF 33(657)-10125), Aug. 1964

6. L. E. Goodman and J. H. Clumpp, "Analysis of Slip Damping with Reference to Turbine Blade Vibration," J. Appl. Mech., Vol. 23, pp. 421-429, Sept. 1956

7. T. H. H. Pian and F. C. Hallowell, Jr., "Structural Damping in a Simple Built-up Beam," Proc. 1st U.S. Nat. Cong. Appl. Mech., ASME, pp. 97-102, 1952

8. Carl C. Osgood, "Force Transmissibilities in Spacecraft Structures," Shock and Vibration Bull. No. 35, Part 7, pp. 205-211, April 1966

9. Technical Information Staff of Industrial Fasteners Institute, "Joint Design," Machine Design, Fasteners Book Issue, pp. 33-40, March 21, 1963

10. R. V. Klint and R. S. Owens, "The Effect of Root Lubrication on the Damping of Cantilever Beams," presented at Lubrication Conf., New York, Oct. 1959

DISCUSSION

Mr. Ungar (Bolt Beranek & Newman): This was a very interesting piece of work. I am particularly gratified to see that your results are very similar to those we got on a slightly different geometry several years ago. We studied a beam riveted to a plate and made some conjectures about the mechanism. Did you determine what caused the damping in the joints?

Mr. Hanks: We were not able to determine the exact mechanism. You determined that air pumping had a considerable effect. We had very little air pumping and we couldn't attribute the joint damping to Coulomb friction because the trends of amplitude dependency was wrong, so we could not identify the mechanism. We did try to extrapolate the curves back to zero value and to identify mechanisms from that but we were unsuccessful.

Mr. Ungar: It was interesting to see that the parametric dependences you got were very similar to those we observed, and although you do not have air pumping in this case you do have oil pumping. We also experimented with oils of different viscosities, but over a range of 1 to 10^4 in increments of orders of magnitude. We found a peak in damping that you get with some intermediate range of oil viscosity. I feel from the things you report that probably the mechanisms are oil pumping for the oily joints and air pumping for the dry joints. Incidentally, Madonic recently published in the Journal of the Acoustical Society an analysis of the mechanism and an analytical prediction. He also showed that there are a couple of dependents of frequency on frequency and viscosity in terms of an oscillatory boundary layer in the fluid between the joints.

Mr. Hanks: We did run the smallest beam in a vacuum, although the vacuum was not a hard one, so that we may not have gotten all the air out of the joint interface. However, the trends were the same in that case as in the atmospheric test.

Mr. Khilnani (Texas Instruments): I notice that the addition of the plastic films interferes with the damping. What was the ratio of film thickness to beam thickness? Were the films double- or single-layered on either side of the joint? Did machining roughness of the beam have any effect on the damping?

Mr. Hanks: The plastic films were very thin, on the order of 1/2 mil. The beams vary from 0.05 to 1 in. in thickness. On the 2/3-scale model, the beam was 2/3 in. in thickness compared to 1 mil for the plastic films. We tried only the 63-μin. rms surface roughness, so I am not prepared to answer any questions as to the effect of the surface roughness.

Mr. Baruch (Kollsman Instrument Corp.): Since your total damping includes the effect of material damping, joint damping and air damping, wouldn't the fact that you decrease the width of your specimen leave a smaller surface area for air damping effects, thus resulting in lower damping in the smaller scale models? Could you possibly give an intuitive percentage of the air damping, or was this just meant to give an overall effect in the study?

Mr. Hanks: We did not go into a detailed study of the air damping, but as well as we could determine, using the works of other people and our tests on small beams in vacuum, air damping accounted for less than 5 percent of the damping in our systems.

* * *

DAMPING OF STRUCTURES BY VISCOELASTIC LINKS

David I. G. Jones
Air Force Materials Laboratory
Wright-Patterson Air Force Base, Ohio

and

Ahid D. Nashif
University of Dayton
Dayton, Ohio

Many complex structures exhibiting vibrational problems contain parallel or substantially parallel elements. The vibrational characteristics of the parallel elements are often different and, under certain circumstances, the use of viscoelastic links between antinodal parts of parallel elements can, with proper use, lead to the introduction of significant amounts of damping into the structure at the expense of very little added weight.

To gain some insight into the possibilities of such a technique, some investigations of the response of parallel beams of different flexural rigidities and weights, joined by such links, have been carried out at the Air Force Materials Laboratory. In the preliminary investigation, attention has been concentrated on a pair of parallel clamped-clamped beams with a viscoelastic link joining the centers. A theory of the response of the system is developed and it is shown that substantial amounts of damping can be introduced into the beams by proper choice of the link stiffness, provided that a natural frequency of one beam is not identical to (or close to) any natural frequency of the other beam, in which case no damping can be achieved no matter what the excitation may be.

An experimental investigation is described in which the theory is verified for links made of one commercially available viscoelastic material. Plans for further investigations of viscoelastic links in more complex structural models, more representative of situations likely to arise in current and future aerospace vehicles and other structures, are briefly discussed.

D. I. G. Jones

INTRODUCTION

It does not appear, from a review of the available literature, that the possibility of using viscoelastic links joining elements of complex structures to achieve high damping has received much attention. An early investigation [1] has shown that the use of distributed viscoelastic links between parallel beams can lead to high damping, provided the frequencies of the fundamental modes of the two beams are not equal.

In this paper, an analysis is presented for the response and effective damping of two parallel clamped-clamped beams with a single viscoelastic link joining the beam centers. It is shown that high damping can still be achieved, provided the fundamental frequency of the beam in question is not equal to any natural frequency of the other beam.

The experimental investigation of the same configuration is described, and it is shown that the theory accurately describes the phenomena occurring for one value of the loss factor of the link, which comprised a ring of a commercially available viscoelastic material.

LIST OF SYMBOLS

a_1, a_2 See Eqs. (7) and (10), respectively

A_1, A_2 Arbitrary constants

A Amplification factor at resonance for beam 1

b Breadth of circular link

b_1, b_2 See Eqs. (8) and (11), respectively

B_1, B_2 Arbitrary constants

c_1, c_2 See Eqs. (9) and (12), respectively

C_1, C_2 Arbitrary constants

cos Circular cosine function

ch Hyperbolic cosine function (cosh)

d Separation of beams; also diameter of circular link used in experimental investigation

D_1, D_2 Arbitrary constants

exp Exponential function

E_1, E_2 Young's moduli of beams 1 and 2, respectively (psi)

i $\sqrt{-1}$ or suffix denoting beam ($i = 1,2$)

I_1, I_2 Second moments of area of beams (in.^{4})

k Real part of stiffness of viscoelastic link (ib/in.)

L Length of beams (in.)

sin Circular sine function

sh Hyperbolic sine function (sinh)

t Time (sec)

T_1 Transmissibility of beam 1

W_1, W_2 Amplitudes of transverse vibrations of beams relative to clamped ends at any point x (in.)

x Station along beams, measured from centers (in.)

X Amplitude of vibration of clamped ends (in.)

Γ $k/E_1 I_1 \lambda_1^3$, nondimensional link stiffness parameter

η Loss factor of viscoelastic link

η_s Effective loss factor of beam 1

λ $E_2 I_2 / E_1 I_1$, nondimensional parameter defining relative stiffnesses of beams

λ_1, λ_2 See Eq. (3)

μ_1, μ_2 Masses per unit length of beams (lb/in.)

τ Thickness of link (ring)

ξ_1 $\lambda_1 L/2$, nondimensional frequency parameter

ϕ μ_2/μ_1, nondimensional mass parameter

ω Circular frequency (rad/sec)

THEORY OF PARALLEL CLAMPED-CLAMPED BEAMS WITH VISCOELASTIC LINK JOINING CENTERS

Consider two parallel clamped-clamped beams joined by a viscoelastic link as shown in Fig. 1. If the amplitude of the harmonic vibration of one beam relative to the clamped ends is $W_1(x)$ and that of the other beam is $W_2(x)$, and the supports are vibrating with harmonic displacement $X \exp(i\omega t)$, then the equations of motion of the two beams are

$$E_i I_i (d^4 W_i / dx_i^4) - \mu_i \omega^2 W_i = \mu_i \omega^2 X, \quad i = 1,2 \qquad (1)$$

at all points apart from the points to which the link is attached. The general solution of Eqs. (1) is:

$$W_i(x) = A_i \mathrm{ch}(\lambda_i x) + B_i \mathrm{sh}(\lambda_i x) + C_i \cos(\lambda_i x) + D_i \sin(\lambda_i x) - X, \quad i = 1,2, \qquad (2)$$

where

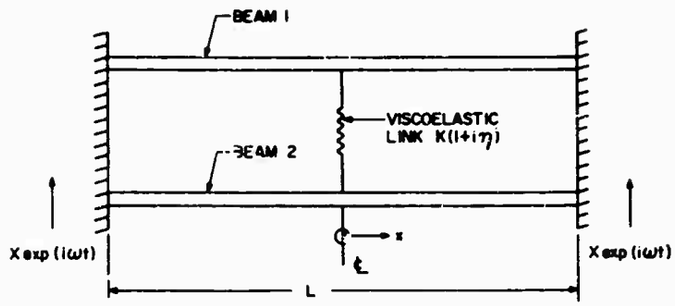

Fig. 1 - Idealized link joining parallel beams

$$\lambda_i^4 = \mu_i \omega^2 / E_i I_i , \quad i = 1,2 . \tag{3}$$

The eight constants A_i, B_i, C_i and D_i are determined from the various boundary conditions:

$$W_i = dW_i/dx = 0 \quad \text{at} \quad x = \pm L/2 ,$$

$$dW_i/dx = 0 \quad \text{at} \quad x = 0 ,$$

$$2E_1 I_1 (d^3 W_1/dx^3) = k(1 + i\eta)(W_2 - W_1) \tag{4}$$

and

$$2E_2 I_2 (d^3 W_2/dx^3) = k(1 + i\eta)(W_1 - W_2) \tag{5}$$

at $x = 0$. From these conditions, the eight equations for the eight unknown constants are readily set up and solved. After some simplification, the solution $W_1(x)$ is readily shown to be:

$$\frac{W_1(x)}{X} = \frac{\Gamma(1 + i\eta)[b_1 c_2 + (b_2 c_1/\lambda)(\phi/\lambda)^{-3/4}] + 4 c_1 a_2}{\Gamma(1 + i\eta)[a_2 b_1 + (a_1 b_2/\lambda)(\phi/\lambda)^{-3/4}] + 4 a_1 a_2} , \tag{6}$$

where

$$a_1 = \text{sh}\, \xi_1 \cos \xi_1 + \text{ch}\, \xi_1 \sin \xi_1 , \tag{7}$$

$$\begin{aligned} b_1 = {} & a_1 [\text{sh}(2\xi_1 x/L) - \sin(2\xi_1 x/L)] \\ & - \text{ch}(2\xi_1 x/L)[\text{ch}\, \xi_1 \cos \xi_1 + \text{sh}\, \xi_1 \sin \xi_1 - 1] \\ & - \cos(2\xi_1 x/L)[\text{ch}\, \xi_1 \cos \xi_1 - \text{sh}\, \xi_1 \sin \xi_1 - 1] , \end{aligned} \tag{8}$$

$$c_1 = \sin \xi_1 \, \text{ch}(2\xi_1 x/L) + \text{sh}\, \xi_1 \cos(2\xi_1 x/L) - a_1 , \tag{9}$$

$$a_2 = \text{sh}\{(\phi/\lambda)^{1/4} \xi_1\} \cos\{(\phi/\lambda)^{1/4} \xi_1\} + \{\text{ch}\, (\phi/\lambda)^{1/4} \xi_1\} \sin\{(\phi/\lambda)^{1/4} \xi_1\} , \tag{10}$$

$$\begin{aligned} b_2 = {} & a_2 \big[\text{sh}\{(\phi/\lambda)^{1/4} (2\xi_1 x/L)\} \\ & - \sin\{(\phi/\lambda)^{1/4} (2\xi_1 x/L)\}\big] \\ & - \text{ch}\{(\phi/\lambda)^{1/4} (2\xi_1 x/L)\}\big[\text{ch}\{(\phi/\lambda)^{1/4} \xi_1\} \\ & + \text{sh}\{(\phi/\lambda)^{1/4} \xi_1\} \sin\{(\phi/\lambda)^{1/4} \xi_1\} - 1\big] \\ & - \cos\{(\phi/\lambda)^{1/4} (2\xi_1 x/L)\} \big[\text{ch}\{(\phi/\lambda)^{1/4} \xi_1\} \\ & \times \cos\{(\phi/\lambda)^{1/4} \xi_1\} \\ & - \text{sh}\{(\phi/\lambda)^{1/4} \xi_1\} \sin\{(\phi/\lambda)^{1/4} \xi_1\} - 1\big] , \end{aligned} \tag{11}$$

and

$$\begin{aligned} c_2 = {} & \sin\{(\phi/\lambda)^{1/4} \xi_1\} \, \text{ch}\{(\phi/\lambda)^{1/4} (2\xi_1 x/L)\} \\ & + \text{sh}\{(\phi/\lambda)^{1/4} \xi_1\} \cos\{(\phi/\lambda)^{1/4} (2\xi_1 x/L)\} - a_2 . \end{aligned} \tag{12}$$

The transmissibility T_1 is defined as the ratio of the response at any point of beam 1, relative to a fixed point in space, to the input amplitude X, i.e.,

$$T_1 = |W_1 + X|/X . \tag{13}$$

METHOD OF SOLUTION

For given values of the ratio ϕ of the beam masses per unit length, beam 1 being taken as reference, and the ratio λ of the flexural rigidities, the transmissibility T_1 can be expressed as a function of the frequency parameter ξ_1, the link loss factor η and the link stiffness parameter Γ (Eq. (6)).

The calculations were performed for ϕ = 0.5, 1.0 and 2.0 and a range of values of λ between 0.01 and 100 at $x = 0$. Transmissibility

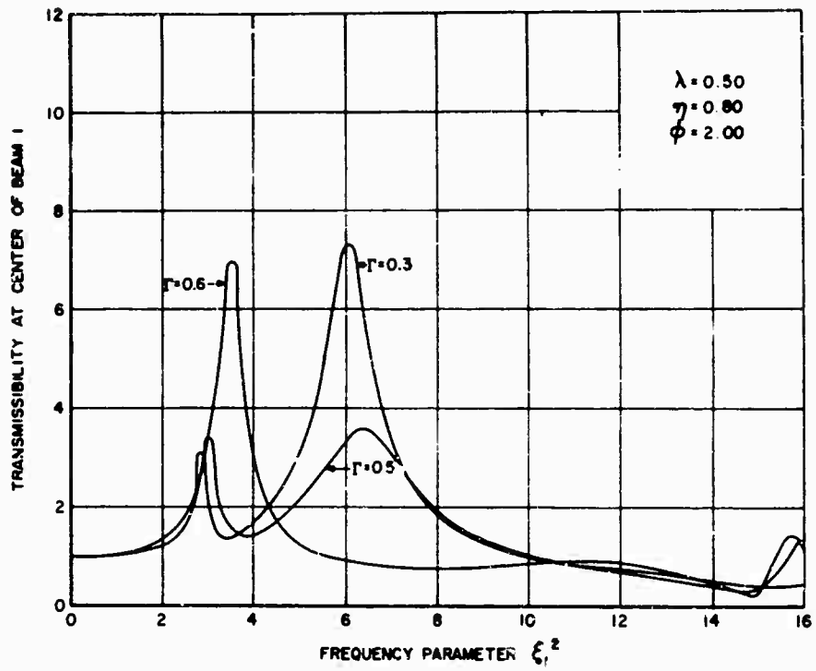

Fig. 2 - Typical transmissibility spectra for $\lambda/\phi < 1$

spectra such as those illustrated in Figs. 2 and 3 were obtained by a digital computer. The characteristics of the response were found to depend on whether $\lambda/\phi = 1$, <1 or >1.

If $\lambda/\phi = 1$, the first resonant frequency of beam 2 is equal to that of beam 1 and the two beams will always vibrate in phase with each other. In this case, no deformation occurs in

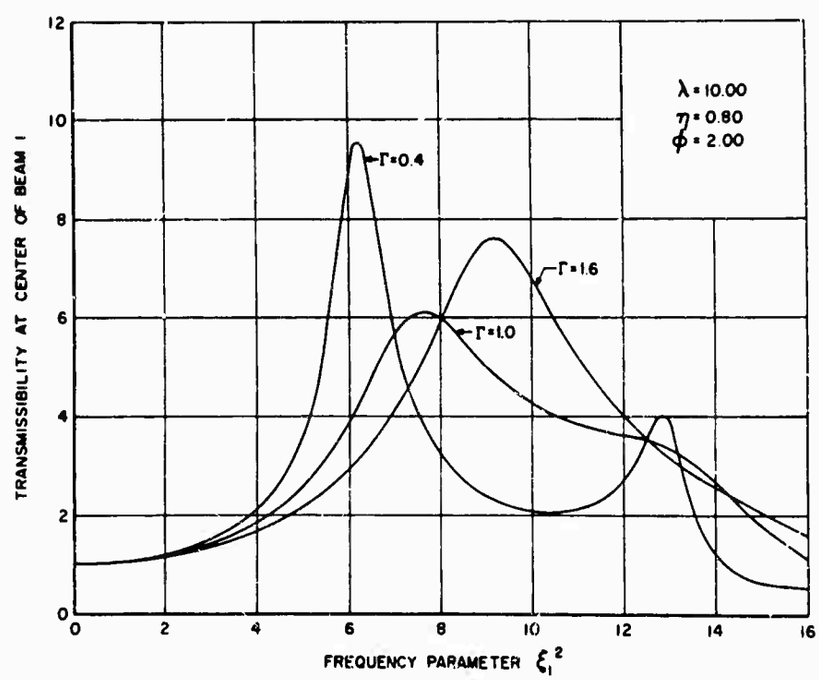

Fig. 3 - Typical transmissibility spectra for $\lambda/\phi > 1$

the viscoelastic link and hence no damping can be introduced into the system by viscoelastic links.

If $\lambda/\phi < 1$, the first resonant frequency of beam 2 is always lower than that of beam 1 and the spectra shown in Fig. 2 are typical. Figure 2 shows that the amplitude of the low-frequency resonance peak is smaller than that of the higher frequency peak for small values of Γ and, as Γ increases, the amplitude of the second peak eventually becomes smaller than that of the first peak. The effective loss factor η_s of a clamped-clamped beam under shaker excitation, for which the clamped ends are vibrated to give the excitation, has been shown [2] to be

$$\eta_s = 1.32\ (A^2 - 1)^{-1/2}, \qquad (14)$$

where A is the amplification factor measured at the center of beam 1 at the resonant peaks corresponding to the first mode. Typical graphs illustrating the variation of the effective loss factors of the two peaks with the stiffness parameter Γ are shown in Fig. 4 for several values of the link loss factor η. It is seen that, for each η, a value of Γ exists for which both peaks will have the same effective loss factor. This loss factor corresponds to the case where the system is "properly tuned" for beam 1, since it represents the maximum loss factor obtainable for given values of λ, ϕ and η, in the frequency range of the fundamental mode of beam 1. This procedure was followed for various values of λ/ϕ between 1 and 0.035. At $\lambda/\phi = 0.035$, the first natural frequency of beam 1 is identical to the third natural frequency of beam 2 and the effective loss factor is again zero. For values of $\lambda/\phi < 0.035$, analysis of the response spectra followed the procedure adopted for values of λ/ϕ between 1 and 0.035. However, in this case, the natural frequency of the fundamental mode of beam 1 is higher than the natural frequencies of the first and third modes of beam 2 and hence the predominant peak due to beam 2 was compared instead with the first peak due to beam 1 to define the optimum effective loss factor.

On the other hand, when $\lambda/\phi > 1$, the first natural frequency of beam 2 is greater than that

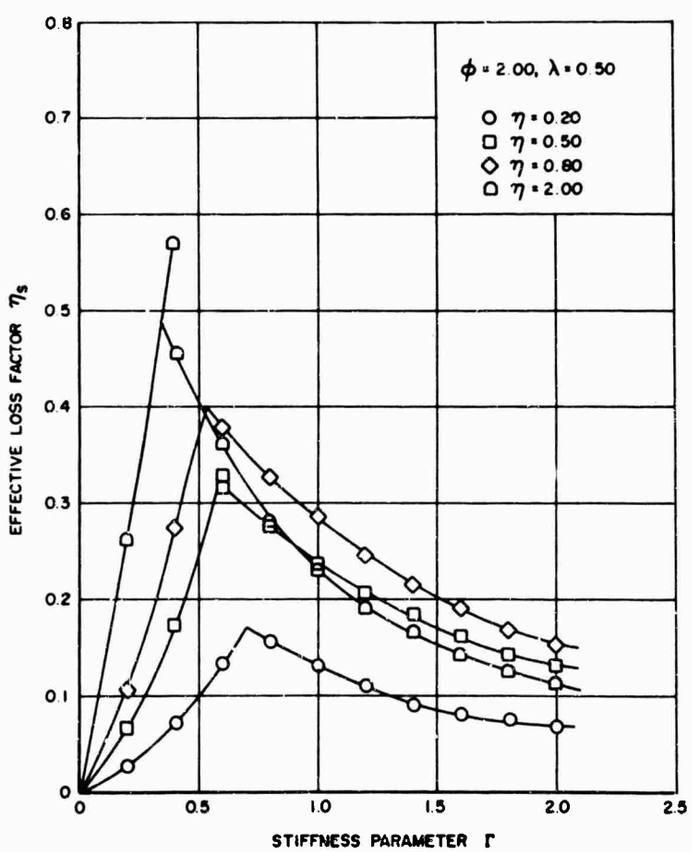

Fig. 4 - Typical graphs of effective loss factor vs link stiffness parameter for $\lambda/\phi < 1$

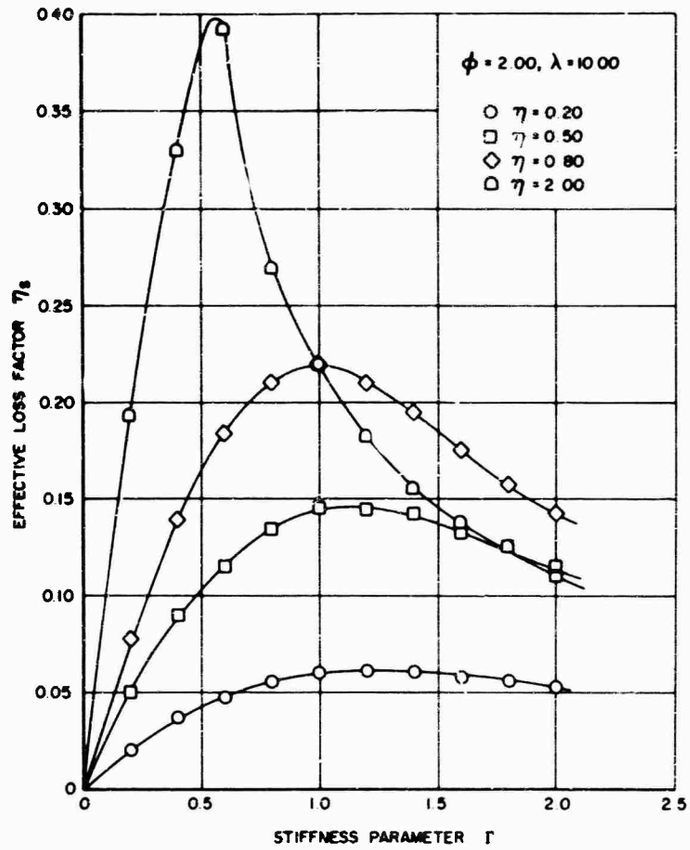

Fig. 5 - Typical graphs of effective loss factor vs link stiffness parameter for $\lambda/\phi > 1$

of beam 1, and the spectra shown in Fig. 3 are typical. It is seen that one peak now dominates the response for all values of the stiffness parameter Γ, even though two peaks still exist. Graphs of η_s against Γ for the predominant peak are illustrated in Fig. 5.

Depending on whether $\lambda/\phi < 1$ or > 1, therefore, one may define the point of optimum damping either as that at which the curves of η_s against Γ cross over, or that at which the curve of η_s against Γ has a maximum, respectively. Graphs of the optimum damping so defined were determined in this manner for many values of λ and ϕ and the results are plotted in Figs. 6, 7 and 8 for ϕ = 0.5, 1.0 and 2.0 and η = 0.2, 0.5, 0.8, 1.0 and 2.0.

EXPERIMENTAL INVESTIGATION

The experiments were carried out for several combinations of parallel clamped-clamped beams joined by viscoelastic links in the center. For these combinations, the weight ratios were ϕ = 0.5, 1.0 and 2.0 and the range of values of the stiffness ratio was from 0.02 to 50. The material used for the viscoelastic link was LD-400 (Lord Manufacturing Co., Erie, Pa.), having a loss factor of approximately 0.8 at room temperature which does not vary greatly with temperature in the vicinity of room temperature.

For each set of values of λ and ϕ, two beams were made and clamped in the mounting fixture which was attached to the shaker table as in Fig. 9. The circular viscoelastic link, of thickness τ, width b and outside diameter d, was attached to both beams to join the centers. An accelerometer was attached to the mounting fixture to measure and control the input acceleration which was kept at a constant amplitude throughout each test. The acceleration output was measured by two miniature accelerometers at the center of each beam. An overall view of the experimental apparatus is illustrated in Fig. 10. For a given width of the link, the acceleration output was measured and recorded continuously on an X-Y plotter over a wide

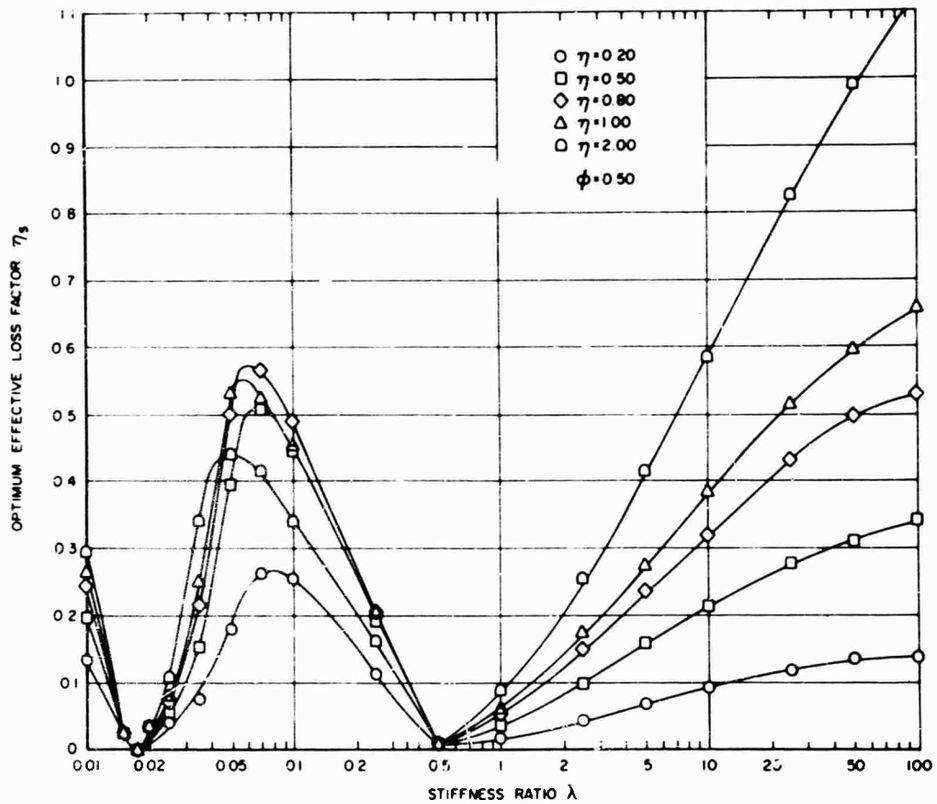

Fig. 6 - Optimum effective loss factor vs beam stiffness parameter for $\phi = 0.5$

range of frequencies. The width b of the link, which is proportional to the stiffness parameter Γ, was then varied to obtain the maximum effective loss factor in the same way as described in the previous section. Typical experimental response spectra for beam 1 are illustrated in Figs. 11 and 12 for $\lambda/\phi < 1$ and > 1, respectively. This test procedure was repeated for every value of ϕ and λ used in the tests.

From all the response spectra so obtained, graphs of the effective loss factor of the significant peaks were plotted against the stiffness parameter (here represented by the link width b) in the same way as in the reduction of the theoretical results. Typical graphs of the effective loss factor measured in the experiments with the link width b are plotted in Figs. 13 and 14 for $\lambda/\phi < 1$ and > 1, respectively. From these graphs, the optimum effective loss factors were determined in the usual manner and plotted against the beam stiffness parameter λ for $\phi = 0.5$, 1.0 and 2.0, as shown in Figs. 15, 16 and 17, for a link loss factor η of 0.8. Theoretically derived curves of η_s versus λ for $\eta = 0.8$, taken from Figs. 6, 7 and 8, are also shown with the experimental results. It is seen that the agreement between theory and experiment is good.

DISCUSSION

The emphasis in both the theoretical and experimental investigations has been placed on the response and effective damping of only one of the parallel beams, referred to as beam 1. This is because we have assumed that, in the real structure which we are endeavoring to simulate in some measure, interest will generally be concentrated on the reduction of vibrations in one part of the structure only. For example, one may be interested only in the vibration levels in the outside skin of an aircraft fuselage and the behavior of the rest of the structure is to some extent secondary. However, it is of little value to reduce vibrations in beam 1, representing the most important part of the structure, if one instead introduces serious vibrations in beam 2. In the experimental investigation, therefore, the response in beam 2 was measured also. It was found, in all cases, that when beam 1 was

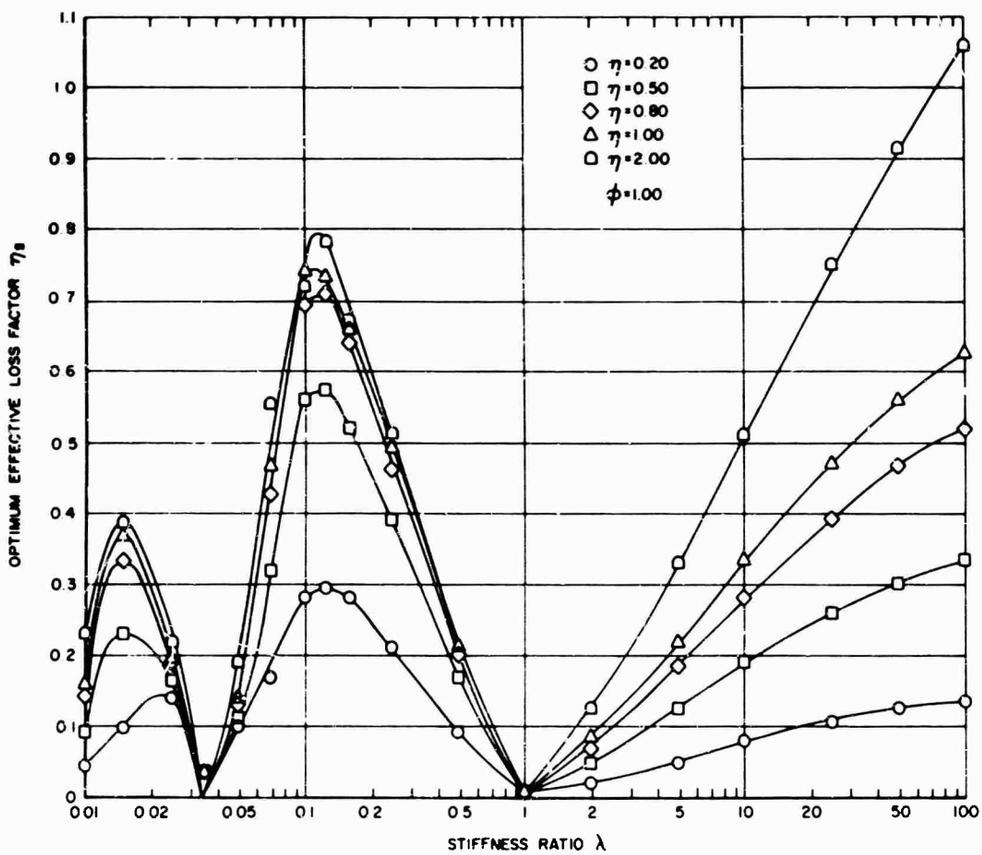

Fig. 7 - Optimum effective loss factor vs beam stiffness parameter for ϕ = 1.0

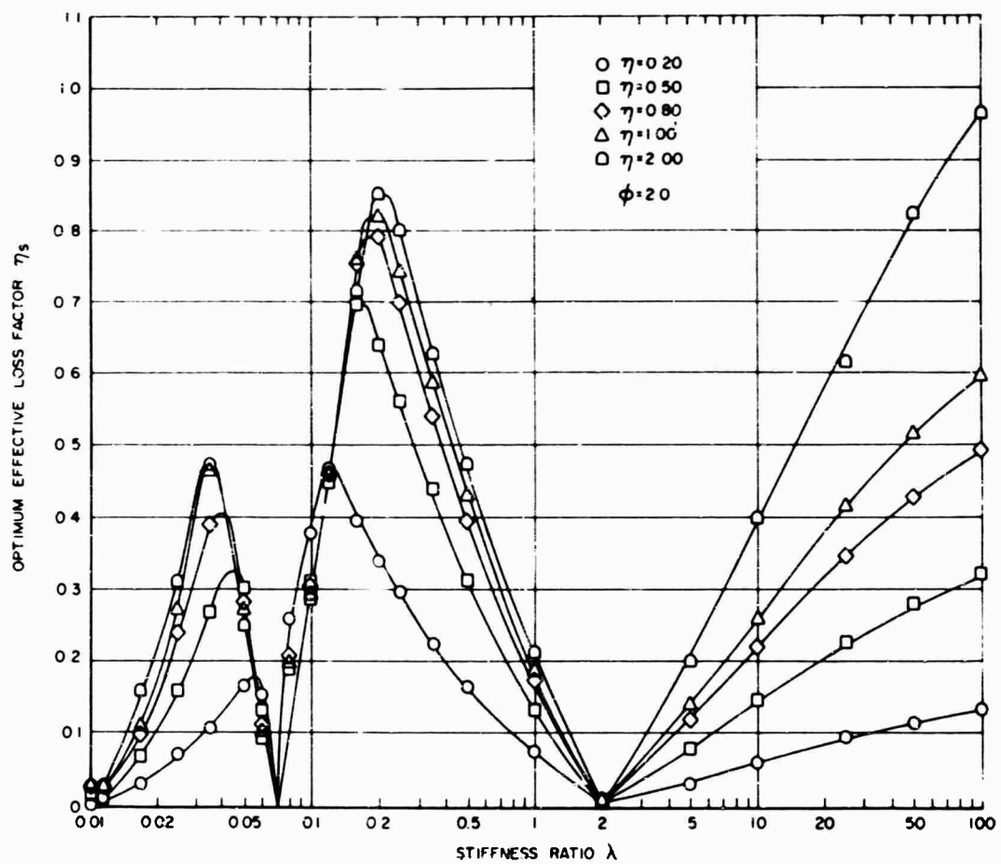

Fig. 8 - Optimum effective loss factor vs beam stiffness parameter for ϕ = 2.0

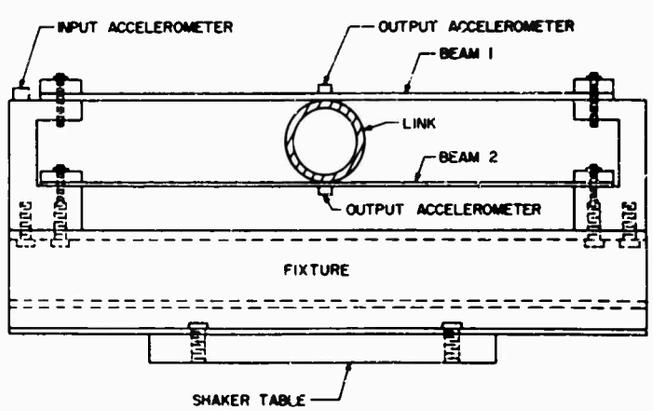

Fig. 9 - Apparatus

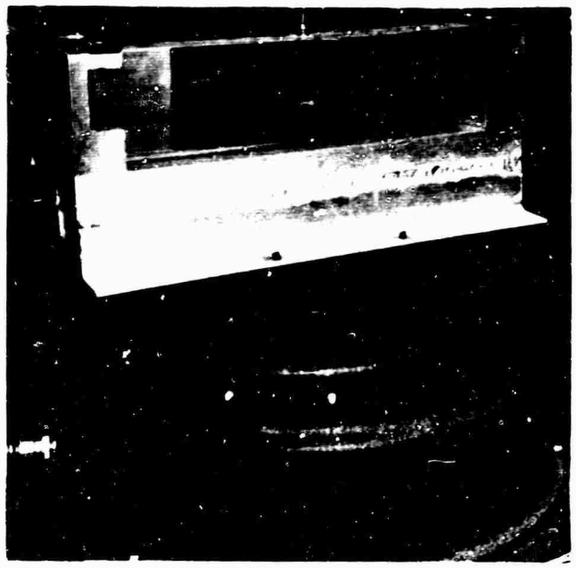

Fig. 10 - Experimental equipment

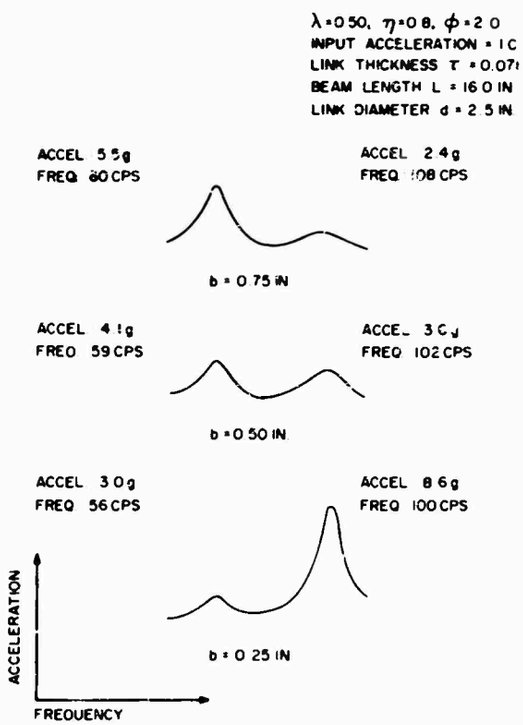

Fig. 11 - Typical measured response spectra for $\lambda/\phi < 1$

properly tuned for optimum damping, high damping was also introduced into beam 2. It was also observed that even the third mode of beam 1 was well damped when the fundamental mode was optimally tuned.

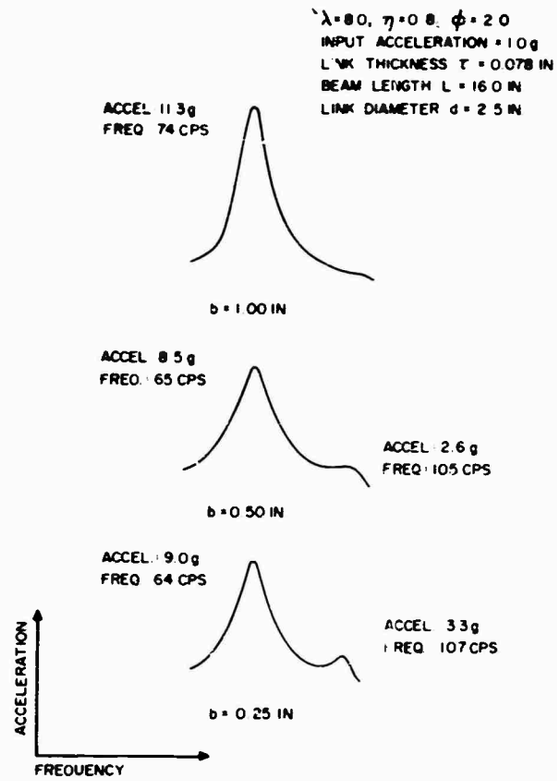

Fig. 12 - Typical measured response spectra for $\lambda/\phi > 1$

The preliminary investigations described in this paper have, therefore, shown that high damping can be introduced into a very simple structure by a viscoelastic link. It remains to be seen whether the same is the case for a complex multi-span skin stringer type structure with such links, as illustrated in Fig. 18. There is considerable hope that such a technique will work well, since the modes of such a structure are closely spaced in frequency compared with those of a simple clamped-clamped beam, and the stored energies are very close [3].

CONCLUSIONS

An analysis has been developed for the response of two parallel clamped-clamped beams, with various relative masses and flexural rigidities, connected at the centers by a viscoelastic link. The effect of link stiffness and loss factor, and of the relative masses and flexural rigidities of the beams, on an arbitrarily defined effective loss factor are described. It is shown that there are certain circumstances in which no damping of the system occurs and others in which high damping is introduced.

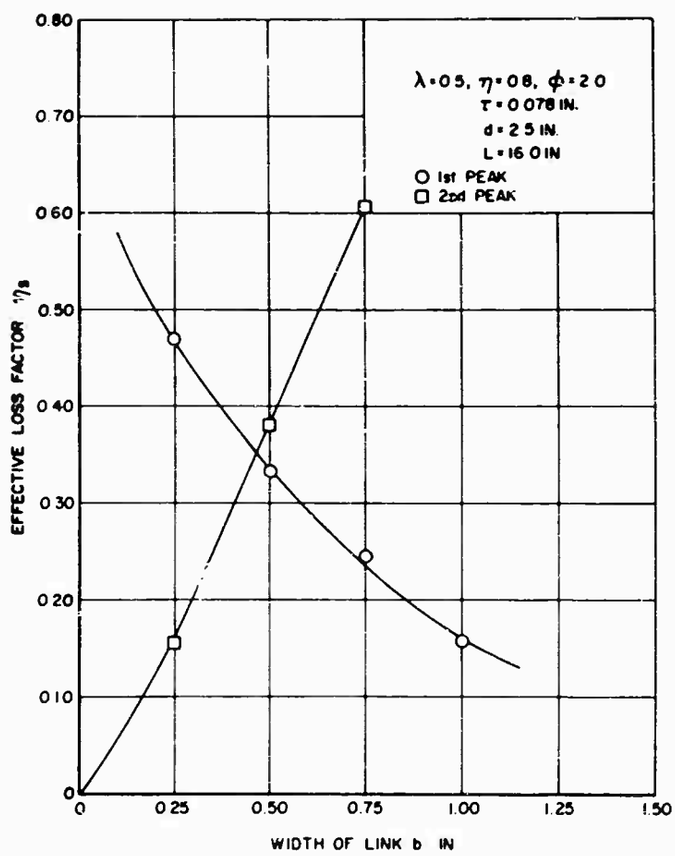

Fig. 13 - Experimentally measured values of effective loss factor vs link width for $\lambda/\phi < 1$

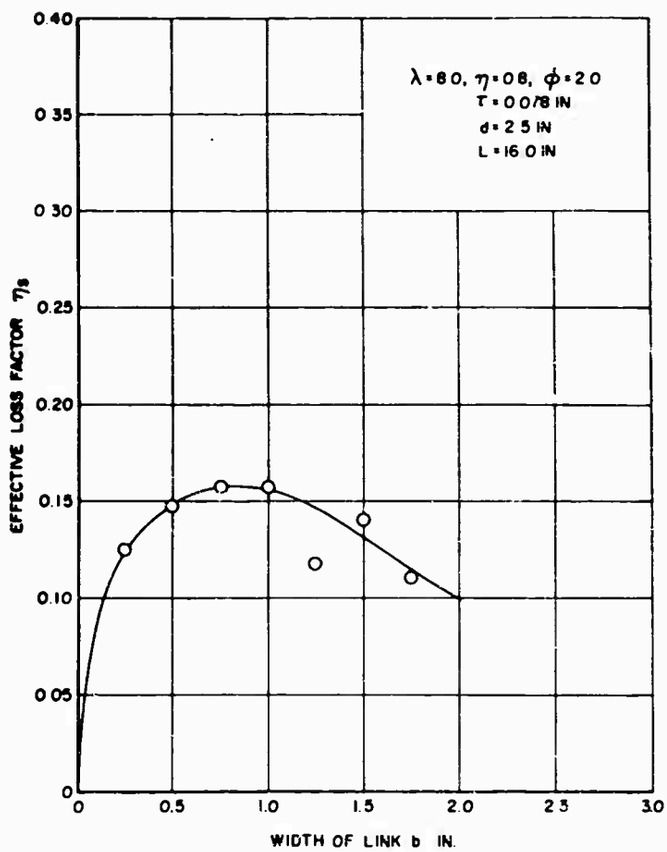

Fig. 14 - Experimentally measured values of effective loss factor vs link width for $\lambda/\phi > 1$

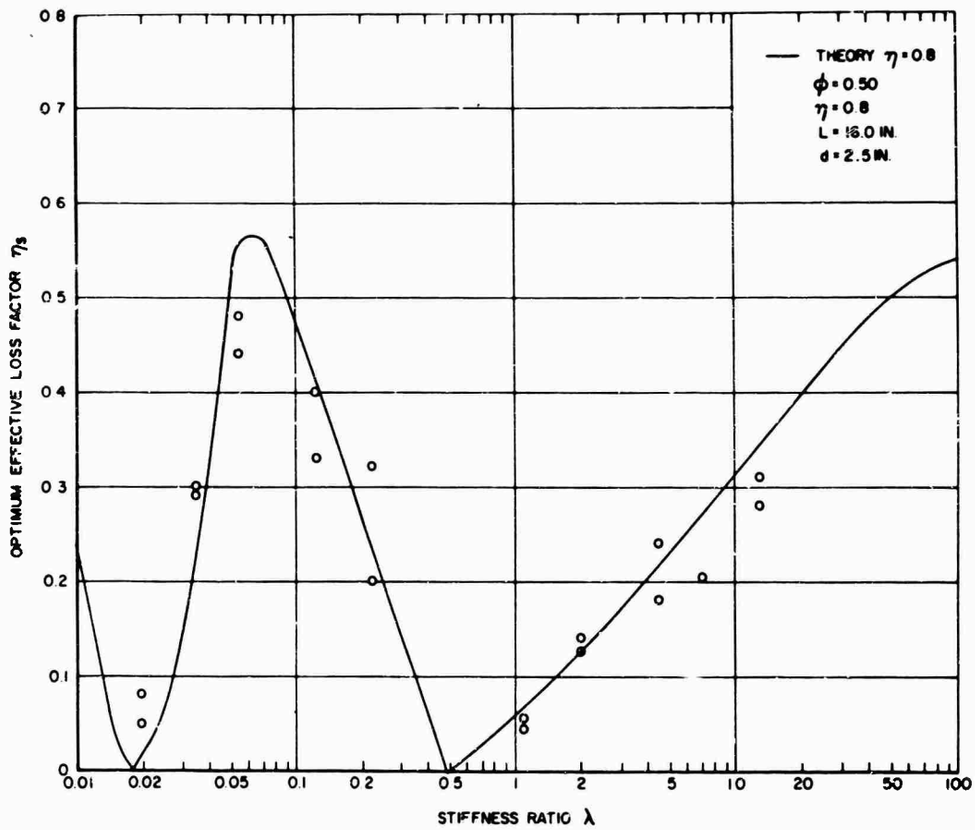

Fig. 15 - Comparison of experimental and theoretical values of optimum effective loss factors for ϕ = 0.5

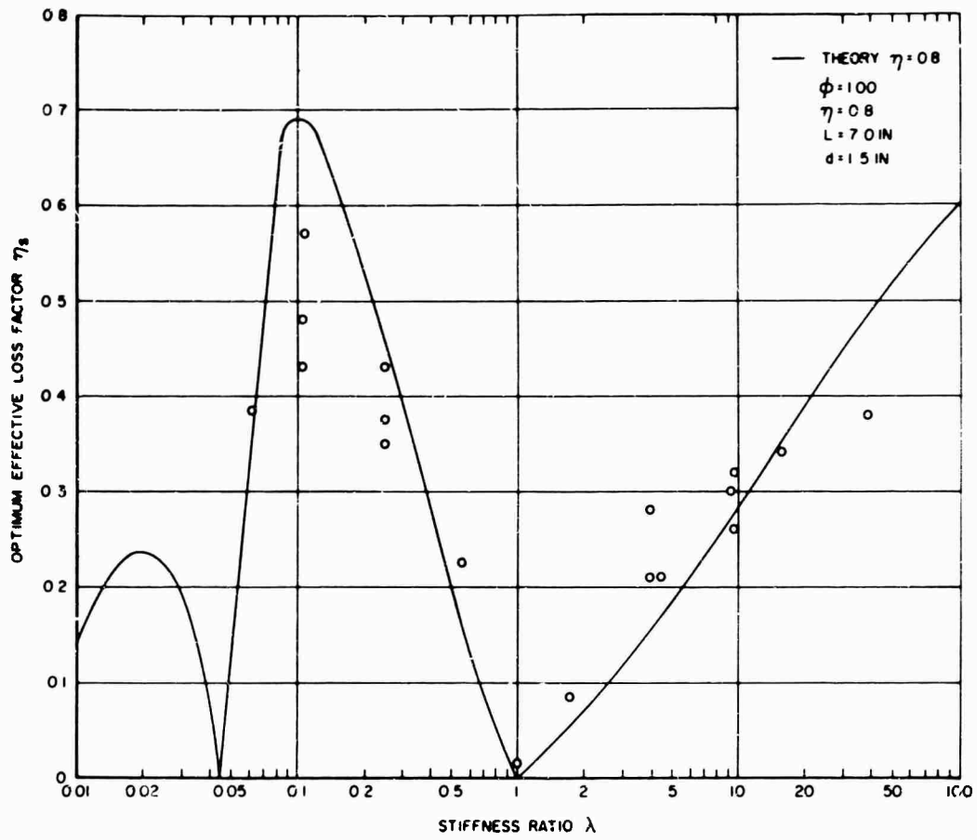

Fig. 16 - Comparison of experimental and theoretical values of optimum effective loss factors for ϕ = 1.0

An experimental investigation is described which shows that the analysis accurately predicts the behavior of the system and that high damping can be introduced into a simple structural system by viscoelastic links.

ACKNOWLEDGMENTS

The experimental investigation described in this paper was carried out on equipment purchased using the Director's Fund of the Air Force Materials Laboratory. The authors would like to thank W. J. Trapp and D. M. Forney, Jr., of the Strength and Dynamics Branch, for their support and encouragement, J. Schmermund and E. D. Goens for support of the experimental investigations, Miss Connie Mantych for preparation of the manuscript and Mr. DeMarey of the University of Dayton for assistance with the figures.

REFERENCES

1. D. I. G. Jones, "Some Aspects of the Analysis of Vibrations and Damping in Simple Structures," Air Force Materials Lab. Rept. AFML-TR-65-151, pp. 82-90, 1965

2. R. L. Adkins and D. I. G. Jones, "Effect of Tuned Viscoelastic Dampers on Response and Damping of a Clamped-Clamped Beam," Air Force Materials Lab. Rept. AFML-TR-66-100, p. 13, 1966

3. J. P. Henderson, "Energy Dissipation in a Vibration Damper Utilizing a Viscoelastic Suspension," Shock and Vibration Bull. No. 35, Part 7, pp. 213-227, April 1966

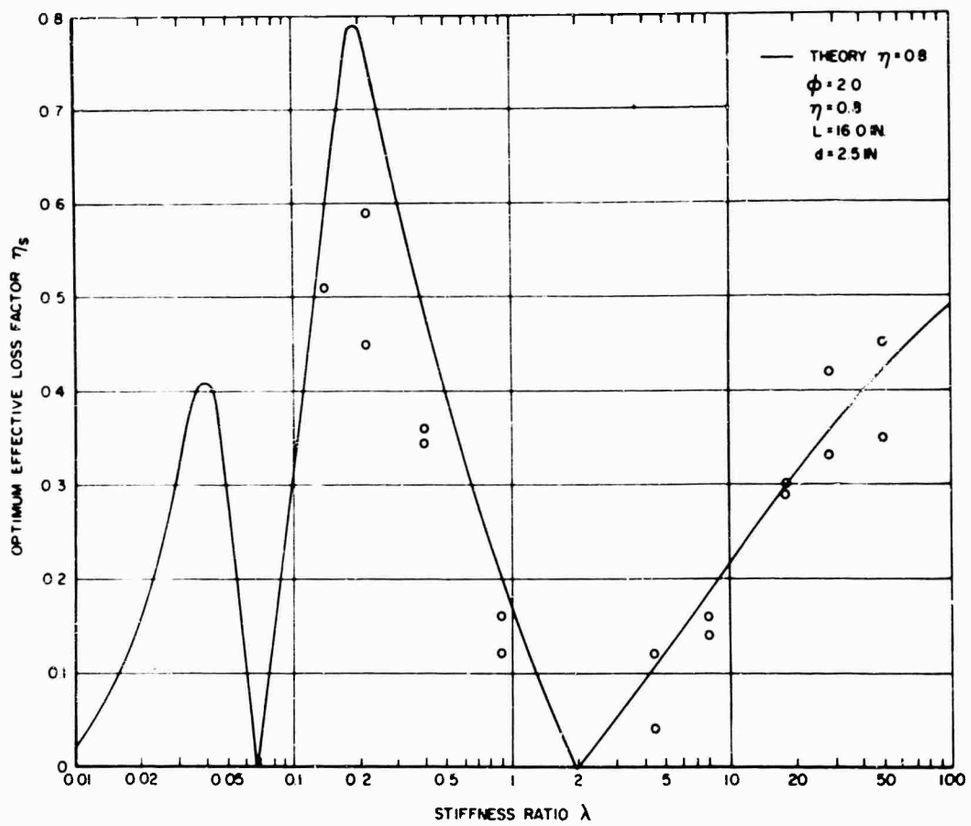

Fig. 17 - Comparison of experimental and theoretical values of optimum effective loss factors for $\phi = 2.0$

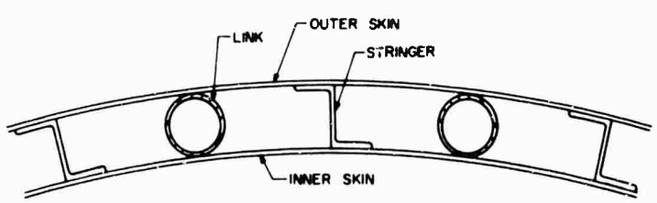

Fig. 18 - Skin-stringer structure with viscoelastic links

DISCUSSION

Mr. Huffington (Martin Co.): Did you have to be concerned with the vibration characteristics of the ring damper as coupling in with the vibrations of the beams? To have a successful energy attenuator it is necessary that the material be capable of continuously dissipating energy without deterioration. Do you have any comments on this?

Mr. Jones: Obviously, material must be capable of withstanding vibration and any other type of environment which occurs. This is a real problem. Certainly for the material we used in this investigation we had no such aims in mind. Maybe one of the papers later in this session will answer that question. As to your first question, in this particular investigation the link was very very light compared to the beams so the problem did not arise. Inevitably if the link is heavy you must bear this in mind. This particular preliminary investigation was not concerned with the practical problems, only

with demonstrating that it was worthwhile or not worthwhile to go ahead and look at the practical problems.

Mr. Huffington: Was there a temperature increase in the material and did it have any effect?

Mr. Jones: It is thought that the temperature rise in this type of situation is not necessarily very great. It might be of the order of 10°F to 30°F, maybe 40°F, and with the specially tailored materials available, that should be no serious problem. We have indeed been working in another investigation altogether with dampers where we have been forced to deal with temperature rises of this sort. Materials can be made to withstand them.

Mr. DiTaranto (PMC Colleges): In your curve of the stiffness ratio, it appeared that if λ goes to a very large number or infinity, you get more damping. This would seem to imply that maybe the thing to do is have just pure mass at the end rather than having any stiffness or beam at the bottom.

Mr. Jones: What we are really dealing with here is a means of using an existing structure. You might have two parts of a powerless structure in which λ, the stiffness ratio, is already defined and there is nothing you can do about it. Since these links can be made very light, and often very cheaply, you can get good damping by adding just a very small amount of weight to your structure. On the other hand, if the other beam does not pre-exist, obviously you must put something else there, and the mass would probably be far more valuable than another beam.

* * *

ELASTOMERS FOR DAMPING OVER WIDE TEMPERATURE RANGES

F. S. Owens
Air Force Materials Laboratory
Wright-Patterson Air Force Base, Ohio

The use of viscoelastic materials for structural damping on aircraft and missiles has been unduly limited because of the temperature sensitivity of these materials. The experimental work here described demonstrates a technique for extending the temperature range over which these materials have useful damping. The approach is based on the phenomenon that viscoelastic polymers exhibit a high level of damping only within a few degrees of their glass transition temperatures and that certain types of polymer blends exhibit more than one glass transition temperature. The dynamic response of blends of polyvinyl acetate and polystyrene with a styrene-butadiene and a nitrile-butadiene rubber were investigated over temperature ranges including all the glass transitions of the polymers used in the blends. The polyvinyl acetate-polystyrene-nitrile rubber blend and the polystyrene-nitrile rubber blend both met the target properties of having a loss factor of 0.1 or more and a modulus of 10^4 psi over a 200°F range. The three polymer blends had a higher level of damping over a wider temperature range than the two polymer blends, and the two polymer blends were better than the base elastomers. Further improvements in high temperature damping materials are anticipated through the use of the fundamental concepts demonstrated in this research effort.

F. S. Owens

INTRODUCTION

Vibrations in high-speed aircraft and missiles arise from turbulent boundary layer conditions, engine thrust, engine noise, unsymmetrical mass distribution of rotary components, etc. Viscoelastic dampers are used to isolate, insulate, and attenuate the unwanted, and at times harmful, oscillations. The dampers protect delicate instruments from vibrations, personnel from undesirable noise, and structural members of the craft from fatigue failure. Ideally, the materials used for dampers should eliminate vibrations of all possible frequencies occurring in the craft at all temperatures from the lowest occurring in the arctic regions up to the highest possible operating temperature. In addition, the material should be strain insensitive and have a low density. However, this ideal material is becoming more difficult to reach because as the speed of the craft increases, the skin and engine temperatures increase, thus widening the temperature requirements for a damping material. In general, elastomers, in the usual sense of the term, cannot act as effective dampers over such a wide temperature range. The reasons for this are evident from Fig. 1, in which the real part of the complex Young's modulus and the loss factor of an elastomeric high polymer are plotted as functions of temperature [1]. The loss factor, η, is a measure of the damping ability of a material [2] and is related to the complex modulus, E^*, as follows:

$$E^* = E' + iE'' \tag{1}$$

$$E^* = E'(1 + i\eta), \tag{2}$$

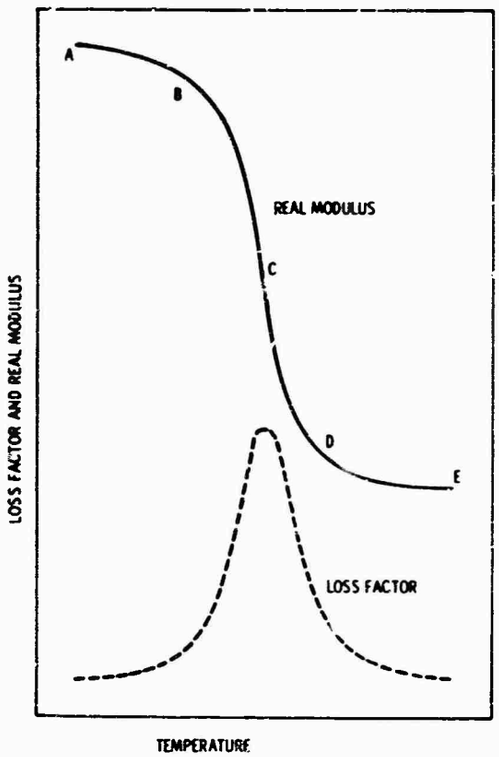

Fig. 1 - Typical loss factor and real modulus vs temperature

where

E' = storage or real modulus,

$i = \sqrt{-1}$, and

$E'' = E'\eta$, the loss or imaginary modulus.

The segment AB of Fig. 1 is called the "glassy" region and is associated with a high modulus and low mechanical losses. The segment BCD is called the "transition" or "dispersion" region. At temperatures within this range, the materials absorb considerable mechanical energy, converting it into heat energy. The temperature corresponding to C, the inflection point of the curve, is of particular interest. It is called the glass transition temperature, usually denoted T_g, and is that corresponding to the maximum energy absorption of the material. The width of the dispersion region, the temperature range corresponding to segment BCD, determines the temperature range over which the material is most effective as a damper. For most elastomers this temperature range is approximately 50°F; butyl rubber, the exception, is about 100°F [3]. Segment DE corresponds to the "rubbery" region and is usually associated with damping that is higher than that in the glassy region but considerably lower than that of the transition region. Since all amorphous viscoelastic materials have modulus and damping curves similar to Fig. 1 [1], and since high damping occurs only within a few degrees of T_g [2,3], the problem of producing wide temperature range viscoelastic dampers is really a problem of producing materials with wider or more numerous dispersion regions. The usual techniques of varying the kind and level of mineral fillers, plasticizers, curing agents, etc., results only in altering the temperature range at which maximum damping occurs and will not greatly improve either the peak damping or the temperature range of satisfactory damping [2,4,5]. Fortunately, such materials can be produced by either chemical modification of existing polymers or by selective blending [1,4,6,7]. The chemical reactions yielding these materials are those reactions which result predominantly in the formation of block and graft polymers [6,7]. Blends in this case are immiscible mixtures of polymers which have a common curing agent [1,4,5]. Block polymers have chains consisting of alternating long sequences of chemically different polymers. Graft polymers consist of one or more polymer chains attached to the backbone of a different type of chemical chain and result from the reaction of a polymer with a monomer. Both graft polymers and polyblends exhibit more than one T_g and, consequently, have more than one damping peak [1,4,5,6,7]. Thus, by the proper selection of grafts or blends, it is theoretically possible to have damping peaks at almost any temperature. Both grafts and blends have been used in this investigation; however, this report is concerned primarily with blends.

OBJECTIVES

The objectives of this research were, first, to satisfy an Air Force need and, secondly, to demonstrate a technique applicable for producing composites having high damping at specified temperatures or over specified temperature ranges. Since the Air Force needs viscoelastic damping materials to cover a wide temperature range, which is not likely to be covered with only one formulation, the initial efforts were directed toward satisfying an immediate need. A rubberlike material having a loss factor of at least 0.1 over a temperature range of about 0 to 200°F within a frequency range of 100 to 1000 cps with a minimum real dynamic Young's E modulus of 10^4 psi was set as the initial objective. Ultimately, our goal is a series of compositions, each having a dynamic modulus of 10^5 psi or greater, with a loss factor of at least 0.3 over at least 200°F to cover the

temperature range where high damping is needed, i.e., within 0 to 400°F and above.

MATERIALS SELECTION

T_g data were the most important criterion used in the selection of the experimental polymers to accomplish the objectives. First, the particular polymer system chosen should be available in a wide variety of T_g's; second, it should lend itself to easy modification, if necessary, by simple chemical reactions not requiring elaborate equipment; and, third, the chemistry of the system should be well known or easily accessible. The polyesters, polyurethanes, and the vinyls met these requirements. The vinyl system was chosen for the initial phases of the research; however, there is evidence that either of the other systems would probably have worked as well. The choice of the particular vinyl polymers to be used was based on the desire to have a composition which was essentially elastomeric at or below room temperature, yet has glass transitions at higher temperatures. Recalling (Fig. 1) that elastomeric behavior is the result of the polymer being above its glass transition temperature, T_g, and that this T_g is shifted to higher temperatures by vulcanization as well as by increasing frequencies [4], the first elastomer selected, a styrene-butadiene copolymer (Firestone Synthetic Rubber #1502) containing 23 percent bound styrene, had a T_g of -65°F. The vinyl polymers selected for blending in the rubber were polyvinyl acetate and polystyrene with T_g's of 84 and 212°F, respectively. As a means of controlling as many variables as possible, these polymers were prepared from the monomers by emulsion polymerization. Composition of the polymers was as follows:

1. Polyvinyl acetate

   Water, 500 ml;
   Vinyl acetate, 340 ml;
   Soap, 5.0 gm; and
   Potassium persulfate, 1.5 gm.

   (Ran for 3 hr at 65°C; air-dried reaction mixture.)

2. Polystyrene

   Water, 500 ml;
   Styrene, 330 ml;
   Soap, 5.0 gm; and
   Potassium persulfate, 1.5 gm.

The results of dynamic measurements on peroxide cures of mixtures of these materials indicated that a higher T_g elastomer would be more desirable. Therefore, the second elastomer chosen was a very high acrylonitrile containing nitrile-butadiene (Paracril-D, U.S. Rubber Co.) rubber which had a T_g of 50°F when cured, as measured dynamically.

BLENDING

The preparation of the blends listed in Table 1 were done according to the usual procedures followed in rubber compounding. First, the gum rubber was banded on a 2-roll 8-in. water-cooled mill. Then zinc oxide was added to neutralize any acid remaining from the coagulation of the polymers and to promote the activity of the curing agent, dicumyl peroxide. The other polymers were added in small amounts as called for in the desired formulation. The polystyrene had to be added next in the styrene-butadiene blends. The order of addition was not critical in the nitrile-butadiene blends. Because these polymers were being milled at temperatures below their T_g's, there resulted very high shearing forces and, consequently, a rise in temperature. After the polymers were taken into the rubber, the mixture was refined by passing one end of the rolled-up compound through a closely set mill. This procedure was repeated several times until the mixture appeared to be homogeneous and then, after cooling, the curing agent was added. Special care to prevent excessive heating had to be exercised while, and after, the curing agent was added. The formulation was again refined several times on a closely set mill, and finally, when the curing agent was uniformly dispersed, it was put back on the mill, sheeted into the desired thickness, and cut into mold preform specimens.

TABLE 1
Experimental Formulations[a]

Material	Amount			
	1	2	3	4
Paracril-D	100	100	100	100
Polyvinyl acetate	-	100	-	100
Polystyrene	-	-	100	100
Zinc oxide	10	10	10	10
Dicumyl peroxide	3	3	3	3

[a]Cure: 1 hr at 280°F.

SPECIMEN PREPARATION

The preform specimens were compression molded into strips 8-in. long, 0.450-in. wide

and in different thicknesses up to 0.125 in. The molding was done at 280°F for 1 hr under a pressure of 500 to 600 psi. Usually, the hot mold was removed from the press and cooled under a stream of tap water before the specimens were removed. The strips of rubber were bonded on the aluminum beams while the rubber was being cured. The same thickness of the viscoelastic material was bonded on both sides of the metal strips as shown in Fig. 2. Rubber-to-metal adhesive systems used were commercial products, Chemlok 203 primer (Hughson Chemical Co.) and Chemlok 220 adhesive. For practical damping applications, a room temperature curing epoxy adhesive may be better, since it contributes to the mechanical losses of the system.

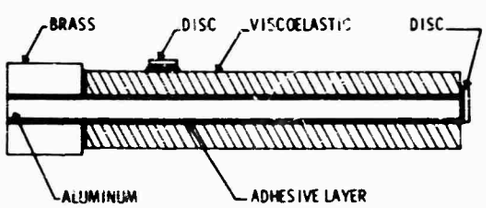

Fig. 2 - Specimen

DYNAMIC MEASUREMENTS

The dynamic mechanical properties of the composite beams were measured by personnel of the Strength and Dynamics Branch, AFML, using the Bruel and Kjaer Complex Modulus Apparatus and ancillary equipment, shown schematically in Fig. 3.

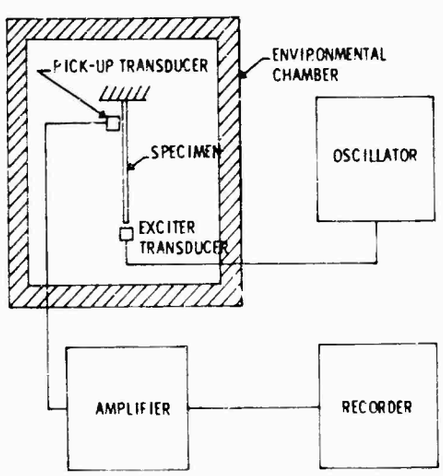

Fig. 3 - Schematic of test equipment

All measurements were made in the temperature test chamber. The room temperature experiments were run first, followed by successively lower temperatures until the temperature was well below the lowest T_g of the particular blend. Next, the higher temperature experiments were run, starting out at room temperature again. A soak period of 30 min was given at each experimental temperature and then the oscillator was calibrated just prior to making the test. At each experimental temperature, the measurements consisted of obtaining the resonant frequencies and the half-power bandwidth points of each resonant frequency of the composite beam. These measurements are related to the physical and mechanical properties of the materials in the composite beam [8,9,10] and were used to calculate the storage modulus and the loss factor of the viscoelastic formulations. A discussion of the mathematical relations used is given by Nashif [10]. For each experimental temperature the storage modulus and the loss factor are plotted as a function of resonant frequencies. The resulting points are then connected by smooth curves, and from these curves the values of the storage modulus and the loss factor at 100 and 1000 cps were interpolated. These values were plotted as a function of temperature, connected with smooth curves, and are the results used for this report.

DISCUSSION

Initial attempts were made to make graft polymers by reacting vinyl acetate and styrene monomers with styrene-butadiene rubber. However, because it was difficult to control the grafting and to analyze the resultant graft polymers, this approach was dropped in favor of making polymer blends. This accomplished the desired results and was much easier to control. Blends of polyvinyl acetate, polystyrene, and the styrene-butadiene rubber were investigated first. The composite beams used for the measurements had only one side of the aluminum coated with the viscoelastic material. The results were not completely reliable because the adhesive being used at that time tended to become ineffective at high temperatures and some of the measurements were taken at resonant frequencies where, as later found, large errors were possible. Even though the results may not be absolutely accurate, they did show that the concept of using blends of polymers having different T_g's will broaden the temperature range of high damping and that adding the plastic polymers to the base elastomer will increase the modulus somewhat. For example, a blend of equal parts by weight of polystyrene

and the styrene-butadiene rubber had a modulus of greater than 10^4 psi over the temperature range of -75 to 225°F. The loss factor curves had peaks corresponding to the dispersions in the modulus curves. However, the loss factor curves were lower than desired; therefore, the experimental work with styrene-butadiene blends was discontinued because it was thought that nitrile rubber had more desirable properties.

Nitrile-butadiene rubbers are more resistant to hydrocarbon fuels, oils, solvents, and heat than the styrene-butadiene rubbers. Hence, they are more desirable for use as dampers on aircraft. The higher the acrylonitrile content of the polymer, the higher the solvent resistance of the rubber. The reason for the hydrocarbon fluid resistance is the presence of the polar nitrile groups in the polymer molecule. These polar groups contribute to the damping of the rubber by making the polymer more sensitive to frequency variations; i.e., the damping under the same temperature conditions is better at higher rather than at lower frequencies. As the acrylonitrile content of the polymer increases, the T_g also increases. There is, however, a reduction of low-temperature properties. The particular nitrile-butadiene rubber, Paracril-D, used was one which had a very high acrylonitrile content and has been successfully applied as liners for fuel hose and as oil seals. It has a T_g just below room temperature and can be blended with many other rubbers and plastics, particularly the polar ones. It is somewhat reinforced by compatible plastic polymers having high T_g's, such as polystyrene. The specimens used for the evaluation of the storage modulus and the loss factor had the rubber bonded with the Chemlok adhesive system on both sides of the aluminum beams. The results are more reliable than those obtained with composite beams having rubber on only one side.

The storage modulus of the gum vulcanizate (Formulation #1) was 4×10^5 psi at 0°F and dropped to 4×10^3 psi at 75°F (Fig. 4). This large change in the modulus is associated with a very high loss factor peak (Fig. 5). The height and width of the damping peak is considerably higher and wider than that obtained for the styrene-butadiene rubber. The maximum in the loss factor was around 1.0, while it was 0.5 for the styrene-butadiene polymer. The temperature range over which the losses were above 0.1 was 20 to 175°F. The width of this temperature range is very frequency dependent; for example, the loss factor at 150°F is 0.1 for 100 cps and 0.3 for 1000 cps. This frequency dependence of the damping can be used to an

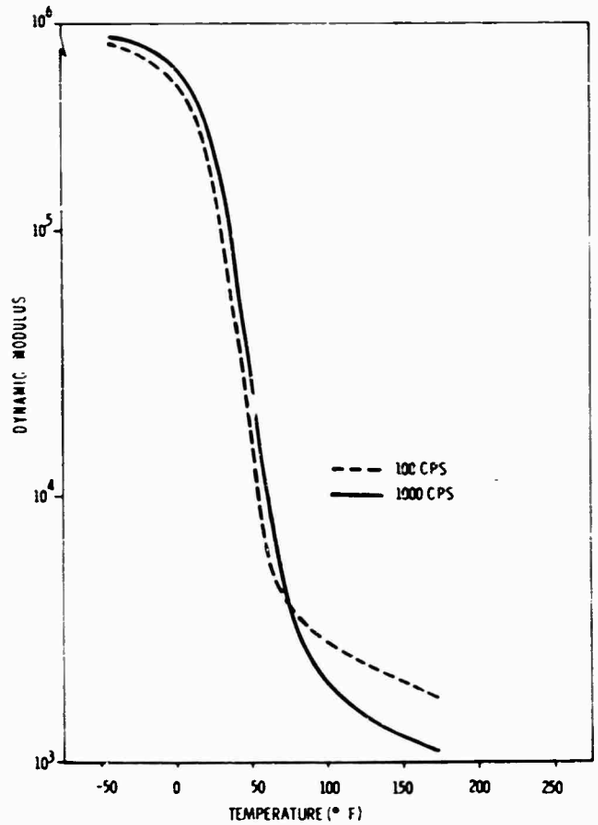

Fig. 4 - Real dynamic modulus vs temperature of a nitrile-butadiene vulcanizate

advantage in applications where adequate damping at low frequencies can be obtained with the nitrile rubber. An equal weight mixture of nitrile-butadiene rubber and polyvinyl acetate (Formulation #2) had two dispersion regions which overlapped so much that they are not obvious from the modulus curves (Fig. 6). The modulus of this blend was greater than 10^4 psi at temperatures below 115°F A 10^2 decrease in the modulus took place over a temperature range of 0 to 175°F. The closeness of the T_g's of the two polymers is the reason why there is not more of a break in the modulus curves and led to the damping peaks being close together (Fig. 7). Also, the nearness of the T_g's helped to keep the damping curves at a high level over a wider temperature range. The loss factor curve is above 0.1 over the 25 to 175°F range and is above 0.3 over the 40 to 175°F. Peak damping of about 1.0 occurred at about 50 and 125°F with the highest peak at 125°F being attributed to the polyvinyl acetate. The damping peak due to the rubber was lowered as a consequence of the dominating effect of the second polymer. The gum rubber met the target

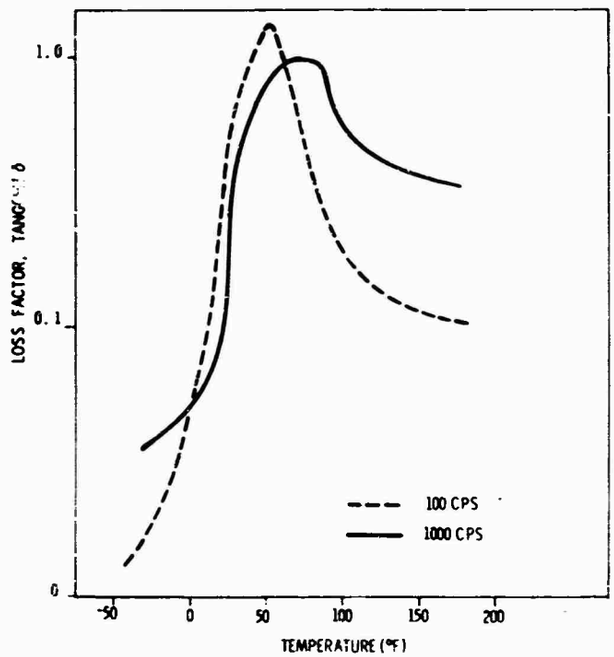

Fig. 5 - Loss factor vs temperature of a nitrile-butadiene vulcanizate

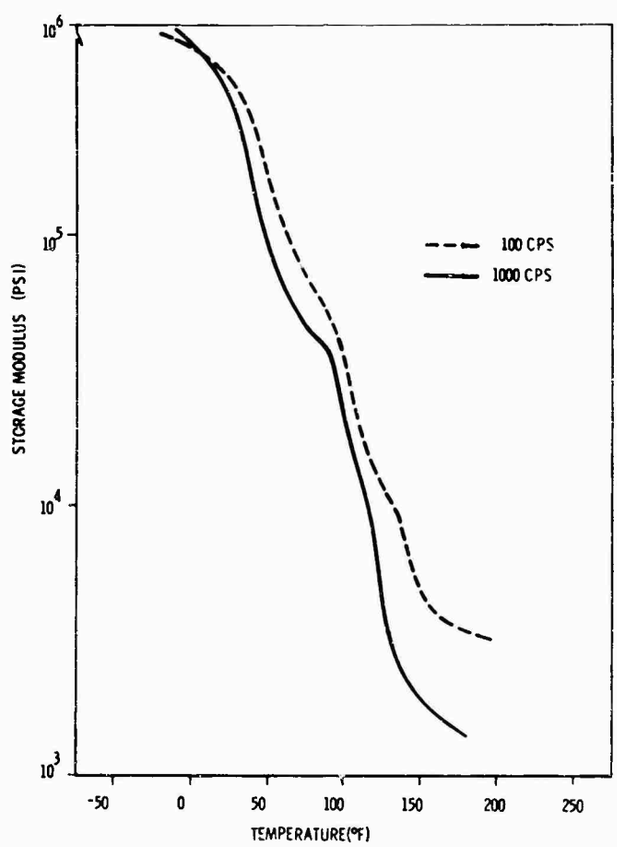

Fig. 6 - Real dynamic modulus vs temperature of a polyvinyl acetate/ nitrile rubber blend

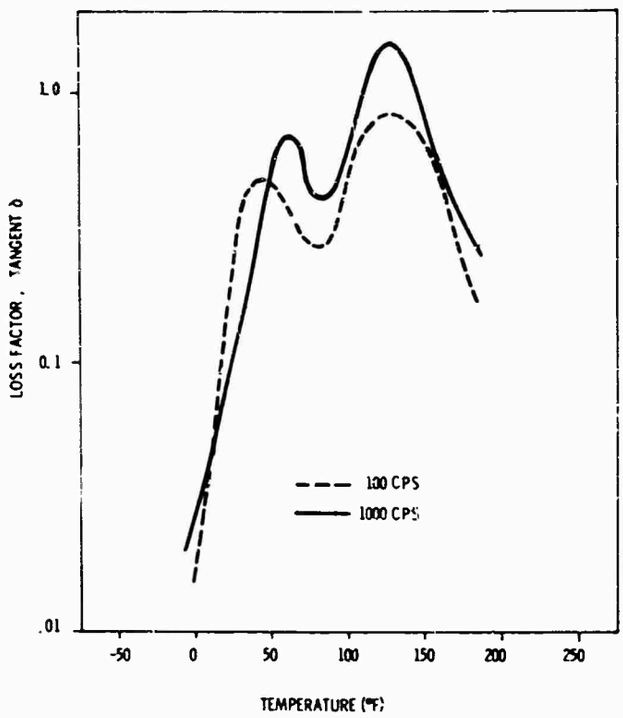

Fig. 7 - Loss factor vs temperature of a polyvinyl acetate/nitrile rubber blend

properties over the temperature range 20 to 60°F, while the two-component blends met the objectives over the 20 to 115°F range. Thus, the addition of polyvinyl acetate to the rubber increased the temperature range by 55°F.

Blends of polystyrene and the nitrile rubber (Formulation #3) had dynamic behavior similar to the polyvinyl acetate blends; however, the modulus curves (Fig. 8) have very definite transitions and there are breaks in the curves at about 150°F. This was a result of the polymers in the blend having widely separated T_g's. Apparently, the polystyrene contributes to the dynamic strength of the rubber and helps to keep the modulus high, particularly at the elevated temperatures. The modulus remained above 10^4 psi up to 225°F. The loss factor curves (Fig. 9) have peaks of 0.6 at 50°F and 0.8 at 250°F. The losses are above 0.1 over the 25 to 275°F range with a minimum value of 0.1 occurring within the range of 50 to 250°F. These two-component blends met the target properties over the range of 25 to 225°F and will function very well as a vibration damper within this range. The equal weight mixture of polyvinyl acetate, polystyrene, and nitrile rubber (Formulation #4) had three transitions which are more evident from the damping curves (Fig. 10) than from the modulus curves (Fig. 11). For this three-polymer blend, the modulus remained above 10^4 psi up to 200°F, which is not as good as obtained with the polystyrene blend. The loss factor vs temperature curves had peaks of 0.3 at 65°F, 0.9 at 130°F, and 0.4 at 230°F for 1000 cps and of 0.15 at 40°F, 0.5 at 120°F, and 0.6 at 230°F for 100 cps. Here again the frequency dependency of the loss factor is very noticeable. While both the two and three polymer blends met the target properties, it is thought that the three component blends have better damping than the two-component mixtures because the area under the loss factor curves is larger. Experiments are now under way to optimize the amount of polymers in the blend so as to have all three of the loss factor peaks of about the same height. This change in the formulation should improve the modulus values at high temperatures. Further improvements can no doubt be made by adding reinforcing fillers. The rubber is not resistant to temperatures above 325°F so no experiments are planned in which the high temperature range is increased.

SUMMARY AND CONCLUSIONS

This preliminary investigation has demonstrated that polymer blends have a higher level

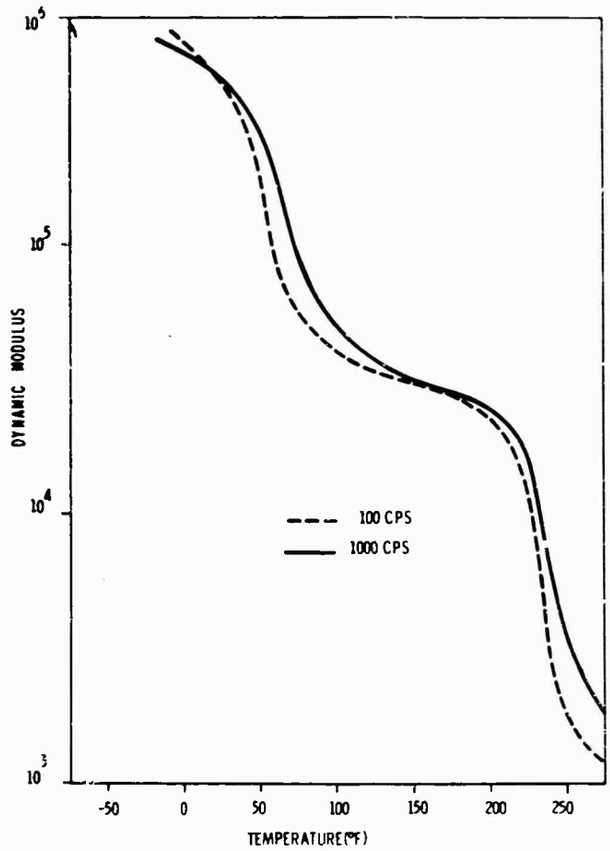

Fig. 8 - Real dynamic modulus vs temperature of a polystyrene/nitrile rubber blend

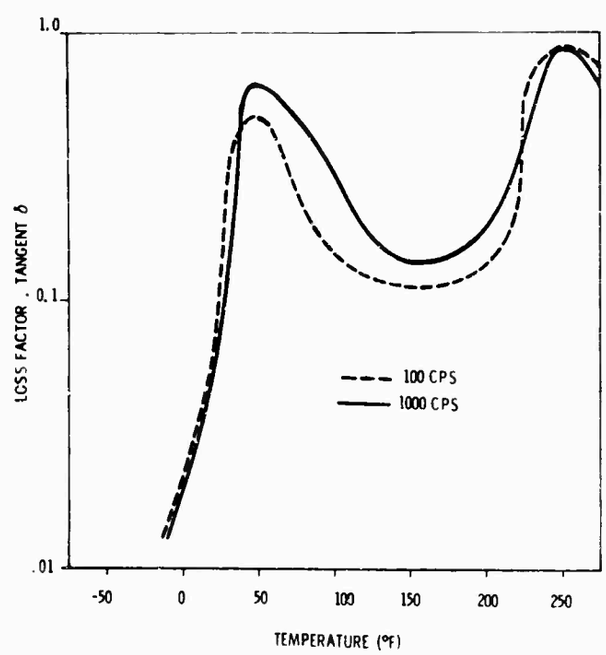

Fig. 9 - Loss factor vs temperature of a polystyrene/nitrile rubber blend

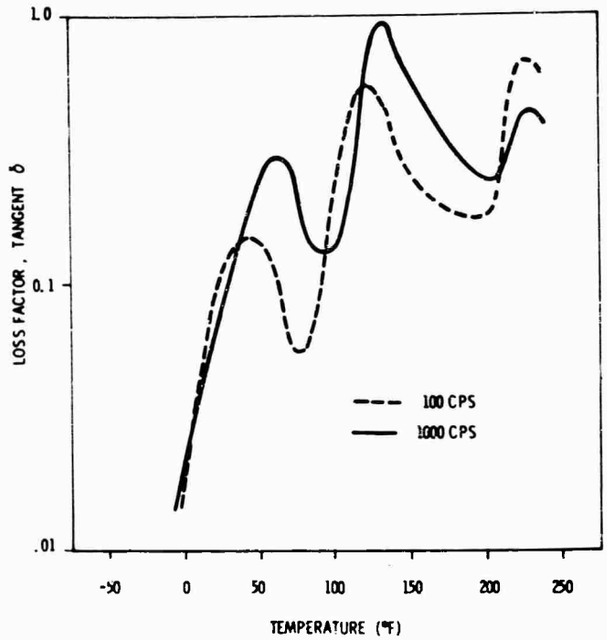

Fig. 10 - Loss factor vs temperature of a polyvinyl acetate/polystyrene/nitrile rubber blend

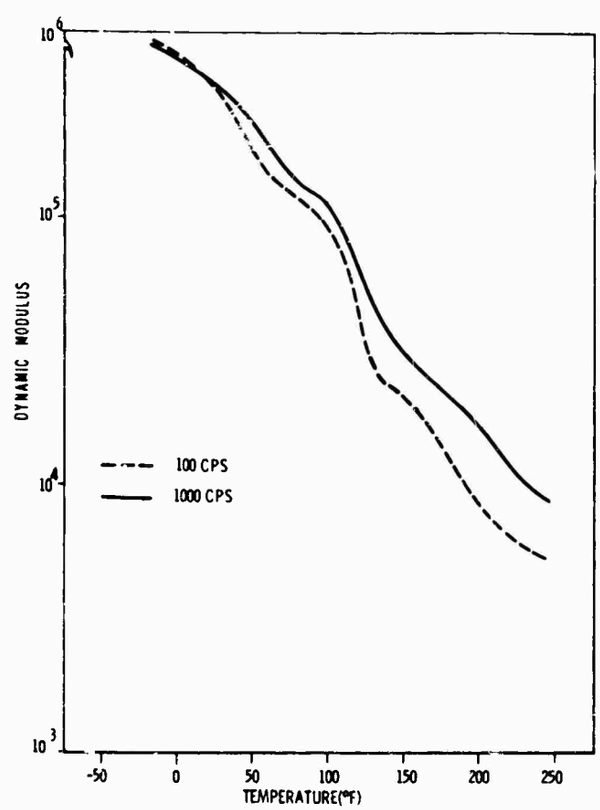

Fig. 11 - Real dynamic modulus vs temperature of a polyvinyl acetate/polystyrene/nitrile rubber blend

of damping than does a homogeneous material. The reason for this is that polymers, in general, are insoluble in each other and that blends actually consist of more than one phase. Each phase exhibits a T_g which is independent of the other polymers used in the blend. Thus, polymer blends can be used to broaden the temperature range of adequate viscoelastic damping. In particular, the three-component blends investigated were better damping materials than the two-component blends, and the two-component blends were better than the base elastomer. The loss factor was 0.1 or more and the real modulus was 10^4 psi or more over 20 to 60°F for the nitrile rubber, 20 to 115°F for the polyvinyl acetate-nitrile rubber blend, and 25 to 225°F for both the polystyrene-nitrile rubber blend and the polyvinyl acetate-polystyrene-nitrile rubber blend.

The above results show that the temperature sensitivity of viscoelastic materials can be used to an advantage to obtain a high level of damping along with a high modulus over a wide temperature range. It seems apparent that the ideas used to achieve the objective can be applied to other temperature ranges where a high level of damping has been difficult to obtain.

ACKNOWLEDGMENTS

This paper is the result of a joint effort between the Nonmetallic Materials Division and Metals Division of the Air Force Materials Laboratory. The author wishes to acknowledge the invaluable assistance of R. E. Headrick, D. Krintzline, and C. M. Cannon.

REFERENCES

1. R. Echer, "Secondary Softening Regions of Copolymer, Mixed Polymers, and Graft Polymers," R. Chem. and Tech., Vol. 30, No. 1, pp. 200-214, 1957
2. J. D. Ferry, Viscoelastic Properties of Polymers. John Wiley and Sons, 1961
3. T. P. Yin and R. Pariser, "Dynamic Mechanical Properties of Several Elastomers and Their Potentialities in Vibration Control Applications," J. Appl. Polymer Sci., Vol. 8, pp. 2427-2443, 1964
4. L. E. Nielsen, Mechanical Properties of Polymers. Reinhold Publishing Corp., 1962
5. D. D. Dunnon and H. K. deDecker, "Versatile Materials for Vibration," Rubber Age, p. 89, Nov. 1965
6. R. J. Cersa, Block and Graft Copolymers. Butterworths, 1962
7. W. J. Burlant and A. S. Hoffman, Block and Graft Polymers. Reinhold Publishing Corp., 1960
8. H. Oberst, "Akustische Messmethoden in Kunstsoff Forshung Prufung und Entwicklung," Proc. 3rd Int. Cong. on Acoustics, reprinted and translated in Bruel and Kjaer Bulletin BB3930, 1959
9. W. P. Van Oort, "A Method For the Measurement of Dynamic Mechanical Properties of Small Samples of Plastic Material," Microtecnic, Vol. 7, No. 5, p. 246, 1952
10. A. D. Nashif, "A New Method for Determining the Damping Properties of Viscoelastic Materials," Shock and Vibration Bull. No. 36, Pt. 4, 1967

DISCUSSION

Mr. Buonagurio (Applied Physics Lab.): What effect would reducing frequency to 10 to 20 cps have on those curves?

Mr. Owens: We tried that on another rubber formulation. As you reduce frequency, ordinarily the loss factor is reduced. As frequency is increased at a constant temperature, the same type of hump appears as was shown here for temperature since there is an inverse relationship between temperature and frequency.

Mr. Thompson (San Francisco Bay Naval Shipyard): What is the nitrile rubber you were using in the blends?

Mr. Owens: Nitrile rubber is commonly called Buna-N. It is a copolymer of acrylonitrile and butadiene. This particular one had greater than 50 percent acrylonitrile. The glass transition temperature of the Buna-N rubbers is a linear function of the acrylonitrile content.

Mr. Forkois (Naval Research Laboratory): Did you monitor the creep characteristics of these polymers? This is a very important consideration. You get into a lot of trouble if you do not consider it.

Mr. Owens: Any time you go through a glass transition temperature, all sorts of things happen. Creep is a bad feature. We have not run any creep tests on the blend, but we probably will. We have not completed the work on this system and want to do some more before we say it is perfected.

* * *

NEW METHOD FOR DETERMINING DAMPING PROPERTIES OF VISCOELASTIC MATERIALS

Ahid D. Nashif
University of Dayton
Dayton, Ohio

Many methods have been developed to measure damping properties of viscoelastic materials. Of these, the complex modulus apparatus developed by Oberst has been one of the most widely used. The generally adopted method of using this apparatus has been to excite the test specimen, comprising a metal cantilever beam with a layer of the viscoelastic material on one side only, by an harmonic force of fixed amplitude generated by a magnetic force transducer, and to measure the frequency response by another transducer. Damping measurements are then made at the resonant frequencies of the specimen by observing either the vibration decay or the half-power bandwidth of each peak, and the relevant material properties are deduced by complicated but well-established theory. However, most viscoelastic materials have higher thermal coefficients of expansion than most metals, so considerable bending of the specimen occurs during high- or low-temperature tests. This problem can be overcome by conducting the damping tests on symmetric specimens, in which the viscoelastic material is coated in equal thicknesses on both sides. This method greatly simplifies the theory from which the viscoelastic material properties are deduced. This theory of symmetric specimens is derived using a simpler approach than has hitherto appeared in the literature, and the formulas by which the damping properties of the viscoelastic material are deduced from experiments on the composite specimen are also presented in a simple form, thereby reducing testing effort.

The simplified equations lead readily to a study of the effect of experimental errors on the measured viscoelastic material properties. For certain combinations of specimen dimensions and environmental conditions, an error magnification phenomenon of serious proportions occurs. Knowledge of the error magnifications, and the circumstances under which they occur, enables one to judge the reliability of the test results and to select appropriate specimen dimensions to minimize the effect of experimental error. Experiments with symmetric and unsymmetric specimens show that agreement between the measured properties is good, except in areas where error magnification is large.

A. D. Nashif

INTRODUCTION

The use of viscoelastic materials in the reduction of vibration problems in structural members and systems has been the subject of many investigations. For a proper understanding of the application of viscoelastic materials to specific vibration problems, the physical properties, and particularly the damping properties, of the materials under consideration must be determined over a wide range of frequencies and temperatures. Many methods have been developed to measure the damping properties of viscoelastic materials. Of these, the complex modulus apparatus developed by Oberst [1] has been one of the most widely used. Oberst's method involves the excitation of a test specimen, comprising a composite cantilever beam of metal and viscoelastic material, by an harmonic force of fixed amplitude generated by a magnetic force transducer, and the measurement of frequency response by another

transducer. The damping measurements are made at the resonant frequencies of the specimen by observing either the vibration decay or the half-power bandwidth of each peak. It has been the general practice to test specimens consisting of a metal cantilever coated on one side only with a layer of the viscoelastic material under investigation. The damping properties of the viscoelastic material are then calculated from the measurements made on the composite specimen using a well-established but complicated theory [1]. Since most viscoelastic materials have a high thermal coefficient of expansion compared with most metals, considerable bending occurs in the test specimen during high- or low-temperature tests. This difficulty can be avoided by conducting the damping tests on symmetric specimens with the viscoelastic material applied in equal thicknesses on both sides. Van Oort [2] has developed a method for measuring the damping properties of viscoelastic materials from tests conducted on symmetric specimens. However, the theory described by Van Oort is complicated, and a simpler formulation is needed.

This paper describes a simplified approach to the problem of measuring the damping properties of viscoelastic materials using symmetric specimens in the Oberst apparatus. It is shown that the procedure for determining the loss factor and Young's modulus of the viscoelastic material is far simpler than that for specimens coated on only one side. Experiments are described which demonstrate good agreement between measurements taken on both types of specimen, thereby demonstrating the accuracy of the new technique.

Finally, experimental errors and their effect on the calculated values of the damping properties of the viscoelastic materials are discussed. The simplicity of the theory for symmetric specimens allows one to demonstrate readily the existence of an intrinsic error magnification phenomenon inherent in the equations, which was not at all apparent for the far more complicated theory of the specimens coated on one side. It is shown that there are certain well-defined combinations of specimen configurations and environments which, if not rejected as unreliable on the grounds of excessive magnification of possible experimental errors, would lead to serious error in the test results obtained from the Oberst apparatus.

LIST OF SYMBOLS

A Function of h_2/h_1, Eq. (25)

b Breadth of cantilever beam, in.

exp Exponential function

e_a Error in calculated value of E_2

e_b Error in calculated value of η_2

E_1 Young's modulus of metal beam, psi

E_2 Real part of Young's modulus of viscoelastic material, psi

EI Effective flexural rigidity of composite beam, psi

E_2' Calculated value of E_2 based on erroneous value of ω_n/ω_{1n}, psi

h_1 Total thickness of metal part of cantilever beam, in.

h_2 Thickness of single layer of viscoelastic material on composite beam, in.

i $\sqrt{-1}$

I_1 Second moment of area of metal beam section about neutral axis, in.^{4}

I_2 Second moment of area of viscoelastic material on beam about neutral axis, in.^{4}

k Function of h_2/h_1, Eq. (11)

L Length of beam, in.

M_a, M_b Error magnification factors

$P(x)$ Applied transverse loading, lb/in.

t Time, sec

$W(x)$ Amplitude of transverse vibration of beam, in.

x Station along beam, in.

X $(\omega_n/\omega_{1n})^2$ or $(f_n/f_{1n})^2$, in.

Y $1 + 2h_2\rho_2/h_1\rho_1$

η Effective loss factor of composite beam

η_n Loss factor of viscoelastic material

η_2' Calculated value of η_2 based on inaccurate values of ω_n/ω_{1n} and η

μ Mass per unit length of composite beam, slug/in.

μ_1 Mass per unit length of bare metal beam, slug/in.

ξ_n Eigenvalue corresponding to nth normal mode of cantilever beam

ρ_1 Density of metal, slug/in.

ρ_2 Density of viscoelastic material, slug/in.

ω Circular frequency, $2\pi f$, rad/sec

ω_n Natural frequency of nth normal mode of composite beam, $2\pi f_n$, rad/sec

ω_{1n} Natural frequency of nth mode of metal beam, $2\pi f_{1n}$, rad/sec

THEORETICAL ANALYSIS

Determination of Material Properties

Consider a metal beam with a viscoelastic layer attached in equal thicknesses to each of its surfaces, as in Fig. 1. If a transverse loading $P(x)\exp(i\omega t)$ is applied to the beam, the equation of motion for the transverse displacement $W(x)\exp(i\omega t)$ is

$$[E_2(1+i\eta_2)I_2 + E_1I_1](d^4W/dx^4) - \mu\omega^2 W = P(x) . \quad (1)$$

where μ is the mass per unit length of the composite beam, I_1 is the second moment of area of the metal beam cross section about the neutral axis (the centerline in the case of symmetric specimens), I_2 is the second moment of area of the viscoelastic material about the neutral axis, E_1 is Young's modulus of the metal, E_2 is the real part of the complex Young's modulus of the viscoelastic material, and η_2 is the loss factor of the viscoelastic material. The loss factor η_1 of the metal beam is assumed to be negligible and will be ignored. Equation (1) may be rewritten in the form:

$$(E_2I_2 + E_1I_1)[1 + i\eta_2 E_2I_2/(E_2I_2 + E_1I_1)](d^4W/dx^4) - \mu\omega^2 W = P(x) . \quad (2)$$

If, however, we define an effective flexural rigidity EI and an effective loss factor η for the composite beam, then the equation of motion may also be written:

$$EI(1+i\eta)(d^4W/dx^4) - \mu\omega^2 W = P(x) . \quad (3)$$

Comparing Eqs. (2) and (3), term for term, we have

$$E_2I_2/E_1I_1 = (EI/E_1I_1) - 1 \quad (4)$$

and

$$\eta_2 = \eta[1 + (E_1I_1/E_2I_2)] . \quad (5)$$

But, for any given mode n the measured resonant frequencies of the composite beam (ω_n) and of the uncoated metal beam (ω_{1n}) are given by

$$\mu\omega_n^2 L^4/EI = \mu_1\omega_{1n}^2 L^4/E_1I_1 = \xi_n^4 ,$$

where ξ_n is the eigenvalue corresponding to the nth mode and is a constant. Therefore,

$$EI/E_1I_1 = (\omega_n/\omega_{1n})^2(\mu/\mu_1) . \quad (6)$$

Putting Eq. (6) into Eq. (4) yields:

$$E_2I_2/E_1I_1 = (\omega_n/\omega_{1n})^2(\mu/\mu_1) - 1 . \quad (7)$$

To determine E_2 and η_2 from the experimentally measured values of η and ω_n/ω_{1n}, it is now necessary to solve for the stiffness ratio E_2I_2/E_1I_1 in terms of the thickness ratio h_2/h_1, where h_1 is the thickness of the metal cantilever and h_2 is the thickness of one layer of the viscoelastic material. The second moment of area about the neutral axis of the viscoelastic material is

$$I_2 = 2[bh_2^3/12 + bh_2(h_1+h_2)^2/4] , \quad (8)$$

and of the metal beam is

$$I_1 = bh_1^3/12 . \quad (9)$$

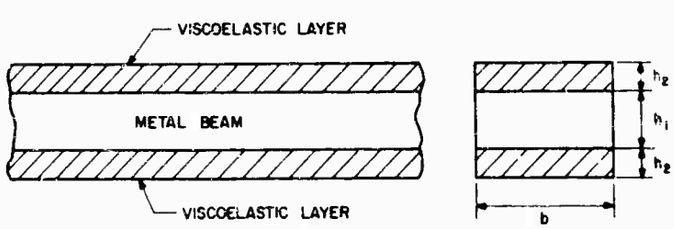

Fig. 1 - Sketch of metal beam with viscoelastic layers coated on both sides

The stiffness ratio E_2I_2/E_1I_1 may, therefore, be written in the form

$$E_2I_2/E_1I_1 = k(E_2/E_1) , \qquad (10)$$

where

$$k = 8(h_2/h_1)^3 + 12(h_2/h_1)^2 + 6(h_2/h_1) . \qquad (11)$$

The nondimensional parameter k is plotted as a function of h_2/h_1 in Fig. 2. Young's modulus for the viscoelastic material is now obtained from Eqs. (7) and (10):

$$E_2 = (E_1/k)\left[(\omega_n/\omega_{1n})^2(\mu/\mu_1) - 1\right] \qquad (12)$$

or

$$E_2 = (E_1/k)\left[(\omega_n/\omega_{1n})^2(1 + 2h_2\rho_2/h_1\rho_1) - 1\right] , \qquad (13)$$

where ρ_1 is the density of the metal and ρ_2 is the density of the viscoelastic material. The loss factor of the viscoelastic material is seen, from Eqs. (5) and (10), to be

$$\eta_2 = \eta(1 + E_1/kE_2) . \qquad (14)$$

Analysis of Error

Equations (12) and (14) represent equations for the Young's modulus and loss factor, respectively, of the viscoelastic material. To obtain these two quantities, it is necessary to determine from experiments on the metal and composite beams the frequency ratio ω_n/ω_{1n} and the composite loss factor η at several resonant frequencies. These experimental measurements are the main sources of error. Therefore, the effect of such errors on the final calculated values of the Young's modulus and loss factor must be determined.

Let the error in measuring the frequency ratio ω_n/ω_{1n} be Δ_a and that in measuring the composite loss factor η be Δ_b. Therefore, the calculated Young's modulus E_2' and loss factor η_2', corresponding to the erroneous frequency ratio $(\omega_n/\omega_{1n}) + \Delta_a$ and the erroneous composite loss factor $\eta + \Delta_b$, become, from Eqs. (12) and (14),

$$E_2' = (E_1/k)\ \{[(\omega_n/\omega_{1n}) + \Delta_a]^2\ (\mu/\mu_1) - 1\} \qquad (15)$$

and

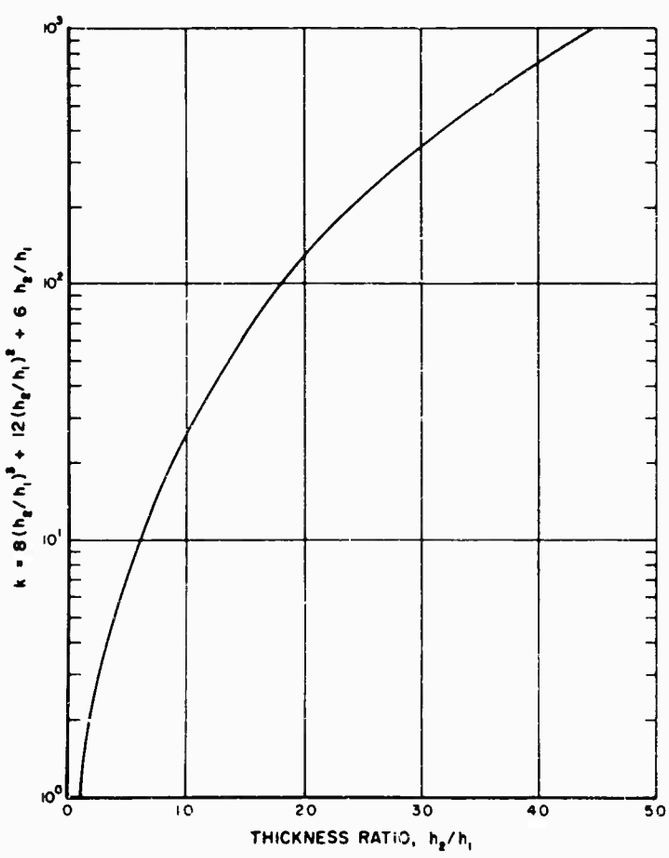

Fig. 2 - Parameter k vs thickness ratio h_2/h_1

$$\eta_2' = (\eta + \Delta_b)(1 + E_1/kE_2') . \quad (16)$$

The errors in the calculated values of the modulus and loss factor are now defined as

$$e_a = (E_2' - E_2)/E_2 \quad (17)$$

and

$$e_b = (\eta_2' - \eta_2)/\eta_2 . \quad (18)$$

By substituting Eqs. (12), (14), (15) and (16) into Eqs. (17) and (18) and assuming that the errors are small, so that Δ_a^2 and $\Delta_a \times \Delta_b$ are negligible, one may show that Eqs. (17) and (18) give

$$e_a = M_a \Delta_a \quad (19)$$

and

$$e_b = \Delta_b/\eta - M_b \Delta_a . \quad (20)$$

where

$$M_a = 2(\omega_n/\omega_{1n})(\mu/\mu_1)/[(\omega_n/\omega_{1n})^2(\mu/\mu_1) - 1] \quad (21)$$

and

$$M_b = 2/(\omega_n/\omega_{1n})\,[(\omega_n/\omega_{1n})^2(\mu/\mu_1) - 1] . \quad (22)$$

The error magnification factors M_a and M_b are plotted in Figs. 3 and 4, respectively, as functions of ω_n/ω_{1n} for several values of μ/μ_1. It can be seen that M_a and M_b are always small except when $(\omega_n/\omega_{1n})^2$ times (μ/μ_1) is of the order of unity. It is seen that errors in the observed quantities ω_n/ω_{1n} and η are magnified in the calculated values of E_2 and η_2 and that, under the specific condition that $(\omega_n/\omega_{1n})^2(\mu/\mu_1)$ approaches unity, these errors may become prohibitively great. The effect of these error magnification factors on experimental data are discussed in more detail in a later section.

EXPERIMENTAL INVESTIGATION

To demonstrate the effectiveness of the new damping measurement technique, the damping properties of a typical viscoelastic material

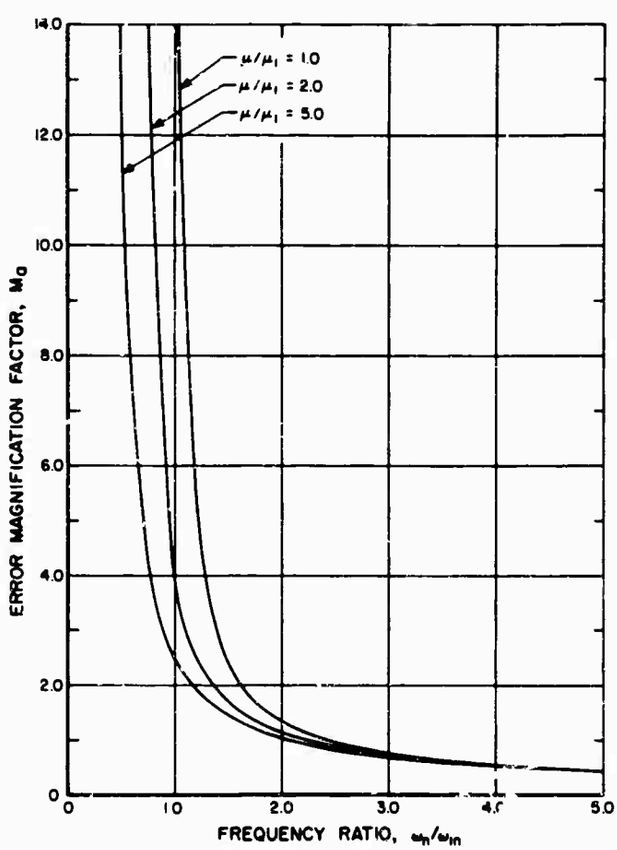

Fig. 3 - Error magnification factor M_a vs frequency ratio ω_n/ω_{1n} for various mass ratios μ/μ_1

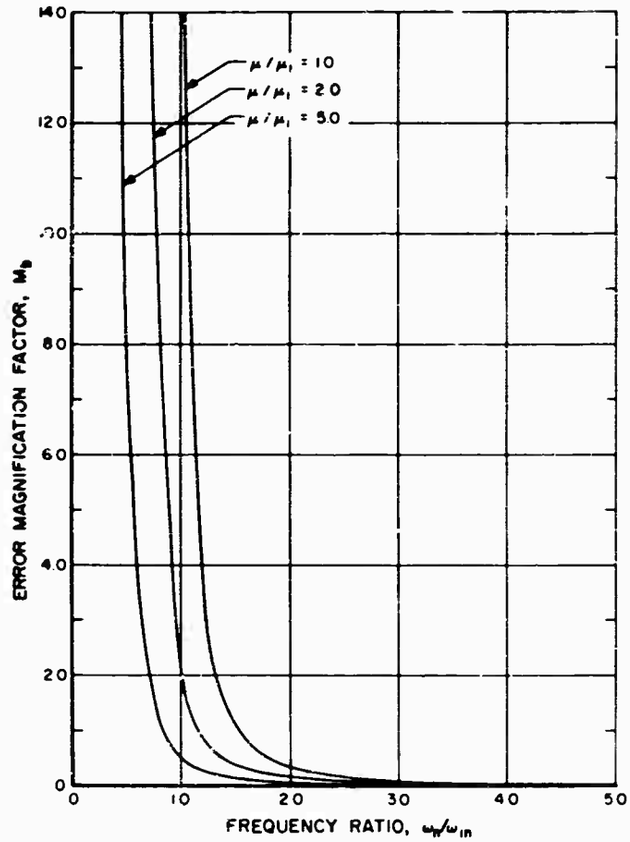

Fig. 4 - Error magnification factor M_b vs frequency ratio ω_n/ω_{1n} for various mass ratios μ/μ_1

were evaluated using both singly and symmetrically coated specimens.

The material used for this investigation was a viscoelastic material known as LD-400 (Lord Manufacturing Co., Erie, Pa.). Two damped specimens were made, as shown in Fig. 5, with LD-400 coated on both sides of one specimen and on one side of the other. Identical undamped metal beams were used, as shown in the same figure. The brass end sections were used to insure that the viscoelastic material was effectively bonded at the clamped ends when the specimen was clamped around these sections. Eastman 910 adhesive was used to hold the viscoelastic material to the metal surfaces.

The complex modulus apparatus used in the investigation consisted of a mounting fixture with two magnetic transducers, an oscillator, an amplifier and a recorder. These elements were assembled as shown in the block diagram in Fig. 6.

For test purposes, the specimen was clamped in the mounting fixture and a harmonic force of constant amplitude was applied to the driving transducer by the oscillator. The output signal was sensed by the pickup transducer and then plotted on the recorder after being amplified. A frequency response spectrum such as that in Fig. 7 was obtained in this manner for each specimen at various temperatures. The frequencies at which each of the modes of vibration occurred were measured for each specimen and the loss factor η in each mode was measured by the half-power bandwidth method. After the various resonant frequencies and loss factors for each of the damped specimens were obtained, the damping properties of LD-400 were calculated. For the symmetric specimen, Eqs. (13) and (14) were used to determine Young's modulus and loss factor, respectively. A sample data sheet for tests on a symmetric specimen at a single temperature is shown in Table 1. For the specimen with the viscoelastic material on one side only, the following formulas [1] were used:

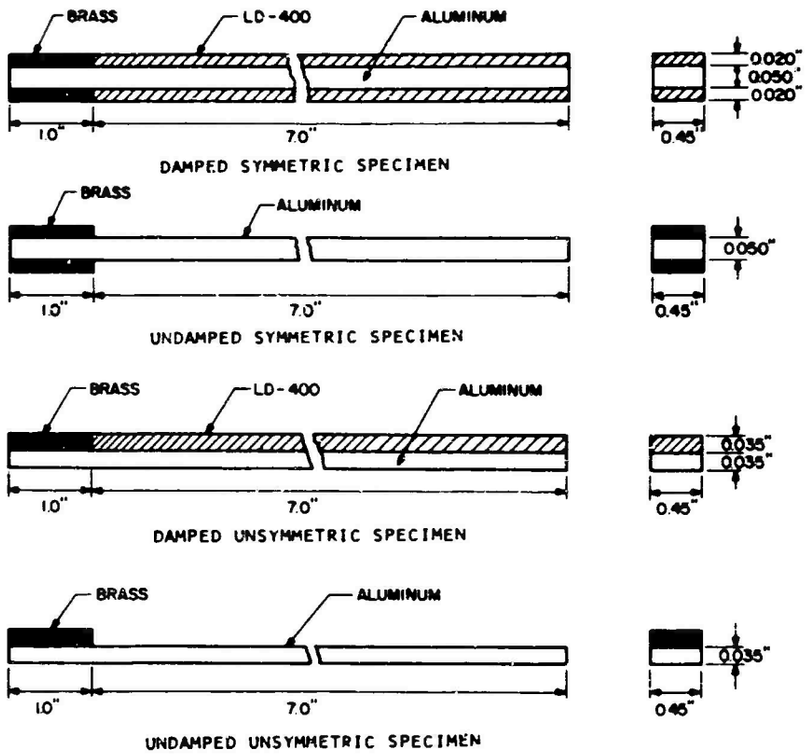

Fig. 5 - Symmetric and unsymmetric test specimens

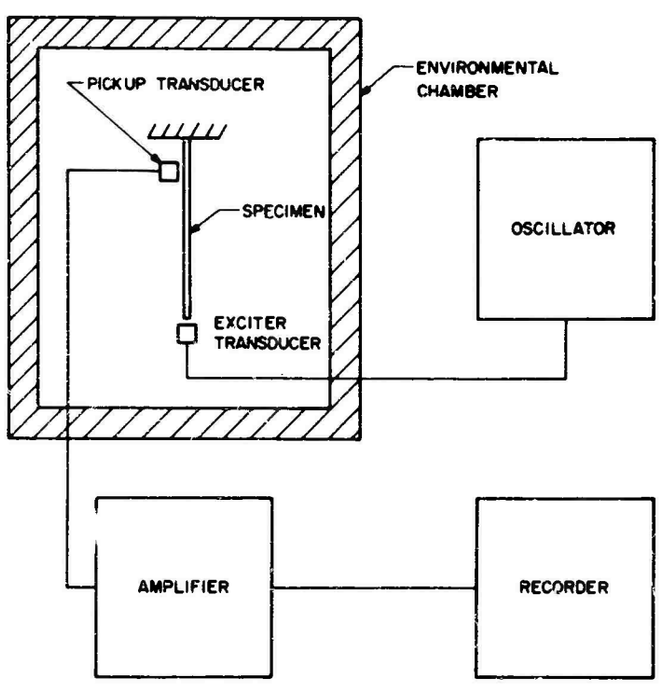

Fig. 6 - Block diagram of experimental setup

TABLE I
Data Reduction Sheet for Damping Measurements on Symmetric Cantilever Beam Specimens

MATERIAL: LD-400			TEMPERATURE: 40°F		
DATE: 12 May 1966			SIGNATURE:		
	1	2	3	4	5
f_n, cps	40.6	274.3	778.7	1536.5	2560.1
f_{1n}, cps	30.4	201.4	561.0	1095.5	1804.0
$X = (f_n/f_{1n})$	1.785	1.855	1.927	1.968	2.014
$Y = 1 + (2h_2\rho_2/h_1\rho_1)$	1.44	1.44	1.44	1.44	1.44
$XY - 1$	1.570	1.671	1.775	1.834	1.900
$E_1/k(\times 10^{-6})$, psi	2.222	2.222	2.222	2.222	2.222
E_2 $(\times 10^{-6})$, psi	3.49	3.71	3.94	4.08	4.22
$Z = E_1/kE_2 = (XY - 1)^{-1}$	0.637	0.598	0.563	0.545	0.526
$1 + Z$	1.637	1.598	1.563	1.545	1.526
η (measured)	0.091	0.059	0.067	0.062	0.056
$\eta_2 = (1 + Z)\eta$	0.149	0.094	0.105	0.096	0.086
$M_a = 2X^{1/2}Y/(XY - 1)$	2.44	2.35	2.26	2.20	2.15
$M_b = 2/X^{1/2}(XY - 1)$	0.96	0.88	0.82	0.78	0.74

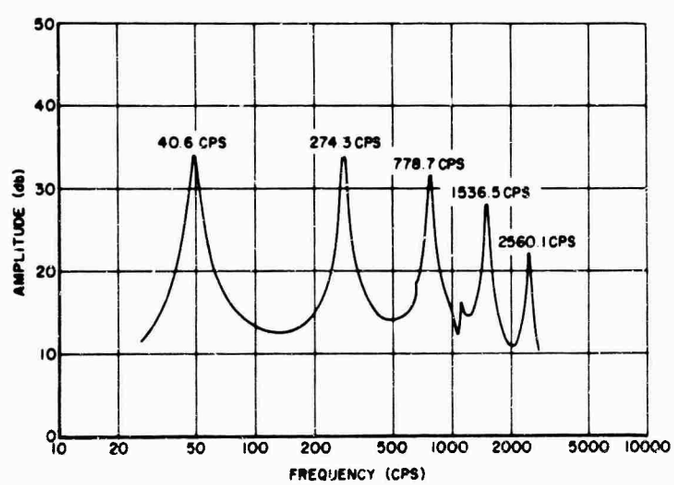

Fig. 7 - Typical frequency response spectrum of damped symmetric specimen

$$(\omega_n/\omega_{1n})^2(1 + h_2\rho_2/h_1\rho_1)$$

$$= \frac{1 + (E_2/E_1)(h_2/h_1)A + (E_2/E_1)^2(h_2/h_1)^4}{1 + (E_2/E_1)(h_2/h_1)} \quad (23)$$

and

$$\eta/\eta_2 = \{(E_2/E_1)(h_2/h_1)\ [2A + 2(E_2/E_1)(h_2/h_1)^3 + (E_2/E_1)^2(h_2/h_1)^4 - 1]\} \Big/ \{1 + (E_2/E_1)(h_2/h_1)\ [1 + 2A(E_2/E_1)(h_2/h_1) + (E_2/E_1)^2(h_2/h_1)^4]\}\ . \quad (24)$$

where

$$A = 2 + 3(h_2/h_1) + 2(h_2/h_1)^2\ . \quad (25)$$

RESULTS AND DISCUSSION

The experimental results are presented in Figs. 8 and 9, which represent graphs of Young's modulus and loss factor, respectively, plotted as functions of frequency at 40°F, 60°F, 90°F and 110°F for the two types of specimen. It can be seen from Fig. 8 that the measured Young's moduli agree well at 40°F and 60°F. The agreement is not as good at the other temperatures because the frequency ratio ω_n/ω_{1n} becomes smaller as the temperature increases and the viscoelastic material becomes softer, and the error magnification factor M_a becomes very large. The error magnification factor was calculated from Eq. (19) for the symmetric specimens and was found to be between 2 and 5 at the low temperatures and greater than 10 at the high temperatures. Therefore, the error in measuring Young's modulus at 40°F and 60°F is small compared with that at 90°F and 110°F. The same behavior can be expected for the results obtained with the sample coated on only one side, since it had the same stiffness ratio EI/E_1I_1 as did the symmetric specimens. However, because of the complexity of Eq. (23), the error magnification factors cannot be so readily demonstrated. It is suggested by Oberst and Frankenfeld [1] that the stiffness ratio EI/E_1I_1 should be greater than 1.1 for accurate results. Equation (6) indicates that this implies that $(\omega_n/\omega_{1n})^2(\mu/\mu_1) - 1 < 0.1$, and this is very much the same criterion as that to which the error magnification factor M_a leads. On this basis, therefore, the results obtained for the specimens coated on one side are unreliable for the two higher temperatures.

The effect of the experimental errors on the loss factor vs frequency data presented in Fig. 9 can also be seen. Equation (20) shows that there are now two sources of error in the estimates of the viscoelastic material loss factor, namely the measured frequency ratio ω_n/ω_{1n} and the composite loss factor η. However, the error in measuring η was found to be very small in several repeated tests of several specimens, so that Δ_b/η is small in comparison with $M_b\Delta_a$. The error magnification factor M_b was calculated from Eq. (22) and is always less than M_a. Again, no accurate method was available for estimating the effect of experimental errors for the specimen coated on one side only, apart from the criterion $EI/E_1I_1 < 1.1$. Again, therefore, all results at 90°F and 110°F were unreliable for the particular specimens used. The thickness ratio of the viscoelastic material to the metal beam thickness was chosen in such a way as to demonstrate readily the effect of the experimental errors on the calculated values of Young's modulus and loss factor of the viscoelastic material. To avoid the inaccuracy found in the high-temperature tests, one could use Figs. 3 and 4 as a guide for selecting appropriate thickness ratios. In this way, the error magnification factors can be minimized.

Finally, several tests were carried out at high and low temperatures for several different viscoelastic materials on symmetric specimens, and no noticeable bending of the specimens was observed at any time. However, prestresses were inevitably set up. Tests on several specimens, cured at room temperature and at about 280°F, showed no noticeable differences in the values of the viscoelastic properties measured. The effect of prestress was not important in these tests, therefore, but one should verify this from time to time during an investigation of any specific material.

CONCLUSIONS

A new method has been described for determining the damping properties of viscoelastic materials from vibration tests carried out on symmetric beam specimens. This method demonstrates a simplified procedure for measuring the loss factor and Young's modulus of viscoelastic materials. With this method, the problem of bending of the test specimens, which usually occurs at high and low temperatures when the specimen is coated on only one side with the viscoelastic material, is avoided. Experimental errors and their effect on the calculated properties of viscoelastic materials were established as functions of derived error magnification factors. These error magnification factors are shown to be useful for judging the reliability of the test results and for selecting the appropriate specimen dimensions to minimize the effects of experimental error.

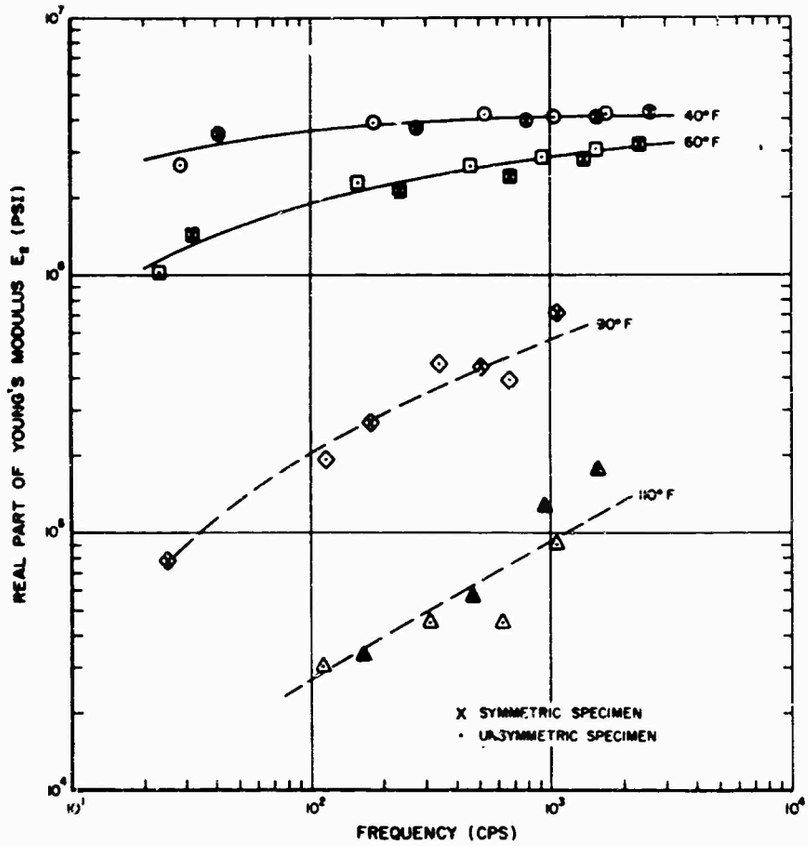

Fig. 8 - Real part of Young's modulus vs frequency for various temperatures

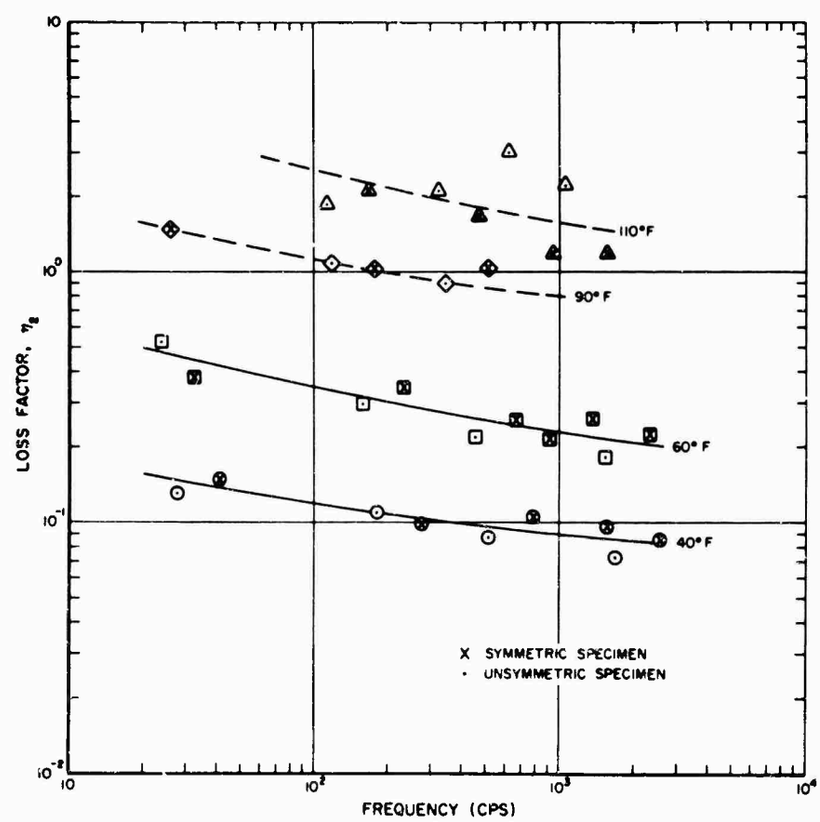

Fig. 9 - Loss factor vs frequency for various temperatures

ACKNOWLEDGMENTS

The author wishes to thank D. I. G. Jones of the Air Force Materials Laboratory for his continued guidance and interest in this investigation, C. M. Cannon of the University of Dayton for his assistance with the experimental work, H. A. DeMarey of the University of Dayton for his help in preparing the figures, and the Lord Manufacturing Company for providing the viscoelastic material.

The investigation was sponsored by the Air Force Materials Laboratory, and the experimental program was carried out on equipment purchased using the Director's Fund of the Laboratory.

REFERENCES

1. H. Oberst and K. Frankenfeld, "Über die Dämpfung der Biegeschwingungen dünner Bleche durch festhaltende Beläge," Acustica, Vol. 2, Leaflet 4, AB 181-194, part 1, 1952; Vol. 4, part 2, p. 433, 1954

2. W. P. Van Oort, "A Method for the Measurement of Dynamic Mechanical Properties of Small Samples of Plastic Materials," Microteknic, Vol. 7, No. 5, p. 246, 1952

DISCUSSION

Dr. Plunkett (University of Minnesota): You assume that damping is due to the tensile modulus rather than the shear modulus. I would assume most of the damping would be due to shear effects in the layers which should be greatly influenced by the ratio of layer thickness to beam thickness.

Mr. Nashif: This problem was investigated at the Air Force Material Laboratory by Dr. Nichols, who found that these assumptions are true as long as the modulus is over 1000 psi and the ratio of viscoelastic material thickness to metal thickness is no larger than 8 to 1.

Dr. Plunkett: Do you mean the viscoelastic layer is thicker than the metal?

Mr. Nashif: Yes.

* * *

EFFECT OF TUNED VISCOELASTIC DAMPERS ON RESPONSE OF MULTI-SPAN STRUCTURES

David I. G. Jones and George H. Bruns
Air Force Materials Laboratory
Wright-Patterson Air Force Base, Ohio

Many complex structures exhibit multi-modal response within certain frequency bands, and the excitation from jet engine, rocket engine or boundary layer sources often leads to early failure or equipment malfunction. Under such conditions, severe vibrational amplitudes often occur near the centers of panels in critical areas. A possible method is presented of reducing this type of problem in complex structures by tuned viscoelastic dampers, an approach which has been generally considered to be limited to single frequency vibrations. It has been shown that using viscoelastic materials with high loss factors in tuned dampers enables energy dissipation over a wide band of frequencies. Therefore, tuned dampers could conceivably be used successfully to damp multi-modal vibrations in typical aerospace structures.

The preliminary investigations reported are concerned with the response of a multi-span beam with tuned dampers distributed uniformly along its length. This idealization of the more practical case of isolated dampers at the center of each span is shown to lead to a simple, easily solved equation of motion. Expressions for the response of the beam, both with distributed tuned damping and with homogeneous viscoelastic damping, are obtained and numerical solutions are discussed for a 9-span pinned beam under uniform harmonic loading. Effective loss factors are defined for the beam-damper system, and the effects of systematic variations of damper loss factor and damper mass on the effective loss factor are discussed. It is shown that substantial amounts of damping can be introduced.

Finally, some preliminary experiments on a skin-stringer-frame structure are described. It is shown that response amplitudes can be reduced considerably, with very moderate weight additions, by proper use of tuned viscoelastic dampers.

G. H. Bruns

LIST OF SYMBOLS

exp Exponential function

E Young's modulus of beam material, psi

F Force transmitted back to structure by tuned damper, lb

i $\sqrt{-1}$

I Second moment of area of beam cross section about neutral axis (in.^{4})

j Span number, counting from left-hand side

k Real part of stiffness of tuned damper spring, lb/in.

ℓ Length of beam occupied by individual tuned damper, in.

L Total length of span, in.

m Mass of tuned damper or number of modal group, slug

n Number of mode in mth group

N Number of spans in beam

$P(x)$ Amplitude of applied loading on beam, lb/in.

P Amplitude of applied uniform loading on beam, lb/in.

P_{mn} Coefficient in generalized Fourier expansion of $P(x)$

Q Amplitude amplification factor at resonance

t Time, sec

w Instantaneous transverse displacement of beam relative to fixed point in space, in.

$W(x)$ Amplitude of w, in.

x Station along beam measured from extreme left-hand support, in.

x_j Station of center of jth span, in.

y Instantaneous displacement of mass m of tuned damper relative to fixed point in space, in.

η Loss factor of viscoelastic material of tuned damper spring or of homogeneous viscoelastic beam

η_s Effective loss factor of beam-damper system

λ $kL^4/\ell EI$, stiffness parameter

μ Mass per unit length of beam, slug/cu in.

ξ^4 $\mu\omega^2L^4/EI$, frequency parameter

ξ_{1n}^4 $\mu\omega_{1n}^2L^4/EI$

ϕ_{mn} nth normal mode in the mth modal group

ψ $m/\mu\ell$, mass parameter

ω Circular frequency, rad/sec

ω_{mn} nth natural frequency in mth modal group, rad/sec

ω_D $(k/m)^{1/2}$, natural frequency of tuned damper, rad/sec

INTRODUCTION

Tuned viscoelastic dampers have often been considered for the reduction of vibrations in one-degree-of-freedom mechanical systems [1,2] and in simple structures [3-5] for which the resonant frequencies are well separated. Little thought has been given, however, to the possibility of utilizing high loss factor viscoelastic materials to increase the useful frequency bandwidth of such dampers so as effectively to damp several modes of vibration of a complex structure. Some preliminary investigations [6] have shown that tuned dampers can be made effective over at least an octave band of frequencies and that, for a class of complex structures typical of many aerospace configurations, the modes of greatest interest often fall within an octave band.

The present investigation has been limited to an analysis of a simple multi-supported beam, representative in many ways of typical aerospace structures, with distributed tuned dampers, each far smaller than an individual span of the beam. The advantage of this idealization of the more practical situation, consisting of isolated dampers at the center of each span, is that the equation of motion is far more readily solved. The essential features of the more complex problem are retained, but the analysis is greatly simplified and some general conclusions can be reached far more readily.

It is shown that high damping can be introduced into a complex structure by proper use of tuned dampers with a sufficiently high loss factor, albeit far less than in the case of a simple structure exhibiting unimodal response. Finally, some preliminary experimental investigations on a multi-span structure with tuned dampers are described. These experiments verify that high damping can be introduced into complex structures by properly utilized tuned viscoelastic dampers.

THEORY

Theory of Multi-Span Beam with Distributed Tuned Dampers

Consider a tuned damper consisting of a mass m connected through a viscoelastic link of stiffness $k(1+i\eta)$ to a point of the beam, vibrating with amplitude $w(x,t) = W(x)\exp(i\omega t)$ as in Fig. 1. The equation of motion of the mass m is

$$m(d^2y/dt^2) + k(1+i\eta)(y-w) = 0 , \qquad (1)$$

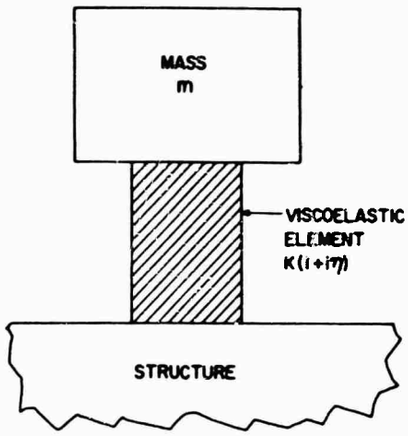

Fig. 1 - Idealized tuned viscoelastic damper

where y is the displacement of the mass from the equilibrium position. The solution of Eq. (1) is

$$y = \frac{\exp(i\omega t)}{1 - m\omega^2/k(1 + i\eta)} . \qquad (2)$$

The force F transmitted back to the beam is then readily shown to be

$$F = k(1 + i\eta)(w - y)$$

$$= \frac{-m\omega^2 w}{1 - m\omega^2/k(1 + i\eta)} . \qquad (3)$$

If the length of the N-span beam, illustrated in Fig. 2, occupied by each individual damper is $\ell(\ell \ll \text{span})$, the force per unit length acting on the beam is F/ℓ and the modified Euler-Bernoulli equation of the damped beam is readily obtained simply by adding the term F/ℓ into the equation for the undamped beam. The equation of motion of the beam for harmonic excitation by loading $P(x)\exp(i\omega t)$, therefore, becomes

$$EI(d^4W/dx^4) - \mu\omega^2 W - \frac{(m/\ell)\,\omega^2 W}{1 - m\omega^2/k(1 + i\eta)} = P(x) , \qquad (4)$$

where E is Young's modulus of the beam and I is the second moment of area of the beam section about the neutral axis.

For the undamped N-span structure, with fairly rigid supports at the ends of the spans, the response consists of a series of groups of modes [7], each with N modes, as illustrated in Figs. 3 and 4. We may, therefore, expand W as a series of these modes, assumed to be known, as follows:

$$W = \sum_{m=1}^{\infty} \sum_{n=1}^{N} W_{mn}\,\phi_{mn}(x/L)$$

$$= \sum_{n=1}^{N} W_{1n}\,\phi_{1n}(x/L) + \sum_{n=1}^{N} W_{2n}\,\phi_{2n}(x/L) + \ldots , \qquad (5)$$

where n refers to the number of the mode in the mth group. The functions ϕ_{mn} are the normal modes or eigenfunctions of the system. The frequency ω_{mn} corresponding to the mnth mode generally satisfies the inequality:

$$\omega_{1n}^2 \ll \omega_{mn}^2 \qquad (6)$$

for $m > 1$, as seen in Fig. 3. The mode ϕ_{mn} satisfies the equation of motion for undamped free vibrations:

$$d^4\phi_{mn}(x/L)/dx^4 - (\mu\omega_{mn}^2/EI)\,\phi_{mn}(x/L) = 0 . \qquad (7)$$

Substituting Eq. (5) back into Eq. (3) and using Eq. (7), we have

$$\sum_{m=1}^{\infty} \sum_{n=1}^{N} \left[\mu\omega_{mn}^2 - \mu\omega^2 - \frac{(m/\ell)\omega^2}{1 - m\omega^2/k(1 + i\eta)}\right] W_{mn}\,\phi_{mn}(x/L)$$

$$= \sum_{m=1}^{\infty} \sum_{n=1}^{N} P_{mn}\,\phi_{mn}(x/L) , \qquad (8)$$

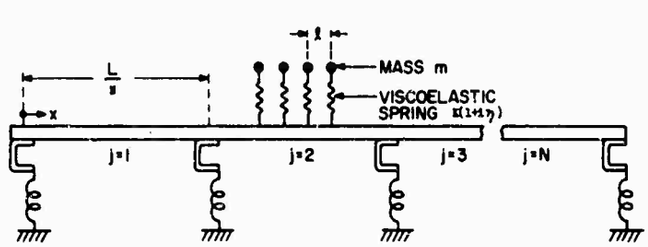

Fig. 2 - Sketch of multi-span beam with distributed tuned dampers

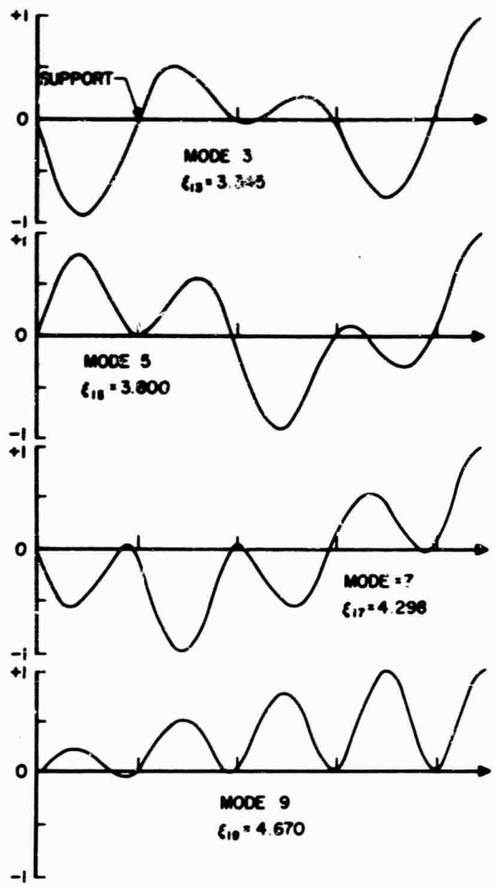

Fig. 3 - Mode shapes for 9-span pinned beam

where

$$P(x) = \sum_{m=1}^{\infty} \sum_{n=1}^{N} P_{mn}\, \phi_{mn}(x/L)$$

and

$$P_{mn} = \int_0^L P(x)\, \phi_{mn}(x/L)\, dx \Big/ \int_0^L \phi_{mn}^2(x/L)\, dx \qquad (9)$$

from the orthogonal property of the normal modes. Equating the mnth terms on the right- and left-hand sides of Eq. (8) gives

$$W_{mn} = \frac{P_{mn}}{\mu\omega_{mn}^2 - \mu\omega^2 - \dfrac{(m/\ell)\,\omega^2}{1 - m\omega^2/k(1 + i\eta)}} \cdot \qquad (10)$$

Therefore,

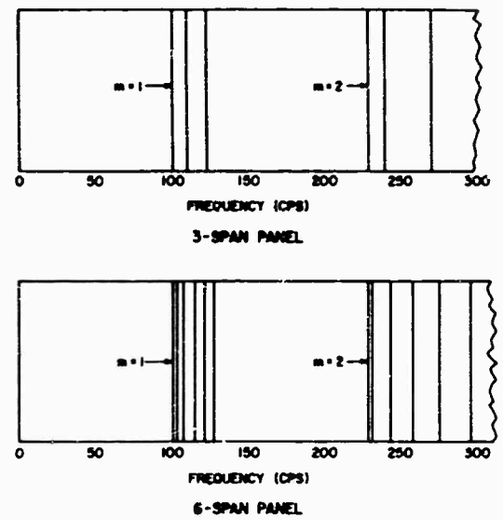

Fig. 4 - Typical frequency bands of response of multi-span structure

$$W = \sum_{m=1}^{\infty} \sum_{n=1}^{N} \frac{P_{mn}\, \phi_{mn}(x/L)}{\mu\omega_{mn}^2 - \mu\omega^2 - \dfrac{(m/\ell)\omega^2}{1 - m\omega^2/k(1 + i\eta)}} \cdot \qquad (11)$$

However, as stated earlier, $\omega_{mn}^2 >> \omega_{1n}^2$ and $P_{mn} << P_{1n}$ for $m > 1$ so that all terms for which $m \geq 2$ will not be significant in the equation for W, in the vicinity of the first group of modes $(m = 1)$. We may, therefore, write approximately

$$W = \sum_{n=1}^{N} \frac{P_{1n}\, \phi_{1n}(x/L)}{\mu\omega_{1n}^2 - \mu\omega^2 - \dfrac{(m/\ell)\omega^2}{1 - m\omega^2/k(1 + i\eta)}} \qquad (12)$$

and

$$\frac{EIW}{L^4} = \sum_{n=1}^{N} \frac{P_{1n}\, \phi_{1n}(x/L)}{\xi_{1n}^4 - \xi^4 - \psi\xi^4/[1 - \psi\xi^4/\lambda(1 + i\eta)]}, \qquad (13)$$

where

$$\xi^4 = \mu\omega^2 L^4/EI,$$

$$\xi_{1n}^4 = \mu\omega_{1n}^2 L^4/EI,$$

$$\psi = m/\mu\ell,$$

and

$$\lambda = kL^4/EI\ell.$$

At zero frequency, the response is

$$(EI/L^4)W = \sum_{n=1}^{N} P_{1n}\, \phi_{1n}(x/L)\, \xi_{1n}^{-4} . \qquad (14)$$

Furthermore the stiffness ratio λ may be expressed in terms of the mass ratio ψ, the first eigenvalue ξ_{11}, and the ratio ω_D/ω_{11} of the damper frequency ω_D to the first natural frequency ω_{11} of the beam. In fact,

$$\lambda = (k/m)(m/\mu\ell)(\mu L^4/EI)$$

$$= (\omega_D/\omega_{11})^2\, \psi \xi_{11}^4 , \qquad (15)$$

since $\omega_D^2 = k/m$. Finally, therefore,

$$\omega_D/\omega_{11} = (\lambda/\psi\xi_{11}^4)^{1/2} . \qquad (16)$$

Theory of Multi-Span Homogeneous Viscoelastic Beam

If the multi-span beam is made entirely of material of complex Young's modulus $E(1 + i\eta)$, where η is the loss factor, the equation of motion is

$$EI(1 + i\eta)(d^4W/dx^4) - \mu\omega^2 W = P(x) . \qquad (17)$$

If we make use of the expansions in normal modes given in Eqs. (5) and (9) in Eq. (17),

$$\sum_{m=1}^{\infty} \sum_{n=1}^{N} \left[\mu\omega_{mn}^2(1 + i\eta) - \mu\omega^2\right] W_{mn}\, \phi_{mn}(x/L)$$

$$= \sum_{m=1}^{\infty} \sum_{n=1}^{N} P_{mn}\, \phi_{mn}(x/L)$$

so that

$$W_{mn} = P_{mn}/\left[\mu\omega_{mn}^2(1 + i\eta) - \mu\omega^2\right] , \qquad (18)$$

and, therefore,

$$W = \sum_{m=1}^{\infty} \sum_{n=1}^{N} \frac{P_{mn}\, \phi_{mn}(x/L)}{\mu\omega_{m,n}^2(1 + i\eta) - \mu\omega^2} . \qquad (19)$$

If we make use, once more, of the fact that $\omega_{mn}^2 >> \omega_{1n}^2$ and $P_{mn} << P_{1n}$, only the first group of modes need be considered, and

$$\frac{EIW}{L^4} = \sum_{n=1}^{N} \frac{P_{1n}\, \phi_{1n}(x/L)}{\xi_{1n}^4(1 + i\eta) - \xi^4} \qquad (20)$$

and, at zero frequency,

$$\frac{EIW}{L^4} = (1 + i\eta)^{-1} \sum_{n=1}^{N} P_{1n}\, \phi_{1n}(x/L)\, \xi_{1n}^{-4} . \qquad (21)$$

DISCUSSION OF SOLUTIONS

It has been shown that the predominant features of the vibrational response of a complex multi-span beam system with tuned dampers can be determined by considering a greatly simplified model in which the tuned dampers are distributed evenly over the beam instead of being concentrated at isolated points. The equation of motion then takes on the greatly simplified form shown in Eq. (4). If the normal modes and natural frequencies of the undamped beam are known [8-10], it is then possible to expand the displacement W at any point of the beam and the loading $P(x)$ in terms of these modal functions and obtain formal solutions such as those given in Eqs. (10) and (13). From Eq. (13), response spectra in the form of graphs of $(EI/L^4)|W|$ against the frequency parameter ξ (or ξ^2) can be evaluated for any chosen values of ψ, λ, η and x/L and any chosen loading $P(x)$. In preliminary calculations on a 9-span pinned beam, $P(x)$ was taken to be a uniform loading P and graphs of $(EI/PL^4)|W|$ against ξ^2, similar to the examples shown in Figs. 5 and 6, have been computed for η = 0.1, 0.2, 0.5, 1.0, 1.5 and 2.0; ψ = 0.1, 0.2, 0.4 and 0.8; λ between 0 and 100; and values of x/L corresponding to the center points x_j/L of the spans $j = 1$ to $j = 5$ only, since the response is symmetric about the center span in this case. Some of the values used in the calculations are given in Tables 1 and 2.

It is not a difficult matter to determine the transmissibility spectra for a system such as this. Interpretation of the spectra, however, is not so simple. In fact, the most that one can do, in the sense of defining a gross measure of the damping introduced by the tuned dampers, is plot a graph of the resonant amplification factor Q against the stiffness parameter λ for various values of the damper loss factor η, the mass ratio ψ and the station x/L. In this particular instance, the spectra contain only two predominant resonance peaks. One of them is at low frequency, corresponding to the stringer torsion mode, and the other is at high frequency, corresponding to the stringer bending mode. The intermediate modes appear to be relatively insignificant in this particular configuration. The graphs of Q against λ for the predominant low- and high-frequency modes have been plotted (Figs. 7-9) for η = 0.1, 0.2, 0.5, 1.0, 1.5 and 2.0; ψ = 0.1, 0.2, 0.4 and 0.8; and $x/L = x_j/L$, $j = 1, 2, 3, 4, 5$.

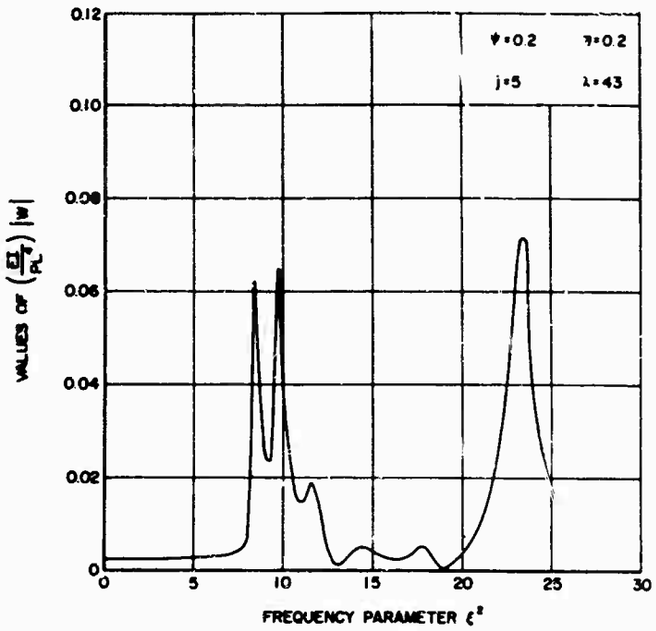

Fig. 5 - Typical response spectrum for 9-span pinned beam with distributed tuned dampers (ψ = 0.2, η = 0.2, j = 5 and λ = 43)

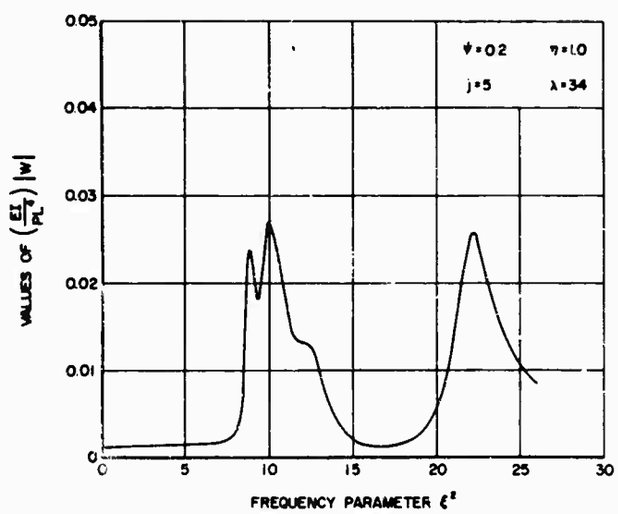

Fig. 6 - Typical response spectrum for 9-span pinned beam with distributed tuned dampers (ψ = 0.2, η = 1.0, j = 5, and λ = 34)

Nothing further can be deduced from these graphs of Q against λ. If one is to define a meaningful effective loss factor for the beam with tuned dampers, one must make comparisons with the transmissibility spectra of the same beam made of homogeneous viscoelastic material of loss factor η. The response of a beam with homogeneous viscoelastic damping is given by Eq. (20) and some typical spectra of $(EI/PL^4)|W|$ against ξ^2 are illustrated in Figs. 10 and 11. Needless to say, the spectra for the beam with homogeneous damping and tuned dampers are not identical. The most that one can do, therefore, is work in terms of the greatest amplification factor Q, corresponding in the present example to the stringer bending

TABLE 1
Characteristics of 9-Span Pinned Beam

Characteristic	Value				
	n = 1	n = 3	n = 5	n = 7	n = 9
ξ_{1n}	3.142	3.445	3.800	4.298	4.670
ξ_{1n}^2	9.870	11.189	14.441	18.469	21.812
ξ_{1n}^4	97.409	125.182	208.528	341.095	475.779
$2\int_0^1 \phi_{1n}(x/L)\, d(x/L)$	+0.637	-1.338	+1.577	-2.265	+6.101
$2\int_0^1 \phi_{1n}^2(x/L)\, d(x/L)$	+4.500	+4.471	+4.360	+4.091	+3.667
P_{1n}/P	+0.142	-0.299	+0.362	-0.554	+1.664
$\phi_{1n}(x_1/L)$	+1.000	-0.940	+0.766	-0.500	+0.737
$\phi_{1n}(x_2/L)$	-1.000	+0.500	+0.500	-1.000	+0.500
$\phi_{1n}(x_3/L)$	+1.000	+0.174	-0.940	-0.500	+0.741
$\phi_{1n}(x_4/L)$	-1.000	-0.766	-0.174	+0.500	+0.940
$\phi_{1n}(x_5/L)$	+1.000	+1.000	+1.000	+1.000	+1.000
$2\sum_{j=0}^{9} \phi_{1n}^2(x_j/L)$	+9.000	+9.000	+9.000	+9.000	+9.000

TABLE 2
Mode Shape Data $\phi_{1n}(x/L)$ for Pinned Beam

x/L	n = 1	n = 3	n = 5	n = 7	n = 9
0.0	0	0	0	0	0
0.1	+0.3044	-0.3035	+0.2822	-0.2268	+0.0975
0.3	+0.8090	-0.7836	+0.7004	-0.5316	+0.2169
0.5	+1.0000	-0.9397	+0.7660	-0.5000	+0.1736
0.7	+0.8090	-0.7205	+0.4866	-0.2039	+0.0252
0.9	+0.3044	-0.2507	+0.1060	+0.0364	-0.0525
1.0	0	0	0	0	0
1.1	-0.3044	+0.2143	+0.0080	-0.1904	+0.1309
1.3	-0.8090	+0.4801	+0.2434	-0.7354	+0.4328
1.5	-1.0000	+0.5000	+0.5000	-1.0000	+0.5000
1.7	-0.8090	+0.3203	+0.5314	-0.7354	+0.2642
1.9	-0.3044	+0.0805	+0.2454	-0.1904	-0.0010
2.0	0	0	0	0	0
2.1	+0.3044	-0.0249	-0.2850	+0.0364	+0.1494
2.3	+0.8090	+0.0461	-0.7849	-0.2039	+0.5965
2.5	+1.0000	+0.1736	-0.9397	-0.5000	+0.7660
2.7	+0.8090	+0.2299	-0.6712	-0.5316	+0.4714
2.9	+0.3044	+0.1273	-0.1912	-0.2268	+0.0505
3.0	0	0	0	0	0
3.1	-0.3044	-0.1762	+0.0910	+0.2268	+0.1481
3.3	-0.8090	-0.5538	+0.0292	+0.5316	+0.6883
3.5	-1.0000	-0.7660	-0.1736	+0.5000	+0.9397
3.7	-0.8090	-0.6724	-0.2983	+0.2039	+0.6217
3.9	-0.3044	-0.2755	-0.1790	-0.0364	+0.0960
4.0	0	0	0	0	0
4.1	+0.3044	+0.2949	+0.2534	+0.1904	+0.1298
4.3	+0.8090	+0.8004	+0.7748	+0.7354	+0.6970
4.5	+1.0000	+1.0000	+1.0000	+1.0000	+1.0000

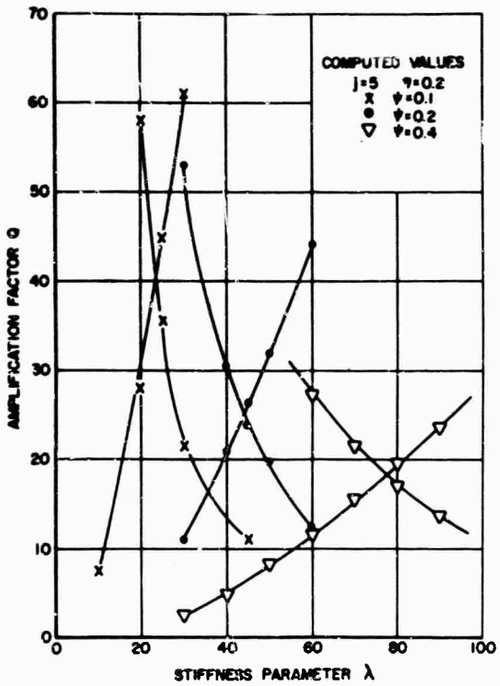

Fig. 7 - Typical graphs of amplification factor vs stiffness parameter for predominant peaks of response ($j = 5$, $\eta = 0.2$)

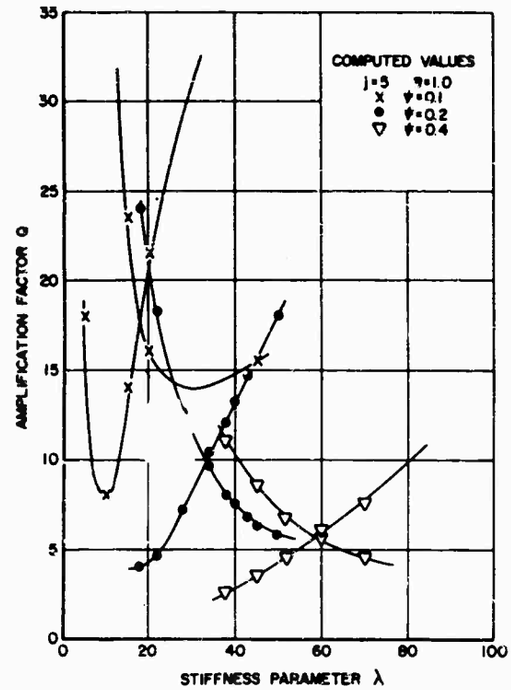

Fig. 9 - Typical graphs of amplification factor vs stiffness parameter for predominant peaks of response ($j = 5$, $\eta = 1.0$)

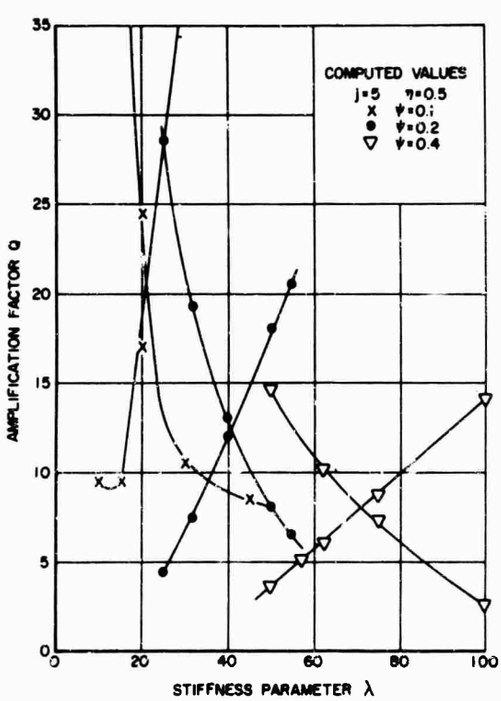

Fig. 8 - Typical graphs of amplification factor vs stiffness parameter for predominant peaks of response ($j = 5$, $\eta = 0.5$)

mode, and plot graphs of Q against η for various values of x/L. As an example, a graph of Q against η for $x/L = x_j/L$, $j = 1, 3, 5$, is plotted in Fig. 12.

For given values of j, η, ψ, one can now read the value of Q for the beam with tuned dampers off the graph of Q against λ and then read the effective loss factor η_s off the graph of Q against η for the beam with homogeneous damping. Graphs of η_s against λ can then be drawn, such as Figs. 13 and 14, for all values of j. It is seen that, in every case, only one value of λ exists for which the value of η_s is the same for all values of j. This value of η_s is the effective loss factor of the beam with properly tuned viscoelastic dampers, for the particular values of ψ and η.

From all such graphs of η_s against λ, the effective loss factor at the point of proper tuning can be plotted against the damper loss factor η for various values of the mass ratio ψ, as in Fig. 15.

Finally, from Eq. (16), one can determine the ratio ω_D/ω_{11} of the damper natural frequency to the first natural frequency of the multi-span beam, at the point of proper tuning, using the

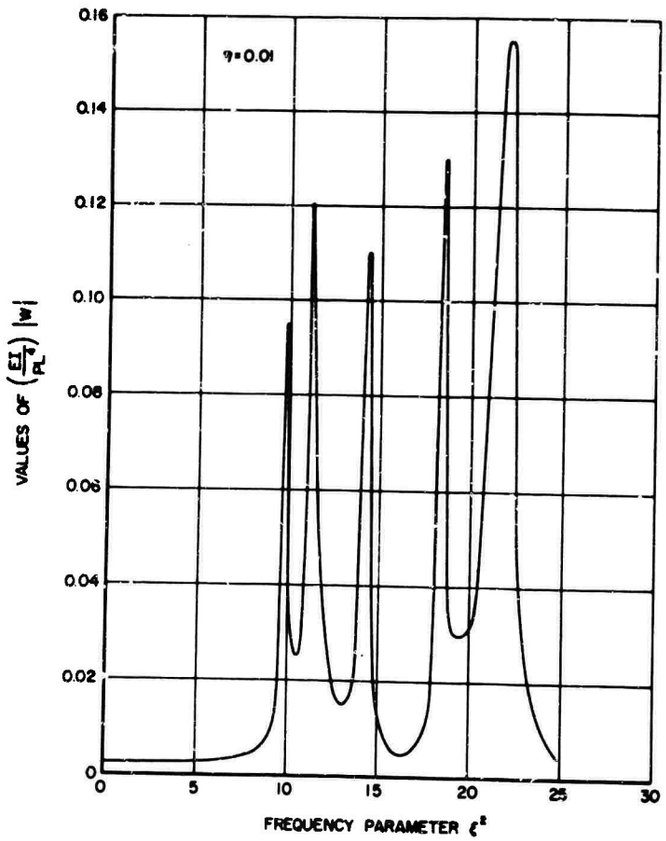

Fig. 10 - Typical response spectrum for 9-span pinned beam with homogeneous viscoelastic damping (η = 0.01)

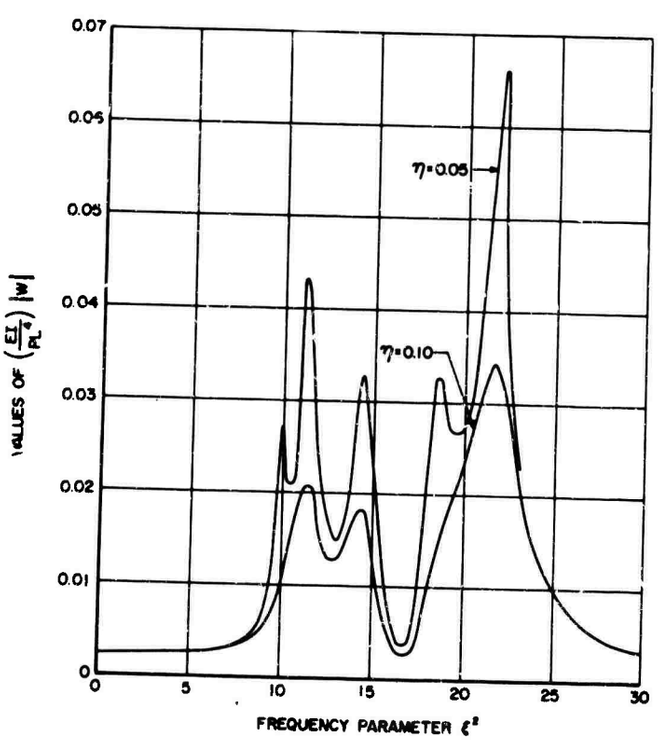

Fig. 11 - Typical response spectrum for 9-span pinned beam with homogeneous viscoelastic damping (η = 0.05, 0.10)

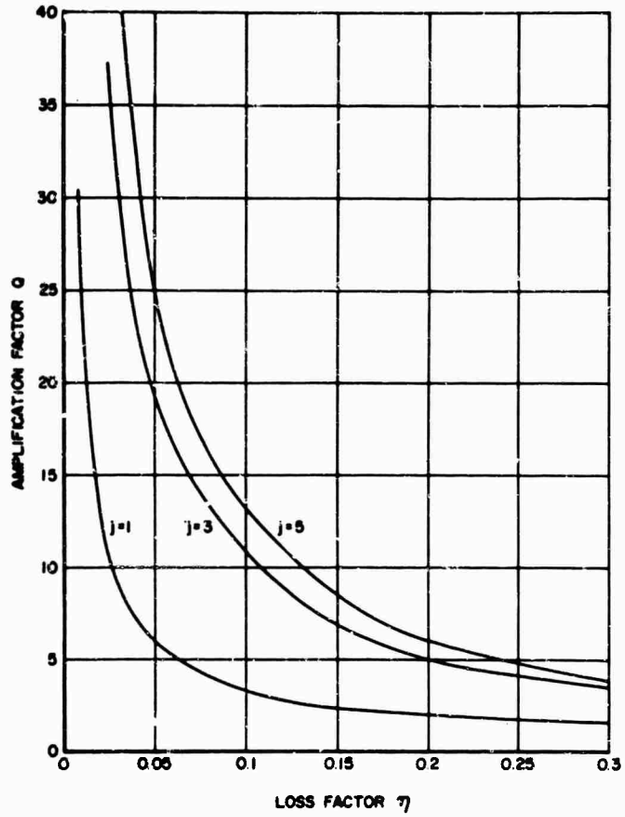

Fig. 12 - Typical graphs of amplification factor of predominant peak vs beam loss factor, for 9-span pinned beam with homogeneous visco-elastic damping

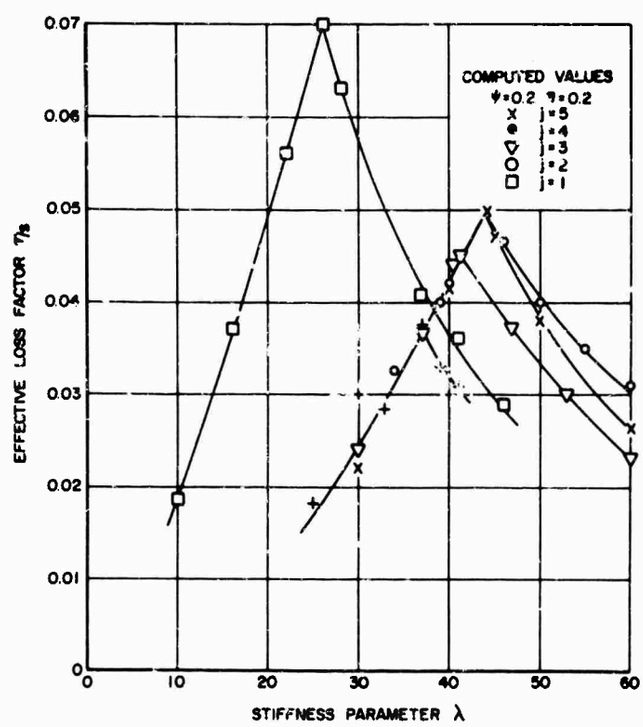

Fig. 13 - Typical graphs of effective loss factor vs stiffness parameter for 9-span pinned beam with tuned viscoelastic dampers (ψ = 0.2, η = 0.2)

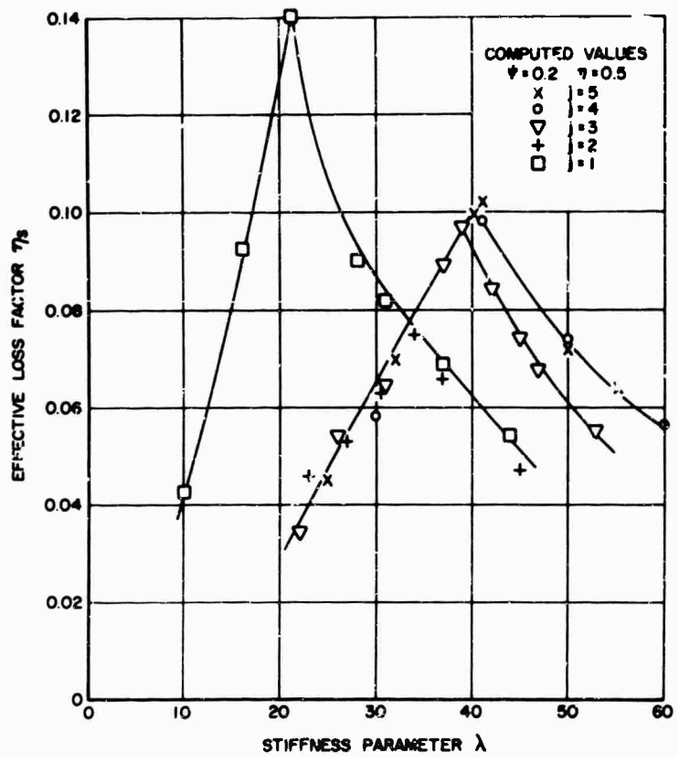

Fig. 14 - Typical graphs of effective loss factor vs stiffness parameter for 9-span pinned beam with tuned viscoelastic dampers (ψ = 0.2, η = 0.5)

value of λ obtained from the graphs of η_s against λ. A graph of $(\lambda/\psi\xi_{11}^4)^{1/2}(1+\psi)^{1/2}(1+\eta^2)^{1/4}$ obtained using Figs. 12 to 14, is illustrated in Fig. 16. The empirical relationship, showing that ω_D/ω_{11} varies in proportion to $(1+\psi)^{-1/2}$ and $(1+\eta^2)^{-1/4}$ has not been proved, but Fig. 16 shows that it gives a good collapse of the computed data. Since, from Fig. 16, the value of ω_D/ω_{11} is equal to 1.56 $(1+\psi)^{-1/2}(1+\eta^2)^{-1/4}$, it follows that, at least for moderate values of η and ψ, proper tuning occurs when the damper is tuned approximately midway between the stringer torsion and stringer bending modes.

EXPERIMENTAL INVESTIGATION OF MULTI-SPAN STRUCTURE WITH TUNED VISCOELASTIC DAMPERS

No experimental investigation has yet been made of a 9-span beam with tuned viscoelastic dampers. However, some recent preliminary experiments with a 5-span skin-stringer-frame structure, typical of a part of an aircraft fuselage, have recently been carried out [11] and have yielded results of sufficient interest to be briefly mentioned in this paper.

The model structure, shown in Fig. 17, was mounted on a rigid fixture which was vibrated harmonically by an electrodynamic shaker. The input acceleration was controlled by an accelerometer along one of the frames, the position being chosen so as to minimize variations of the input acceleration at all points along the frames. The response measured by miniature accelerometers at the center span (span C) is shown in Fig. 18. The multi-modal response is clearly seen, the stringer bending mode being predominant.

Tuned dampers in which the stiffness was provided by a ring or loop of viscoelastic material (LD-400, Lord Manufacturing Co., Erie, Pa.) were then attached at the center of each panel, as in Fig. 19. The dampers were nominally identical and similar to those used in previous investigations [3, 4, 6]. The experimental setup is illustrated in Fig. 20. Response records were again taken for each span and a typical record, taken for the center span, is shown in Fig. 21. It is seen that the greatest amplification factor at resonance is reduced from about 30 in the nominally undamped case to about 6 in the damped case, for a total weight

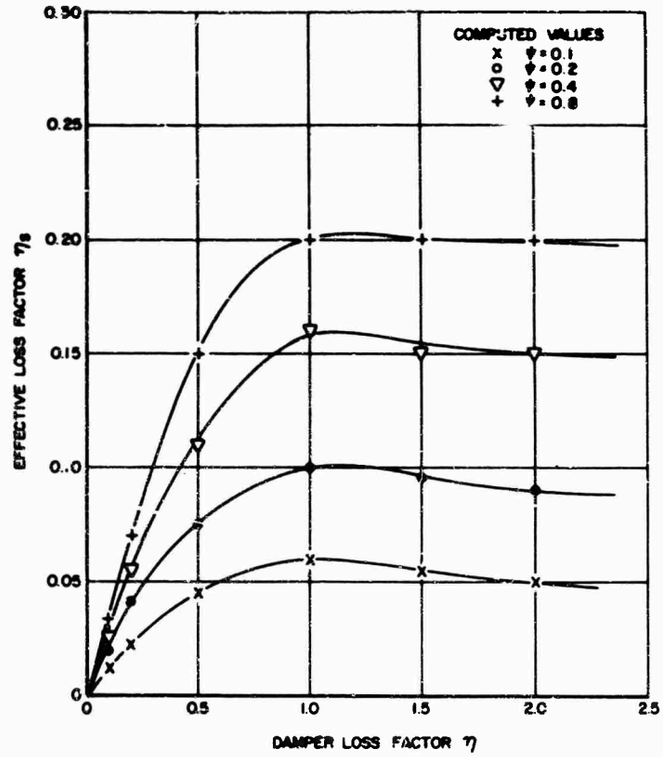

Fig. 15 - Typical graphs of effective loss factor vs damper loss factor for 9-span beam with optimally tuned viscoelastic dampers

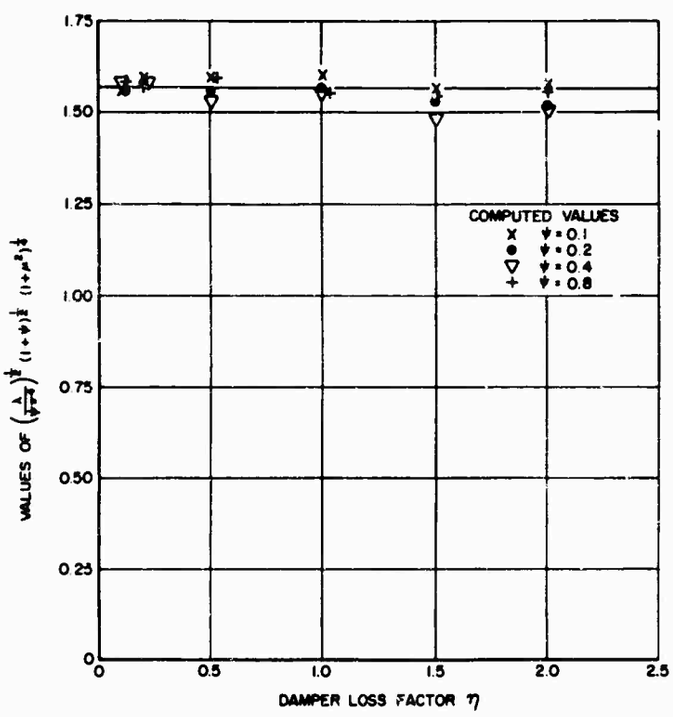

Fig. 16 - Graphs of $(\lambda/\psi\xi_{11}^4)^{1/2}(1+\psi)^{1/2}(1+\eta^2)^{1/4}$ against damper loss factor for 9-span pinned beam with optimally tuned distributed tuned dampers

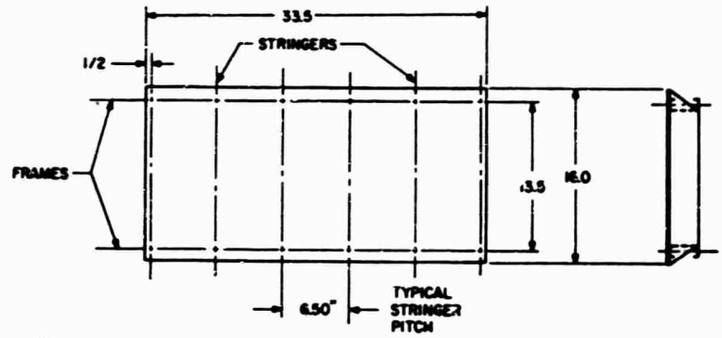

Fig. 17 - Diagram of five-span skin-stringer structure

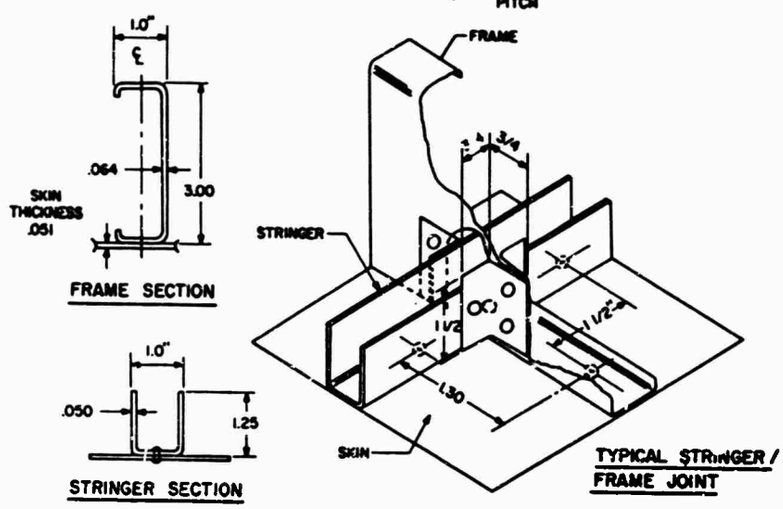

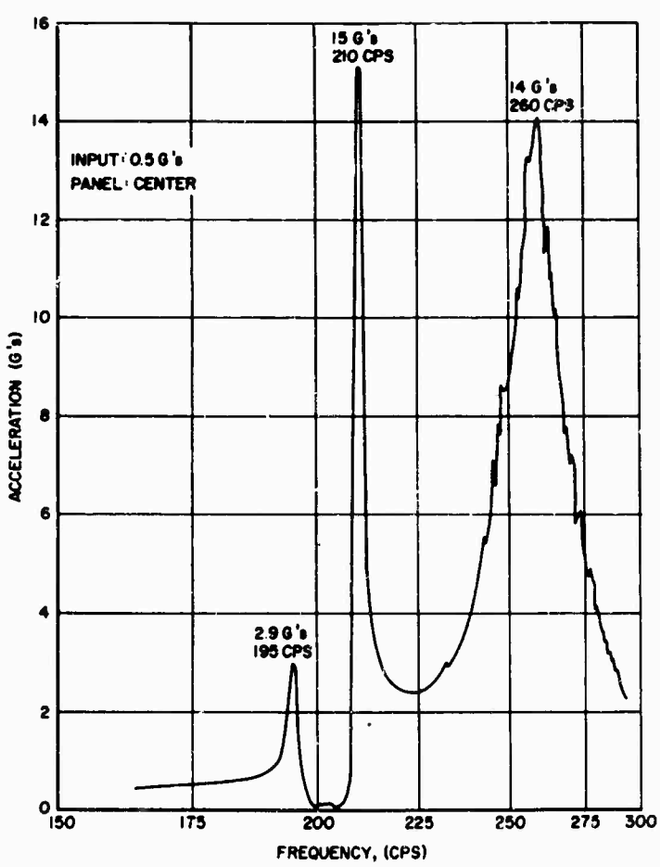

Fig. 18 - Typical measured response spectrum at center panel of 5-span skin-stringer structure excited by shaker

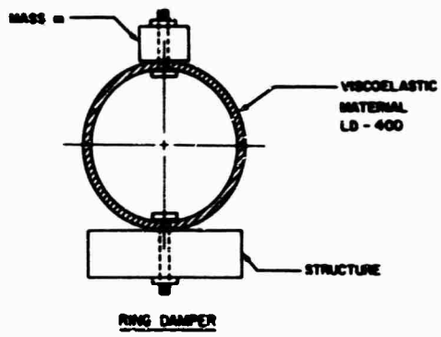

Fig. 19 - Sketch of typical ring damper used in experimental investigation

addition of about 6 gm per damper, which amounts to about 3 percent of the weight of the skin of the structure.

Needless to say, no direct comparisons can be made between the present theory and these experimental results. However, they do serve to show that excellent damping can be introduced into multi-span structures, exhibiting multi-modal response, by properly optimized tuned dampers.

CONCLUSIONS

An analysis has been developed for the response of a multi-span beam, with tuned

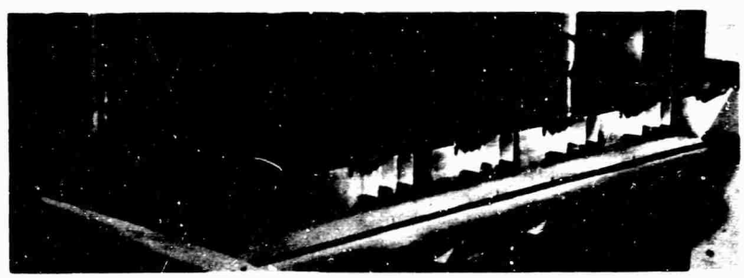

Fig. 20 - Photograph of skin-stringer structure with tuned dampers at center of each panel

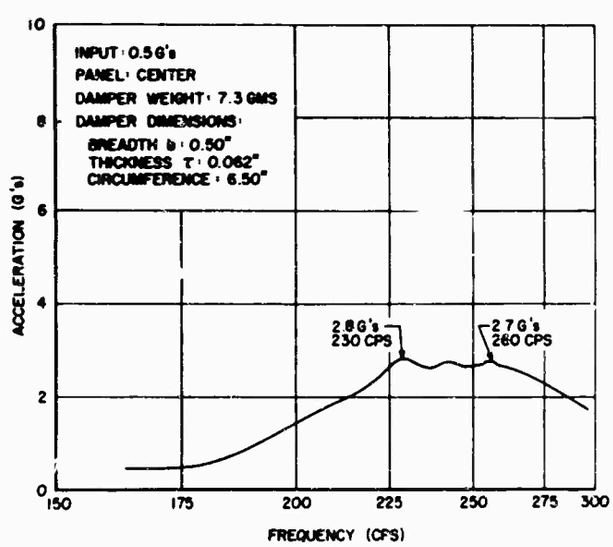

Fig. 21 - Typical response spectrum measured at center panel of 5-span skin-stringer structure excited by shaker, with tuned dampers close to optimal tuning

viscoelastic dampers distributed along the beam, to a harmonically varying loading of arbitrary spatial dependence. The solution is expressed in terms of the normal modes of the undamped beam, and a knowledge of these modes and the corresponding natural frequencies is a prerequisite of the analysis. By comparisons between the response of the beam with tuned dampers and the same beam configuration with homogeneously distributed viscoelastic damping, an effective loss factor giving a measure of the damping introduced by the tuned dampers is defined. The variation of the effective loss factor with damper mass, loss factor and stiffness is demonstrated, and it is shown that high damping can be introduced into structures exhibiting multi-modal response by tuned dampers. Preliminary experiments, described in the paper, support this conclusion.

ACKNOWLEDGMENTS

The experimental investigation described in this paper was carried out on equipment purchased using the Director's Fund of the Air Force Materials Laboratory. The authors would like to acknowledge the help given by B. J. Lazan during the very early phases of the investigation. Thanks are owed to W. J. Trapp, Chief of the Strength and Dynamics Branch, for his support and encouragement of the work, D. J. Mead of the University of Southampton, England, and J. P. Henderson for assistance with the investigation, Miss Connie Mantych for assistance with preparation of the manuscript, and Mr. DeMarey of the University of Dayton for assistance with preparation of the figures.

REFERENCES

1. J. C. Snowdon, "Steady State Behavior of the Dynamic Absorber," J. Acoust. Soc. Am., Vol. 31, pp. 1096-1103, Aug. 1959
2. J. P. Den Hartog, Mechanical Vibrations. McGraw-Hill, New York, 1934
3. A. D. Nashif, "Effect of Tuned Dampers on Vibrations of Cantilever Beams," AFML-TR-66-83, March 1966
4. R. L. Adkins and D. I. G. Jones, "Effect of Tuned Viscoelastic Dampers on Response and Damping of a Clamped-Clamped Beam," AFML-TR-66-100, April 1966
5. J. C. Snowdon, "Vibration of Cantilever Beams to which Dynamic Absorbers are Attached," J. Acoust. Soc. Am., Vol. 39, pp. 878-886, May 1966
6. J. P. Henderson, "Energy Dissipation in a Vibration Damper Utilizing a Viscoelastic Suspension," Shock and Vibration Bull. No. 35, Part 7, pp. 213-229, April 1966
7. Y. K. Lin, "Free Vibration of Continuous Skin-Stringer Panels with Non-Uniform Stringer Spacing and Panel Thickness," AFML-TR-64-347, Part 1, Fig. 4, Feb. 1965
8. J. W. Miles, "Vibrations of Beams on Many Supports," Proc. ASCE, Jan. 1956
9. C. A. Mercer, "Response of a Multi-Supported Beam to a Random Pressure Field," Inst. Sound and Vibration Res., Univ. of Southampton, Eng., Memo. 103, March 1964
10. D. J. Mead, Personal communication
11. D. I. G. Jones, J. P. Henderson, and G. H. Bruns, "Use of Tuned Viscoelastic Dampers for Reduction of Vibrations in Aerospace Structures," presented at 13th Ann. Air Force Sci. and Eng. Symp., Arnold AFB, Tenn., Sept. 1966

DISCUSSION

Mr. Hooper: How much change in acceleration would have been brought about just by the dead weight of your added dampers apart from their viscoelastic properties?

Lt. Bruns: I don't quite understand you. Do you mean if we had invested this weight in a thicker skin?

Mr. Hooper: No, if you had just added concentrated weights.

Lt. Bruns: In other words, a sprung mass without any damping?

Mr. Hooper: No, if you had just taken the weight of your rings and put it in those spots as

a rigid mass. That would probably make quite a dramatic change.

Lt. Bruns: You are just adding a lumped mass to the system?

Mr. Hooper: Yes.

Lt. Bruns: This, to the best of my knowledge, would only result in a shift of the curve. The same peaks would result; in fact, I should think they would be a little worse. True, the frequency would shift as it would when you add mass to any elastic system, but you certainly would not eliminate the peaks the way we did there.

Mr. Woolam (Southwest Research Inst.): It appears that we presently have two very good methods of damping. What are future uses for this? Can we expect to see this in the Flight Dynamics Lab now?

Lt. Bruns: My boss is sitting in the front row. He can answer this if he likes. We are working more and more toward getting a practical solution. You cannot envision a fuselage with these rings hanging all over the inside. There are problems, and there is work to be done. I think our major goal in the two papers presented by Dr. Jones and myself is to show that this is a fruitful area of investigation. This is something you should consider when you run into problems in this area. Of course, we will be continuing to work in this area but we also hope that maybe some other people in the industry who are closer to the problems will help.

Mr. Smith (Bell Aerosystems Co.): Under random loading, of course, the reduction in response, while still being pretty dramatic, will decrease as the square root of the damping instead of the damping. Have you compared the local strains for a panel both with and without the tuned dampers at the center of the panel? Are you eliminating one potential problem but perhaps introducing another?

Lt. Bruns: We realized that there is more than one criterion in evaluating what is being done to the response of the system. We chose amplitude of vibration. We feel that anything else will be in some way involved with this, possibly, even probably, proportional to it. I fully admit that there are other criteria to be used and you could run this whole investigation over using a different criterion, such as maximum bending stress.

Mr. West (Aerojet-General Corp.): Very often in vibration testing fixture resonances present a serious problem. Would you expect that this viscoelastic damper system could be used to help out in this situation?

Lt. Bruns: Yes, although I should think that if it is just a fixture, the solution would be to stiffen it and to raise the fixture natural frequency above the area of interest. The primary reason for using the tuned damper is to get a lot of reduction with a low weight penalty and this is, of course, extremely important when you have anything airborne. You can solve most vibration problems by adding weight, but this is usually not acceptable.

* * *

METHOD FOR IDENTIFYING AND EVALUATING LINEAR DAMPING MODELS IN BEAM VIBRATIONS

M. W. Wambsganss, Jr., B. L. Boers, and G. S. Rosenberg
Argonne National Laboratory
Argonne, Illinois

This paper presents the results of an effort to identify and evaluate effective linear damping models in beam vibration. The study was motivated by the desire to model mathematically the dynamic response of a beam-type element in which significant energy dissipation could be attributed to the contact of the component with adjacent similar components. The usual method of modeling damping, that is, assuming damping mechanisms and empirically evaluating the coefficients, is employed. The three damping mechanisms considered are viscous, stress, and load damping. The problem is that of identifying the dominant damping mechanism(s) for inclusion in the mathematical model and of evaluating the associated damping coefficients.

A theoretical analysis, based on the usual assumptions in (Euler) beam theory and the further assumption of the damping being small enough that the natural frequencies and mode shapes are unaffected, is carried out. The analysis leads to a sensitive method, compatible with results obtained from tests on a vibration exciter, for identifying the effective damping mechanisms. The technique involves a comparison of the experimentally determined ratio of first to second mode magnification factors, related to a common point on the beam, with the constant values of this ratio corresponding to "pure forms" of the proposed damping. The method is illustrated by application to the modeling of the response of a cluster of cantilevered beams clamped together at the base. This model is being employed in the preliminary analysis of the interaction effects of vibrating fuel rods in a nuclear reactor core. Damping models are identified and curves of damping coefficients as a function of cluster size are presented.

M. W. Wambsganss, Jr.

INTRODUCTION

A nuclear reactor core is made up of a large number of structural elements, usually in the form of slender plates or rods, which contain the fuel material. These fuel elements are often arranged in small subassemblies which, in turn, are mounted on a support grid, forming a relatively tightly spaced bundle. High velocity coolant flows axially through this arrangement while the entire core is additionally subjected to severe thermal and pressure loads.

Parallel coolant flow is known to induce oscillations of plates and rods. In a reactor, large amplitudes of oscillation must necessarily be avoided, not only for conventional structural reasons, but because ensuing coolant channel closure may have a critical effect on heat transfer and reactor neutron dynamics. In addition to flow-induced vibration, mobile reactors for use on submarines or space vehicles are subjected to disturbances from the environment in

which the vehicle operates. This paper stems from a part of the study directed toward acquiring pertinent design insights.

The mathematical modeling of the dynamic behavior of an in-core fuel assembly is immediately complicated by the fact that interaction occurs among the clustered fuel subassemblies. Because of this interaction, and the fact that critical displacements are small, damping becomes an important consideration of the modeling.

The study of the interaction and damping using a full-size core mock-up becomes prohibitive due to the high cost of fabricating prototype fuel assemblies. Therefore, as a preliminary model, the fuel subassemblies are simulated by hexagonal rods. The cluster is formed by clamping a rod bundle together at the base. Among the objectives of the study of this preliminary model are the following:

1. Determine the effect of cluster size on the natural frequencies and damping of a rod within the cluster;

2. Identify damping models and associated damping coefficients to describe satisfactorily the dissipation of energy in a rod; and

3. Determine the experiment size in terms of the number of elements in the experimental cluster that would be required to obtain experimental estimates of certain corresponding features (listed above) without requiring the full prototype compliment of cluster elements.

The damping force associated with the dissipation of energy can be a linear or nonlinear function of displacement, velocity, stress, temperature, and/or other factors. The mathematical modeling of this force is difficult and the dynamicist must generally assume a damping mechanism and rely on empirical determination of the effective damping coefficients. The most widely used model, which leads to the simplest mathematical treatment, is that of viscous damping, in which the damping force is assumed proportional to the velocity. Structural, or material, damping is often modeled assuming the damping force to be proportional to the displacement but in phase with the velocity. Various other damping mechanisms can be conceived.

This basic approach to modeling damping, that is, assuming damping mechanisms and utilizing empirical results for evaluation, is followed in studying the energy dissipated in the vibration of simulated fuel assembly clusters.

The three damping mechanisms considered are viscous, stress, and load damping. They are defined by the distributed damping force intensity as

$$f_D(x,t) = \begin{cases} c_V y_t, & \text{viscous damping;} \\ c_S y_{xxt}, & \text{stress damping;} \\ c_L y_{xxxxt}, & \text{load damping.} \end{cases} \quad (1)$$

In the analysis it is assumed that the damping is sufficiently small that the natural frequencies and mode shapes are unaffected.

The selection of the dominant damping mechanisms is based on a comparison of the experimentally determined ratio of first to second mode magnification factors, with the constant values of this ratio corresponding to "pure forms" of the proposed damping, as obtained from theoretical considerations. Evaluation of the associated damping coefficients is performed via solution of a set of independent simultaneous equations. The set of equations is constructed by expressing the coefficients as a linear combination and using experimental results obtained at resonant conditions.

THEORETICAL ANALYSIS

Forced Vibration of Lightly Damped Beam

Consider a transverse motion imparted to a uniform beam by giving the support the harmonic displacement,

$$z(t) = A_o \cos \omega t . \quad (2)$$

With $y(x,t)$ defined as the relative lateral displacement of the beam with respect to the support, the absolute displacement of the beam can be written

$$Y(x,t) = y(x,t) + z(t) . \quad (3)$$

Including the three proposed damping mechanisms and using Euler beam theory, the equation of motion for the beam becomes

$$EIY^{IV} + c_L \dot{Y}^{IV} + c_S \dot{Y}^{II} + c_V \dot{Y} + \rho A \ddot{Y} = 0 , \quad (4)$$

or

$$y^{IV} + \left(\frac{c_L}{EI}\right) \dot{y}^{IV} + \left(\frac{c_S}{EI}\right) \dot{y}^{II} + \left(\frac{c_V}{EI}\right) \dot{y} + \left(\frac{\rho A}{EI}\right) \ddot{y}$$

$$= - \left(\frac{c_V}{EI}\right) \dot{z} - \left(\frac{\rho A}{EI}\right) \ddot{z} . \quad (5)$$

For structural systems the amount of damping is generally small. Based on this observation, the assumption will now be made that the relative motion of the beam can be represented as a superposition of the undamped free vibration modes, or eigenfunctions, as found from solving

$$\phi_m^{IV} = \lambda_m \phi_m ,$$
$$\lambda_m = \frac{\rho A}{EI} \omega_m^2 , \tag{6}$$

with the appropriate boundary conditions. Therefore, the relative motion of the beam can be written

$$y(x,t) = \sum_{k=1}^{n} \phi_k(x)\, q_k(t) . \tag{7}$$

Application of Galerkin's method by substituting Eq. (7) into Eq. (5), multiplying through by $\phi_m(x)$ and integrating over the length, gives, using the orthogonality property of the normal modes, a set of n-ordinary differential equations to solve for the n-generalized coordinates. In general, because of the nature of the stress damping term, the equations will be coupled. However, noting a further property [1] of the normal modes, that

$$\int_0^{\ell} \phi_m(x)\, \phi_n''(x)\, dx = 0 , \quad \text{for } (m+n), \text{ odd}, \tag{8}$$

a two-term approximation to the motion, made up of an even and an odd harmonic term, will give uncoupled equations. Since a two-degree-of-freedom approximation often gives satisfactory results in slender beam vibrations, this requirement for uncoupling is not serious. Further, higher degree of freedom approximations may be used with this procedure when the stress damping term is included, if it can be shown, say by an "order of magnitude" comparison, that the coefficients in front of the coupling terms are such that the coupling terms can be neglected relative to the remaining terms. With these comments regarding the uncoupling of the equations of motion, the analysis will be developed in general for a n-term, or n-degree-of-freedom, approximation, under the assumption that uncoupled equations can be obtained. The resulting set of uncoupled equations can be written

$$\ddot{q}_m + 2\zeta_m \omega_m \dot{q}_m + \omega_m^2 q_m = -(2\zeta_m^V \dot{z} + \ddot{z}) \frac{1}{\ell} \int_0^{\ell} \phi_m(x)dx, \tag{9}$$

where

$$\zeta_m = \zeta_m^V + \zeta_m^S \frac{1}{\ell} \int_0^{\ell} \phi_m \phi_m'' dx + \zeta_m^L \frac{1}{\ell} \int_0^{\ell} \phi_m \phi_m^{IV} dx ,$$

$$\zeta_m^V = \frac{c_V}{(c_{cr})_m} ,$$

$$\zeta_m^S = \frac{c_S}{(c_{cr})_m} ,$$

$$\zeta_m^L = \frac{c_L}{(c_{cr})_m} ,$$

$$(c_{cr})_m = 2\rho A \omega_m ,$$

and the eigenfunctions have been normalized such that

$$\int_0^{\ell} \phi_m^2(x)\, dx = \ell . \tag{10}$$

The steady-state forced vibration response to the sinusoidal forcing function, Eq. (2), can be written, using superposition, as

$$q_m(t) = B_m \left\{ \cos(\omega t - \gamma_m) + \frac{2\zeta_m^V}{\beta_m} \sin(\omega t - \gamma_m) \right\} , \tag{11}$$

where

$$B_m = \frac{A_o \beta_m^2 \frac{1}{\ell} \int_0^{\ell} \phi_m(x)\, dx}{\left[\left(1 - \beta_m^2\right)^2 + 4\zeta_m^2 \beta_m^2 \right]^{1/2}} ,$$

$$\gamma_m = \tan^{-1} \frac{2\zeta_m \beta_m}{\left(1 - \beta_m^2\right)} ,$$

and

$$\beta_m = \frac{\omega}{\omega_m} .$$

The relative motion of the beam can then be represented by

$$y(x,t) = \sum_{m=1}^{n} B_m \phi_m(x) \left\{ \cos(\omega t - \gamma_m) + 2 \frac{\zeta_m^V}{\beta_m} \sin(\omega t - \gamma_m) \right\} \tag{12}$$

or

$$y(x,t) = \sum_{m=1}^{n} y_m(x) \cos(\omega t - \gamma_m - \theta_m), \quad (13)$$

where

$$y_m(x) = A_o \phi_m(x) \beta_m^2 \left\{ \frac{1 + 4\left(\frac{\zeta_m^V}{\beta_m}\right)^2}{\left(1 - \beta_m^2\right)^2 + 4\zeta_m^2 \beta_m^2} \right\}^{1/2}$$

$$\times \frac{1}{\ell} \int_o^\ell \phi_m(x)\, dx,$$

and

$$\theta_m = \tan^{-1} 2\left(\frac{\zeta_m^V}{\beta_m}\right).$$

Therefore, the absolute motion of the beam is given by

$$Y(x,t) = A \cos \omega t + \sum_{m=1}^{n} y_m(x) \cos(\omega t - \gamma_m - \theta_m). \quad (14)$$

When vibrating at one of the natural frequencies, assume all the energy input goes into that mode of vibration. Under this assumption, when $\omega = \omega_n$,

$$Y(x,t) = A_o \cos \omega_n t + y_n(x) \cos(\omega_n t - \gamma_n - \theta_n). \quad (15)$$

Also, when $\omega = \omega_n$, $\beta_n = 1$ which gives

$$y_n(x) = \frac{A_o \phi_n(x)}{2\zeta_n} \left(1 + 4\zeta_n^{V^2}\right)^{1/2} \frac{1}{\ell} \int_o^\ell \phi_n(x) dx, \quad (16)$$

where $\gamma_n = \pi/2$, and leads to

$$\frac{Y(x,t)}{A_o} = \cos \omega_n t + \frac{y_n(x)}{A_o} \sin(\omega_n t - \theta_n). \quad (17)$$

At a resonance, with small damping,

$$\left|\frac{Y(x,t)}{A_o}\right| >> 1,$$

and (18)

$$4\zeta_n^{V^2} << 1;$$

therefore,

$$Y(x,t) \approx y_n(x) \sin \omega_n t, \quad (19)$$

where

$$y_n(x) = \frac{A_o \phi_n(x)}{2\zeta_n} \frac{1}{\ell} \int_o^\ell \phi_n(x)\, dx.$$

Vibrating a beam on a vibration exciter, the beam displacement at a resonance can be observed to be of the form

$$Y(x,t) = A_n(x) \sin \omega_n t, \quad (20)$$

where the amplitude $A_n(x)$ can easily be measured. Equating Eqs. (19) and (20) gives

$$\zeta_n = \frac{\phi_n(x) \int_c^\ell \phi_n(x)\, dx}{2\ell\, \mu_n(x)}, \quad (21)$$

where

$$\mu_n(x) = \frac{A_n(x)}{A_o}.$$

Damping Model Identification

Three damping mechanisms have been proposed in mathematically modeling the damping in a beam. The problem which now arises is that of identifying, from the three, the dominant damping mechanism(s). In this regard, it would be desirable to have a rather sensitive method of making the identification from simple experimental tests.

Assume, for the moment, that only one damping mechanism is dominant; take the other two damping coefficients to be zero. Then the remaining damping coefficient can be obtained from Eq. (21) as

$$c = \frac{\rho A \omega_n \phi_n(x) \int_o^\ell \phi_n(x)\, dx}{\mu_n(x) \int_o^\ell \phi_n \phi_n^{(r)}\, dx}, \quad (22)$$

where

$$c = \begin{cases} c_V, & \text{for } r = 0; \\ c_S, & \text{for } r = 2; \\ c_L, & \text{for } r = 4. \end{cases}$$

Equating the expressions for the damping coefficient (which is being assumed constant) as obtained from first and second mode considerations gives

$$R(x) = \left[\frac{\mu_1(x)}{\mu_2(x)}\right] = \left(\frac{\omega_1}{\omega_2}\right)\left[\frac{\phi_1(x)}{\phi_2(x)}\right]$$

$$\times \left[\frac{\int_0^\ell \phi_1\, dx}{\int_0^\ell \phi_2\, dx}\right]\left[\frac{\int_0^\ell \phi_2 \phi_2^{(r)}\, dx}{\int_0^\ell \phi_1 \phi_1^{(r)}\, dx}\right] . \qquad (23)$$

That is, the ratio of first to second mode magnification factors is a constant at a particular value of x or section along the beam. Knowing the eigenfunctions and the ratio of natural frequencies, the constant depends only on the order of the derivative of the eigenfunction under the integral, which in turn is directly related to the form of damping. Therefore, experimental determination of the ratio of magnification factors, related to a section on the beam, and comparison with the corresponding ratio constants, associated with a particular damping mechanism, gives a method of determining if one particular damping mechanism alone is present, or which two are dominant.

As an example, consider a clamped-free or cantilevered beam. The required modal properties of beams are given by Bishop and Johnson [2]. An additional property, required in evaluating Eq. (23), is given by Langhaar [1], that is,

$$\int_0^\ell \phi_m \phi_m''\, dx = \frac{1}{\ell}\left[\sigma_m \gamma_m \ell (2 - \sigma_m \gamma_m \ell)\right] .$$

The symbols correspond to those in Ref. 2. Using these to evaluate Eq. (23) gives as the ratio of magnification factors, related to the tip of a cantilevered beam,

$$R(\ell) = \begin{cases} 0.288, & \text{viscous damping } (r = 0) ; \\ 4.46 , & \text{stress damping } (r = 2); \\ 11.3 , & \text{load damping } (r = 4). \end{cases} \qquad (24)$$

Therefore, a comparison of the ratio of magnification factors gives a rather sensitive method, compatible with results derived from tests on a vibration exciter, for evaluating or selecting a damping model for a uniform beam.

It should be noted that similar sets of ratio constants can be developed for beams mounted in various other basic configurations. Also, although it is not always practical, modes other than the first and second may be employed to give a ratio of magnification factors. The effect of shear and rotatory inertia, which have been neglected, increase with frequency. Therefore, if higher modes are used, care must be taken to be sure that the effective length (modal "wavelength") in comparison with the depth of the beam, is still such that slender beam theory applies. Further, it must be remembered that for the modal property given by Eq. (8) to hold, which allows stress damping to be included in general, an even and odd harmonic mode must be used.

In general, a two-mode approximation is often sufficient in the description of the dynamic response of most structural components. Unless the boundary conditions or type of excitation indicates that other modes might be expected, the two modes selected are generally the first and second. Therefore, it is logical to use the first and second mode magnification factors in the damping model identification scheme.

Damping Coefficient Evaluation

Once the damping mechanisms and corresponding damping models have been selected, completing the formulation of the mathematical model requires evaluation of the associated damping coefficients. If a consideration of the ratio of magnification factors indicates, by a close comparison with one of the ratio constants given by Eq. (24), that only one form of damping is dominant, the corresponding damping coefficient can be readily evaluated with Eq. (22). In general, however, more than one type of damping will be indicated.

Equation (21) can be expanded and written in the form

$$c_V + c_S \frac{1}{\ell}\int_0^\ell \phi_n \phi_n''\, dx + c_L \lambda_n^4$$

$$= \frac{\rho A \omega_n \phi_n(x) \int_0^\ell \phi_n(x)\, dx}{\ell \mu_n(x)} . \qquad (25)$$

Let only two damping mechanisms be included in the model by assuming one of the damping coefficients to be zero. By vibrating a beam on a shaker through its first two resonant modes, the corresponding natural frequencies and magnification factors can be measured. With this information and Eq. (25), two equations can be written and the two unknown damping coefficients can be computed.

As an example, consider once again the cantilevered beam and let viscous and stress damping be the two damping mechanisms included in the mathematical model for the beam. With Eq. (25) and the properties previously given for a clamped-free beam, the viscous and stress damping coefficients can be expressed as

$$c_V = \frac{EI}{\ell^4}\left(\frac{18.2}{\omega_1\,\mu_1(\ell)} - \frac{25.5}{\omega_2\,\mu_2(\ell)}\right),$$

and (26)

$$c_S = \frac{EI}{\ell^2}\left(\frac{1.37}{\omega_1\,\mu_1(\ell)} + \frac{29.8}{\omega_2\,\mu_2(\ell)}\right).$$

In the above equations, the ratios of magnification factors are referred to the beam tip or free end. Note that all that is required to compute the damping coefficients is a knowledge of the flexural rigidity and length of the beam and values for the first and second mode natural frequencies and magnification factors.

APPLICATION TO REACTOR CORE FUEL ASSEMBLIES

Experiment Design

As discussed earlier, the preliminary model, simulating the reactor fuel subassemblies, consists of a cantilevered cluster of hexagonal rods. For the experiment, 1/2-in. rods were used. The clamping fixture consisted of two square 2-in. thick plates of aluminum with an 8-in. diameter hole in the center. The plates were cut into halves which could be bolted together. The maximum size cluster, which fits inside an 8-in. diameter circle (163 rods), was made one row larger by adding 4-in. long stubs. The resulting bundle was then turned down to an 8-in. diameter to fit inside the clamping fixture. Thus, the fixture clamps on the lower 4 in. of the rods. Any size cluster, up to the maximum size of 163 rods, could be tested by replacing rods with 4-in. stubs. For this study, eight cluster sizes of 1, 7, 19, 37, 61, 91, 127 and 163 rods were tested. The clamping fixture and a 37-rod cluster are shown in Fig. 1.

The test fixture was mounted on a slip plate and excited by a 10,000-lb shaker. The shaker was servocontrolled to maintain a constant input displacement amplitude as sensed by a variable reluctance displacement transducer. The experimental test setup is shown in Fig. 2.

Fig. 1 - Clamping fixture for model cluster

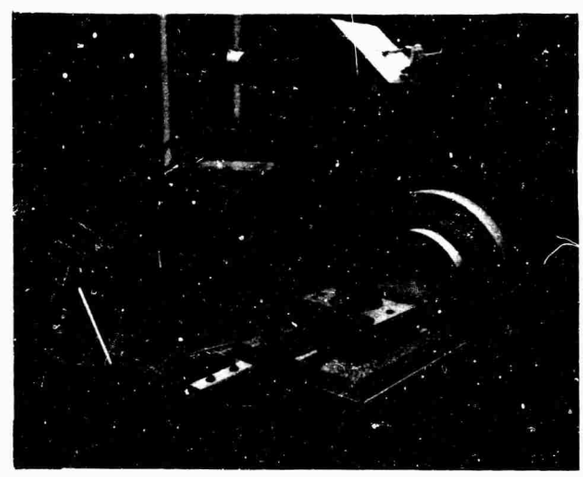

Fig. 2 - Experimental test setup

The input displacement and acceleration, strain at the root of the center rod, and strain at the root and acceleration at the free end of a rod in the outer row, were measured and recorded on magnetic tape. The data were then processed on a spectrum analyzer to give frequency response plots of the measured variables.

Tests were conducted using both aluminum and steel rods. The effective length of the aluminum rods was 25-3/8 in.; the steel rods were 24 in. long. Three sets of tests were run with each type of rod. In the first set of tests, the initial cluster consisted of a single element and a row was added for each successive test. The second set started with the maximum size cluster and for each succeeding test the outer

row would be removed and replaced with 4-in. long stubs. In the third set of tests, the clusters were formed from randomly selected rods.

Test Results

The results of the tests, applicable to the subject matter of this paper, are presented as sets of curves in Figs. 3 and 4. In running the tests at second mode with the larger size clusters (61 to 163 rods), large vertical g-levels were measured at the fixture. It must be remembered that the influence of these large vertical accelerations is present in the given results. Redesign of the fixture or mounting is required for future tests.

For the purpose of this analysis, a natural frequency was assumed to be equal to the corresponding resonant frequency as defined by a maximum in magnification factor. Figure 3 indicates that the natural frequencies of vibration of a rod in a cluster do not vary significantly from the corresponding natural frequency of a single rod.

The strain versus frequency plots for the center rod compared favorably with those for an instrumented outer rod. Therefore, it was assumed that an outer rod was representative of the behavior of a typical rod in a given cluster. This was an advantage in data reduction. The outside rod could easily be instrumented with a miniature accelerometer, and since acceleration is proportional to displacement, for the harmonic response at resonance, the magnification factor becomes simply the ratio of tip to input acceleration. The first and second mode magnification factors calculated in this manner are plotted in Fig. 4.

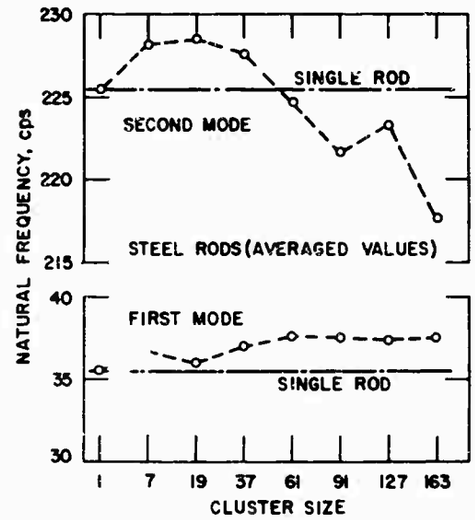

Fig. 3 - Natural frequency vs cluster size

As illustrated in Fig. 4, as the number of rods in the cluster is increased from one to the maximum of 163, the magnification factors decrease continuously. Sensitivity of the magnification factor to input amplitude is ruled out by the fact that a controlled constant amplitude input was used. Therefore, the difference in response between a single rod and a rod in a multi-rod cluster is demonstrated by the increased dissipation of energy with increasing cluster size; hence, it is important to include damping in the equation of motion for a fuel assembly.

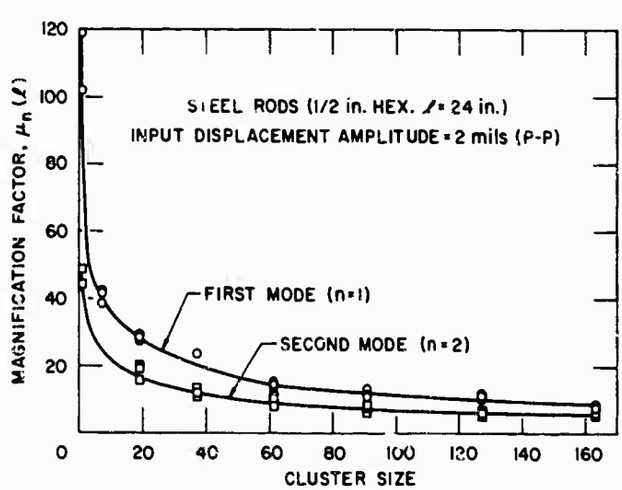

Fig. 4 - Magnification factor vs cluster size

The theoretical analysis, developed in the previous part of this paper, is based on the assumption that the natural frequencies and mode shapes are unaffected by the damping. Figure 2 shows the natural frequencies remained relatively constant with cluster size. Based on this observation one would intuitively expect the mode shapes to also remain effectively unchanged. This was shown to be the case via observation of slow-motion movies and measuring and comparing, with theory, strains at a number of locations along the length of a rod.

Damping Model Identification

To model the damping, the three damping mechanisms given by Eq. (1) were considered. The method developed earlier, for identifying linear damping models using test results obtained on a vibration exciter, will now be applied to determine the dominant damping mechanisms, describing the dissipation of energy which occurs during the vibration of simulated fuel subassemblies.

The identification scheme is based on the comparison of the ratio of first to second mode magnification factors with theoretically determined constants corresponding to "pure" forms of the proposed damping mechanisms. Using the averaged experimental data points given in Fig. 4, the ratios of first to second mode magnification factors can be calculated. The results are given in Fig. 5, where comparison can be made with ratio constants corresponding to pure viscous, stress, and load damping as obtained from Eq. (24).

The experimental data can be seen to lie between the lines corresponding to viscous and stress damping. Therefore, it is deduced that these may be the two dominant damping mechanisms to be included in the equation of motion for a fuel subassembly. The ratio of first to second mode magnification factors is employed as a means of identifying the damping mechanisms present. Since the experimentally determined ratios are approximately constant, and hence independent of cluster size, it may be concluded that the damping mechanisms themselves are invariant with cluster size.

In summary, based on a consideration of the ratio of magnification factors, viscous and stress damping are assumed to represent the dominant energy dissipative mechanisms.

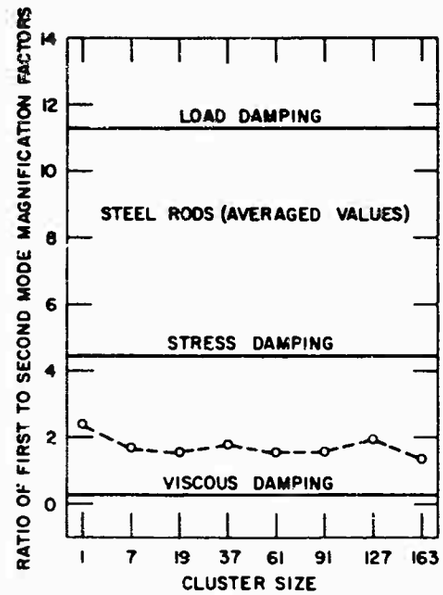

Fig. 5 - Ratio of first to second mode magnification factors as function of cluster size

Damping Coefficient Evaluation

Having selected the damping models, that is, viscous and stress damping, the remaining problem is to determine the appropriate damping coefficients to use in the models. This is easily accomplished by substituting the experimental results into Eq. (26), which was derived for a cantilevered beam. The magnification factors averaged over the three sets of tests were used. The damping coefficients, so calculated, are plotted versus cluster size in Fig. 6.

With the results given in Fig. 6, a two-mode, or two-term, approximation for the equation of motion of a rod in a particular size cluster can be written including damping. The response to an arbitrary input, e.g., $p(x,t)$, which might result from a pressure loading, would take the form

$$y(x,t) = \phi_1(x)\, q_1(t) + \phi_2(x)\, q_2(t) . \qquad (27)$$

The generalized coordinates are determined by solving

$$\ddot{q}_m + 2\zeta_m \dot{q}_m + \omega_m^2 q_m = \frac{\int_0^{\ell} p(x,t)\, \phi(x)\, dx}{EI\, \ell} , \qquad (28)$$

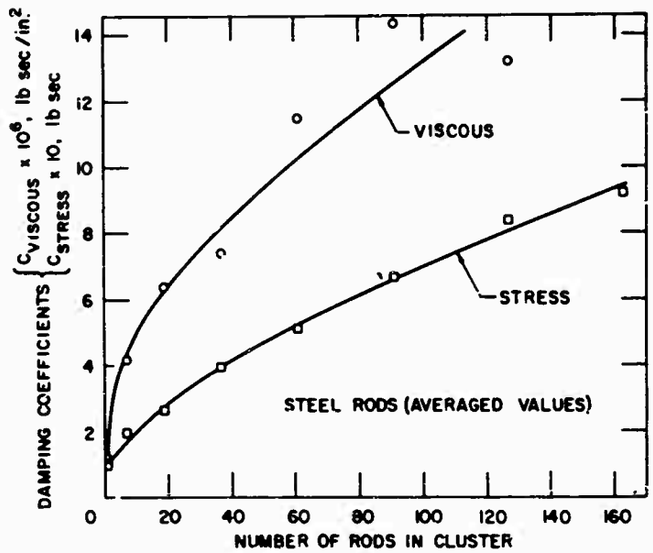

Fig. 6 - Damping coefficient vs cluster size

where

$$\zeta_m = \frac{1}{2\rho A\omega_m} \left\{ c_v + c_s \frac{1}{\ell} \int_0^\ell \phi_m \phi_m'' \, dx \right\} .$$

The coefficients c_v and c_s are read from Fig. 6 for the particular size cluster.

SUMMARY AND DISCUSSION

A study of the dynamic response of reactor fuel assembly clusters indicated the importance of including damping in the model. The effort to model the damping led to the development of a method for identifying assumed damping mechanisms and calculating the associated damping coefficients. The method is based on a comparison of experimental results with theoretically determined values. The required experimental results are easily obtained from tests performed on a vibration exciter. The method is sensitive to the ratio of first to second mode magnification factors and appears well-suited to formulating mathematical models for structural components, amenable to vibration testing, which can be modeled as two-degree-of-freedom systems.

Experimental results were obtained using a constant displacement amplitude input. Linearity is assumed in the mathematical model and in application should be checked experimentally in investigating the dependence of the magnification factor on the input displacement amplitude. Also, in conducting such tests, the fixture or connection damping is included implicitly in the results. In certain cases this may be desirable. However, it must be remembered that to obtain quantitative results from such tests, the tests must closely resemble the final application.

The mathematical model, formulated in the manner outlined in the paper, has been forced to give the correct response at the first two natural frequencies for the given input. This results from using information obtained while operating at the resonances to compute the required damping coefficients. Since a system is most sensitive to damping at, or near, a resonant frequency, it may be reasonable to expect the mathematical model to predict satisfactorily the dynamic response throughout the frequency range for which the model is derived. The ability of the mathematical model to predict system response to arbitrary loadings must be checked via experiment.

It is obvious that any two damping models might have been chosen and the coefficients forced to give the required responses at the resonances. However, the proposed models of viscous, stress, and load damping do have certain physical significance. Also, the location of experimental data in relation to the theoretical values on the plot of the ratio of magnification factors versus cluster size lends support for the use of these models to represent the energy dissipative mechanisms.

With regard to satisfying the objectives of the study, the following concluding remarks can be made:

1. The cluster size and, hence, the interaction phenomena have little, if any, effect on the natural frequencies of an individual element within the cluster.

2. The magnification factor, related to the free end of the rod, decreases continuously with cluster size, but appears to be approaching a limiting value.

3. In the attempt to determine the experiment size required to give results typical of a full-size core, the only invariant observed was the ratio of first to second mode magnification factors. This is the ratio employed in the damping model identification scheme. The magnitude of this ratio indicates that viscous and stress damping may be the dominant damping mechanisms.

ACKNOWLEDGMENTS

The authors acknowledge the work of J. A. Jendrzejczyk, W. Lawrence, and K. C. Stair in performing the experiments on the vibration exciter, solving various instrumentation problems, and processing the data.

REFERENCES

1. H. L. Langhaar, Energy Methods in Applied Mechanics, p. 283. John Wiley and Sons, New York, 1962

2. R. E. D. Bishop and D. C. Johnson, Vibration Analysis Tables. Cambridge University Press, 1956

DISCUSSION

Mr. Smith (Bell Aerosystems Co.): Did you calculate only the coefficients for the first two modes?

Mr. Wambsganss: That's right.

Mr. Smith: The results are obviously a function of the type of damping assumed in the first place. Why did you choose load damping for both a solid structure and the clustered type of structure? Wouldn't a shear type of damping be more appropriate? Secondly, do you intend to extend this to see whether you get the same sort of coefficients from other combinations of modes, for example, second and third or first and third? This might illustrate whether the types of damping that you have chosen or other types of damping could be used generally for any number of modes.

Mr. Wambsganss: I am not sure if I can answer the first question satisfactorily. Mr. Rosenberg, one of the coauthors, chose the damping models, so I cannot give a good reason why we included the low damping mechanism. In answer to your second question, I would like to extend the work. We have not done any more than that reported here.

Mr. Dobson (Knolls Atomic Power Lab.): You showed that stress damping increased with the number of rods in the cluster. Previously, I believe, you had showed decreasing amplitude or decreasing Q factor for a number of rods in the cluster. There seems to be a paradox. Stress damping normally would increase with deflection, assuming the stress increases somewhat proportionally. Could you explain the fact that apparently the stress coefficient is increasing with cluster size? Isn't the stress coefficient you are trying to determine related to material damping? Or is it unknown exactly what you are determining?

Mr. Wambsganss: Actually it is unknown, because the damping is due to an interaction of all the rods and is not necessarily material damping. We are looking for some damping mechanism that we can use to describe what is going on within a nuclear reactor core where these rods can interact, rub together, and provide damping in that manner, so this is not related directly to material damping.

* * *

EFFECT OF AIR DAMPING ON STRUCTURAL FATIGUE FAILURE*

John R. Fagan
Radio Corporation of America
Princeton, New Jersey

The response of a single-degree-of-freedom resonant system is dependent on the amount of damping present; the stress induced is dependent on the system response. Fatigue data of most structural materials can be expressed mathematically as a power function relating stress to number of cycles to failure. After determining the expression described for sine and random forcing excitations, it is possible to plot curves relating the ratio of damping parameters in air and in a vacuum to the time to failure of the structure. The principal conclusion is that when low-mass large-area structures are vibration excited in a vacuum, they should be tested in a manner that will reflect the lack of air damping on the structure. This consideration is especially pertinent in relation to the application to lunar ascent and descent functions, such as are now being planned.

INTRODUCTION

Significant levels of structural excitation will probably be generated during lunar ascent and descent functions. Because of the environment, the coupling will be almost exclusively through the hardware, and this condition must be recognized during environmental testing. This analysis does not encompass the entire problem but merely serves to indicate the significance of the impact of these factors on the test specification.

The response of a single-degree-of-freedom resonant system is effectively described by the Q of the system. For a sine input dwelling at resonance, the response ratio is Q; for a flat random input, the response ratio is approximately $(Qf_n)^{1/2}$, where f_n is the natural frequency of the system [1]. The units determining the ratio are g rms divided by g rms. For our purposes, we desire a ratio that consists of the displacement response to the g rms input to the system; this ratio is proportional to $(Q/f_n)^{1/2}$ (Fig. 1). Now

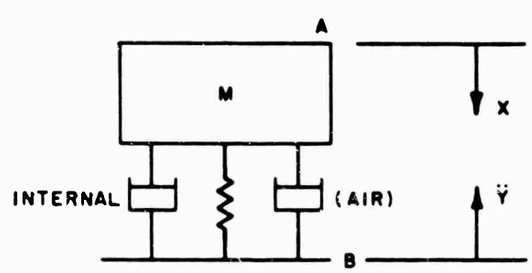

$$\frac{X}{\ddot{Y}} \propto \sqrt{\frac{Q}{f_n}}$$

X = RELATIVE DISPLACEMENT RESPONSE A WITH RESPECT TO B

Ÿ = ACCELERATION INPUT

Fig. 1 - Schematic representation of displacement response ratio

$$Q = 1/2\zeta = \pi/\delta \qquad (1)$$

for light damping, where ζ is the damping ratio and δ_t is the total log decrement (decay of amplitude at a logarithmic rate) of the system. Let

$$\delta_t = \delta_i + \delta_a, \qquad (2)$$

*This paper was presented by H. W. Lekuch, Radio Corporation of America, Princeton, N. J.

where δ_i is the internal log decrement of a system and δ_a is the log decrement due to air damping.

FATIGUE FAILURE FOR CASE OF SINE EXCITATION

All structural materials have a certain fatigue life described by the well-known S-N fatigue curves, as exemplified in Fig. 2. These curves follow a law that can be mathematically expressed as

$$NS^b = C, \tag{3}$$

where B and C are material constants [2], N is the number of stress cycles to failure, and S is the peak stress. Also $N = f_0T$ and substitution into Eq. (3) results in

$$Tf_0 S^b = C, \tag{4}$$

where T is the total time to actual fatigue failure of the material.

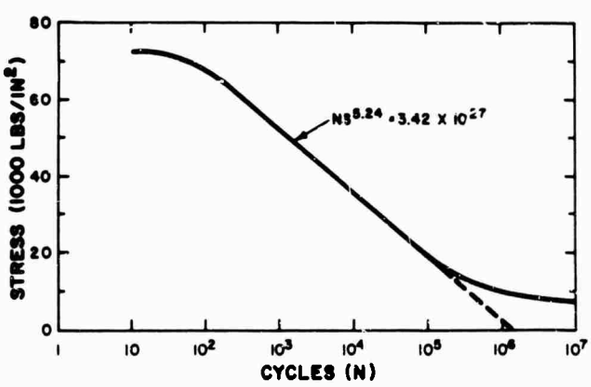

Fig. 2 - Typical S-N fatigue curve for aluminum alloy

A simple system has a response, at resonance, described by

$$X/X_0 = 1/2\zeta \cong \pi/\delta_t, \tag{5}$$

where X is the response amplitude and X_0 is the zero-frequency (static) deflection.

Since $S = AX$, where A is the coefficient relating stress to displacement,

$$S_a = A\pi X_0/\delta_t$$

at atmospheric pressure, and

$$S_v = A\pi X_0/(\delta_t - \delta_a) \tag{6}$$

in vacuum. Setting a ratio,

$$S_a = S_v(1 - \delta_a/\delta_t). \tag{7}$$

Solving for T in Eq. (4) and establishing a ratio of T_v to T_a, where T_v is time to failure in a vacuum and T_a is time to failure at atmospheric pressure, results in

$$T_v/T_a = (1 - \delta_a/\delta_t)^b. \tag{8}$$

FATIGUE FAILURE FOR CASE OF RANDOM EXCITATION

The problem is effectively described by Crandall and Mark [2]. The mean square stress response of a simple resonator to an ideal white-noise input is (Fig. 3)

$$S^2 = A^2 \frac{W_0}{8} \frac{(386)^2}{\zeta(2\pi f_n)^3}, \tag{9}$$

where A^2 is a coefficient relating S^2 to the mean square of the displacement response, W_0 is the input spectral density level (g^2/cps), ζ is the damping ratio, and f_n is the system natural frequency. Also, $\zeta = \delta_t/2\pi$; therefore,

$$S_{rms} = A\sqrt{\frac{W_0}{8} \frac{(386)^2}{\delta_t(2\pi)^2 f_n^3}}. \tag{10}$$

It is now necessary to select a failure theory. The Palmgren-Miner hypothesis is general in scope and the most widely used (within its limits) of any [2]. The theory is simply stated as:

$$D = \sum_{i=1}^{\infty} [n(S_i)/N(S_i)], \tag{11}$$

where $N(S_i)$ is the number of cycles to failure in a constant-amplitude fatigue test with stress amplitude S_i, $n(S_i)$ is the number of cycles experienced at stress amplitude S_i, and i is an arbitrarily assigned stress level (i = 1,2,3, etc.). When D = 1, failure occurs.

Cyclical stress damage is dependent on the stress peaks. The distribution of peaks in a random process (if the process is assumed to be normal or Gaussian) is Rayleighian. Therefore, to determine $n(S_i)$ for any specific S_i, it is necessary to multiply f_nT by the probability of the occurrence of these peaks. Thus,

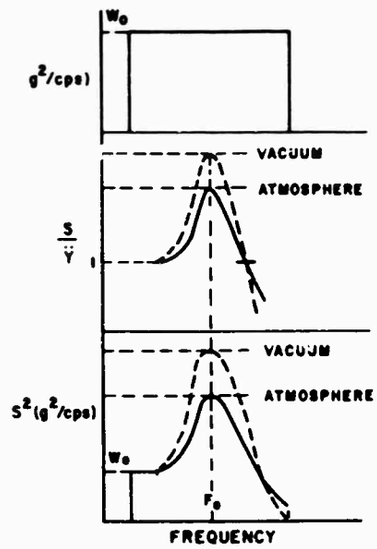

Fig. 3 - Curve of resonator response to flat noise input

$$n(S_i) = f_n T \Delta P(S_i) , \tag{12}$$

where $f_n T$ is the total number of cycles of the responding system and $\Delta P(S_i)$ is that fraction of all the peaks associated with stress cycles $n(S_i)$. It can be further stated that $\Delta P(S_i)$ is the incremental area under the probability density curve of a Rayleigh distribution.

To determine the damage contribution of a specific $n(S_i)$, we divided by $N(S_i)$

$$n(S_i)/N(S_i) = [f_n T \Delta P(S_i)]/N(S_i) . \tag{13}$$

The total damage is the sum of the damage contributions at all the stress amplitudes:

$$\text{Accumulated damage} = f_n T \int_0^\infty \frac{d[P(S)]}{N(S)} , \tag{14}$$

where $d[P(S)] = S/S_M^2 \exp(-S^2/2S_M^2)\, ds$, and S_M is the mean stress of the process. Now

$$\text{Accumulated damage} = f_n T \int_0^\infty \frac{S^{b+1}}{CS_M^2} \exp(-S^2/2S_M^2) ds . \tag{15}$$

Solving this expression results in

$$\text{Accumulated damage} = (f_n T/C)\left(\sqrt{2}\, S_{rms}\right)^b \Gamma(1 + b/2) , \tag{16}$$

where T is the duration of the excitation.

For failure to occur, accumulated damage becomes unity, and we can write

$$1 = (f_n T/C)\left(\sqrt{2}\, S_{rms}\right)^b \Gamma(1 + b/2) . \tag{17}$$

Equation (9) at atmospheric pressure is

$$S_{rms} = A \sqrt{\frac{(386)^2}{8} \frac{W_0}{(2\pi)^2 f_n^3} \frac{1}{\delta_t}} , \tag{18}$$

and in vacuum is

$$S_{rms} = A \sqrt{\frac{(386)^2}{8} \frac{W_0}{(2\pi)^2 f_n^3} \frac{1}{\delta_t - \delta_a}} . \tag{19}$$

Substitution in Eq. (17) results in

$$T_v = \frac{C}{f_n} \frac{1}{\left[\sqrt{2}\, A \sqrt{\frac{(386)^2}{8} \frac{W_0}{(2\pi)^2 f_n^3} \frac{1}{\delta_t - \delta_a}}\right]^b} \Gamma\, 1 + \frac{b}{2}$$

and (20)

$$T_a = \frac{C}{f_n} \frac{1}{\left[\sqrt{2}\, A \sqrt{\frac{(386)^2}{8} \frac{W_0}{(2\pi)^2 f_n^3} \frac{1}{\delta_t}}\right]^b} \Gamma\, 1 + \frac{b}{2} ,$$

and the ratio is

$$T_v/T_a = (1 - \delta_a/\delta_t)^{b/2} . \tag{21}$$

The constant b of Eq. (3) ranges between 5 and 20, depending on the material. T_v/T_a for random excitation and for values of b from 5 to 20 is plotted against air damping (δ_a/δ_t) in Fig. 4.

An attempt to determine the air-damping decrement was made by Stevens and Scavullo [3]. They state that the air damping can be as small as 5 or as large as 83.3 percent. For the smaller value and a typical material constant of 6.09,

$$T_v/T_a = (1 - 0.05)^{6.09/2} = 0.856 .$$

This means that if the structure fails in 10 min at atmospheric pressure with 5 percent air damping, it will fail in 8.56 min in vacuum under equal conditions of excitation. For 83.3 percent of air damping,

$$T_a/T_v = (1 - 0.833)^{6.09/2} = 0.0043 .$$

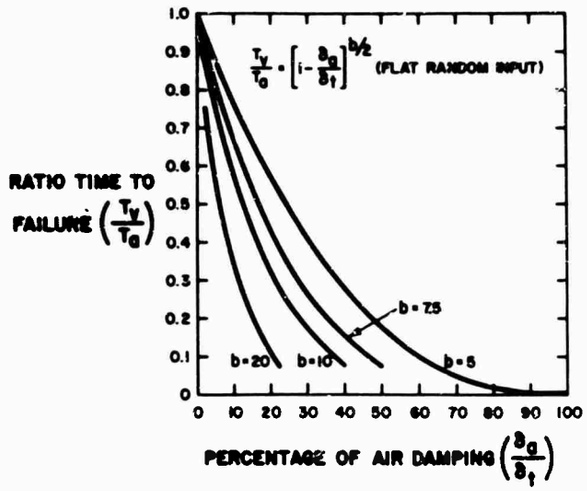

Fig. 4 - Curve of time to failure in vacuum vs percent of air damping

Thus, if the structure fails in 10 min at atmospheric pressure, it will fail in 0.043 min in a vacuum environment.

The statistical variation of the solution has not been attempted; an excellent discussion of the effect of the magnitude of damping is given by Crandall and Mark [2].

Intuitively, air damping would exhibit the greatest effect on structures that have large areas and small masses associated with these areas (panels, printed-circuit boards, sheet metal beams, radar antennas, and solar panels).

CONCLUSIONS

The subject of the vibrating structure in a vacuum is of no interest when no excitation exists; the most severe vibration environment presently occurs during booster lift-off and at Mach 1 velocities. Both of these conditions occur within the Earth's atmosphere. Further, rocket firings in space have been of minor significance and short duration. With the advent of Apollo, the requirements for withstanding relatively severe excitations in a vacuum first appear.

Lunar descent and ascent functions will probably result in the generation of significant levels of structural excitation. Obviously, no acoustic coupling can exist in the lunar environment and structural vibration would be transmitted almost exclusively through the hardware; the environmental test must include consideration of this effect. The analysis presented here hardly describes the entire problem; it does, however, indicate the significance of the test specification. (Should testing be specified for longer times, or should the combined vibration-vacuum environment be simulated? Are there other failure modes that are affected?) Any performance parameter affected by an increased level of response would serve to lower the overall reliability of a system.

REFERENCES

1. C. T. Morrow, Shock and Vibration Engineering, Chapter 3, p. 87. John Wiley and Sons, New York, 1963

2. S. H. Crandall and W. D. Mark, Random Vibration in Mechanical Systems, Chapter 3, Sections 3.5 and 3.6. Academic Press, New York, 1963

3. D. G. Stevens and M. A. Scavullo, "Effect of Pressure Environment on Damping of Vibrating Structures," Shock and Vibration Bull. No. 34, Part 5, pp. 197-203, Feb. 1965

DISCUSSION

Mr. Plunkett: I think the estimate as to how much influence air damping can have is a little conservative, because we know from other results that air damping in connection with joint damping may have an influence of perhaps 99 percent rather than only 40 percent. In this case, the change in life would be very significant.

Mr. Lekuch: We agree with that. We have not done any specific testing, but we have seen cases where structures that have undergone vibration in vacuum have responded to an extent that we did not expect. I should refer again to the paper by Stephens and Scavullo [3].

Mr. Jacisin (Bell Telephone Labs.): You made a statement that the lifetimes of these structures were reduced in vacuum. Possibly this conclusion was reached primarily from an air damping standpoint. There has been much work done on fatigue of various metals, a phenomenon existing here, which shows that the fatigue is increased considerably in vacuum. Have you also investigated this effect?

Mr. Lekuch: We have not looked into the fatigue mechanism; we simply accepted, in this case, the Miner failure hypothesis. I realize that a great deal of investigation into fatigue in vacuum has been made, but we have not specifically gone into it.

* * *

DEVELOPMENT OF DAMPED MACHINERY FOUNDATIONS

W. Blasingame and E. V. Thomas
Navy Marine Engineering Laboratory
Annapolis, Maryland

and

R. A. DiTaranto
Pennsylvania Military Colleges
Chester, Pennsylvania

R. A. DiTaranto

INTRODUCTION

A program designed to reduce the vibratory energy transmitted through machinery foundations in naval ships is currently under way at the Navy Marine Engineering Laboratory (MEL), Annapolis, Md. The objective is being pursued through the development of damped machinery foundations capable of attenuating vibratory energy before it reaches a ship's hull where it can be transformed into acoustical energy and radiated overboard as undesirable noise. To obtain a reduction in radiated noise, it is proposed that foundations be fabricated from highly damped laminated plates and a pipe-within-a-pipe configuration separated by a viscoelastic material. These members, composed of alternate layers of steel and viscoelastic material, have been shown to dissipate large amounts of vibratory energy through cyclic shear induced in the viscoelastic material. For laminated plates the dissipation of energy occurs through flexural vibration, whereas the pipe-within-a-pipe member produces damping primarily by shearing the viscoelastic material through axial vibration. However, damping occurs for this configuration for all planes of vibrations. The program has been directed towards the development of highly damped structural laminates and means of being able to design and predict their performance, the investigation of the effects of dynamic mechanical properties of viscoelastic material on composite damping and the reliability in measuring these properties, and the design and evaluation of damped machinery foundations. In particular, the program has led to a general specification of test samples for damping evaluation, analytical means for predicting damping and determining composite behavior, development of a method for reasonably determining the dynamic properties of a particular viscoelastic material, and the design and evaluation of laminated foundations for effectiveness in reducing vibration transmission. The problems and highlights of the development program are described in this paper.

ANALYSIS OF LAMINATED BEAMS

To design foundations properly with laminated material, it is necessary to be able to predict the composite loss factor vs natural frequency and the natural frequencies of the system if the elastic and viscoelastic physical properties, cross-sectional geometry and end conditions are known.

Historically the analyses of laminates began with the investigation by Oberst [1] who predicted the composite loss factor vs natural frequency for an elastic plate having an unconstrained viscoelastic layer. In this case the primary mechanism of dissipation is the extension and compression of the viscoelastic material as the composite is subjected to bending. It is found that the composite loss factor, η, in this case is

$$\eta = \frac{\eta_1 E_1' H_2 (3H_1^2 + 6H_2H_1 + 4H_2^2)}{EH_1^3 + EH_2(3H_1^2 + 6H_2H_1 + 4H_2^2)} \qquad (1)$$

where

E = elastic modulus of elastic material;

E' = real part of elastic modulus of viscoelastic material;

$\eta = E_1''/E_1'$, loss of viscoelastic material;

H_1 = thickness of elastic layer; and

H_2 = total thickness of viscoelastic layer.

It was further found that a limited amount of damping is obtained by the unconstrained viscoelastic layer configuration. In the late 1950's, Kerwin et al. [2] investigated the damping capability of constrained layers, i.e., a material composed of alternate elastic and viscoelastic layers. They developed a bending theory for constrained layers based on several reasonable assumptions:

1. The elastic modulus of the viscoelastic is small compared to that of the elastic layer and thus extensional forces in the viscoelastic layer may be neglected.

2. The predominant motion of the viscoelastic material is due to shear.

3. The beams are simply supported or infinitely long.

It was found that more damping could be obtained over a discrete frequency range by using the laminated beams or constraining the viscoelastic material. With respect to this program, Kerwin's results left several questions unanswered:

1. What is the effect of having more than three layers?

2. Since the beams to be considered by MEL are finite, what is the effect of end conditions, other than simply supported, on the composite loss factor and natural frequencies?

3. What is the effect on the composite loss factor of varying geometric and physical properties of the laminated beam?

Analytical investigations were conducted in an effort to answer these questions. The results of Kerwin et al. were programmed for a high-speed digital computer in which the composite loss factor was found for three- and five-layer laminated beams. These computer results are reported in Ref. 3, and the salient curves are shown in Figs. 1 and 2. It is seen that for a given overall thickness, the composite loss factor is higher for a five-layer laminate at the optimum and higher frequency range than that obtained for a three-layer laminate for the same viscoelastic material. Higher values of the viscoelastic material loss factor β is seen generally to produce higher composite loss factors. In the low-frequency region, however, there appears to be a value of β between 1 and 2 for which maximum damping is obtainable. Increasing the shear modulus of the viscoelastic material produces a frequency shift of the damping curve.

Many of the results obtained in Ref. 3 can be seen better in a curve of η vs h_1 recently obtained in the course of this program (Fig. 3). The parameter h_1 is given by

$$h_1 = \frac{12\,\gamma E\, H_2^2\, \omega_2^2}{G_1^2}\,, \qquad (2)$$

where γ is the average mass density of the composite, G_1 is the real part of the shear modulus of the viscoelastic material, H_2 is the thickness of the viscoelastic layer, and ω_1 is the natural frequency of vibration. It can be seen that the variation of η vs ω with variations of G_1, β and H_2 can be predicted. Thus, a typical η vs ω curve will shift to the left as G_1 is increased. The curve will move up bodily as β increases and shift to the left for increasing H_2. This last curve of η vs h_1 is based on a sandwich construction in which the thickness of the viscoelastic layer is small compared to the thickness of the two equal elastic layers. Thus, one can find the composite loss factor of a three-layer sandwich beam if G_1, β, H_2 and ω are known.

The results of DiTaranto [4], in which the differential equation of motion is derived for a three-layer beam, indicate that composite loss factor vs frequency curve is independent of the boundary conditions. This finding implies that the results of Kerwin for an η vs ω curve of a simply supported beam are applicable to all nondissipative end conditions. A series of tests conducted at MEL on the effect of end conditions [5] has shown good correlation with the theoretical results.

The effect of the viscoelastic layers on the natural frequencies of vibration of laminated beams is presently being considered and forms the basis of current results. The natural frequencies can be calculated using the results of Ref. 4, but the resulting set of equations must be satisfied in general by the nulling of a 12×12 determinant. In itself, this is not an impossible task, but for all the possible variations in each elastic layer thickness, viscoelastic layer

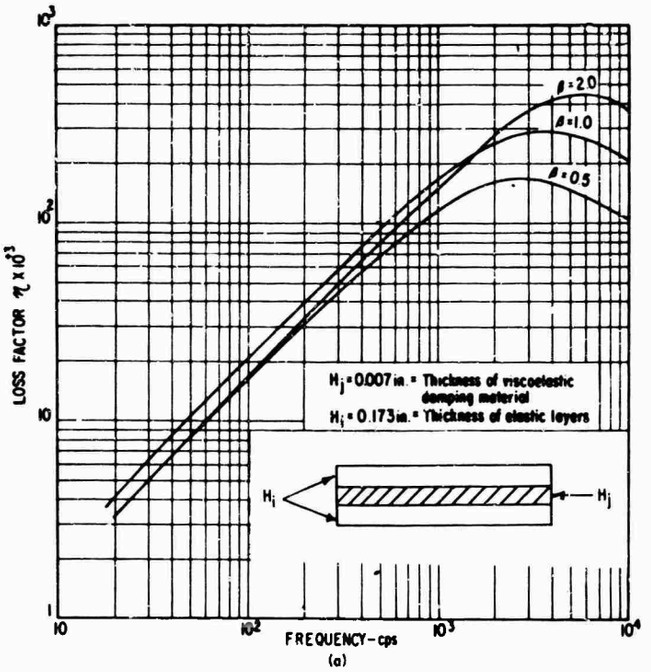

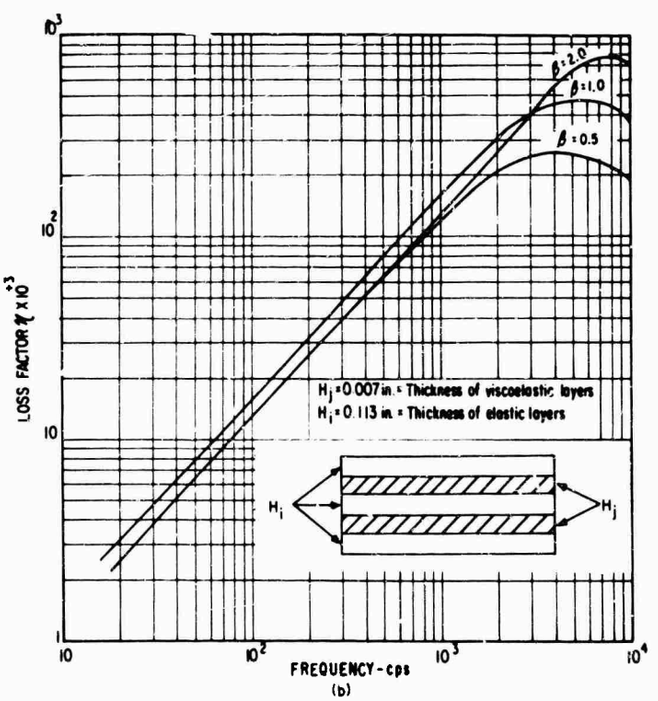

Fig. 1 - Computed composite loss factor values: (a) for three-layer laminated beam with cross-sectional area equal to that of five-layer beam, and (b) for five-layer laminated beam

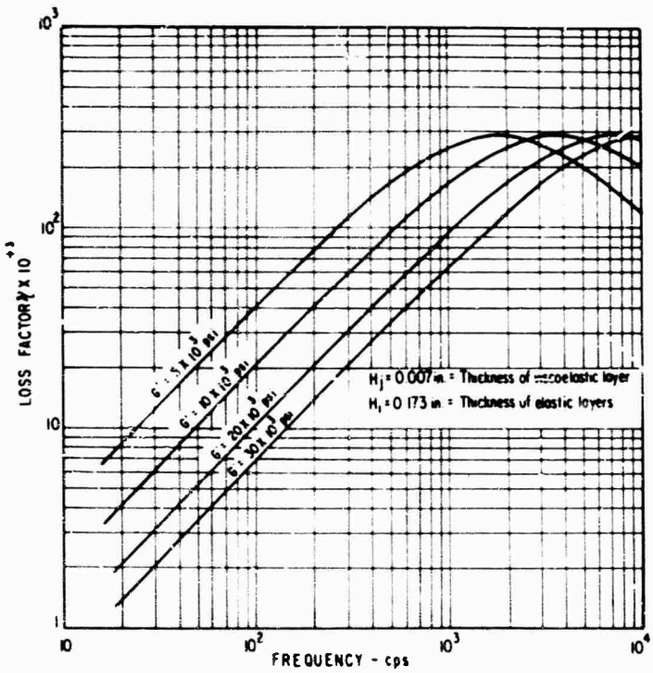

Fig. 2 - Loss factor values for three-layer laminated beam computed for several values of shear storage modulus and constant value of viscoelastic material loss factor

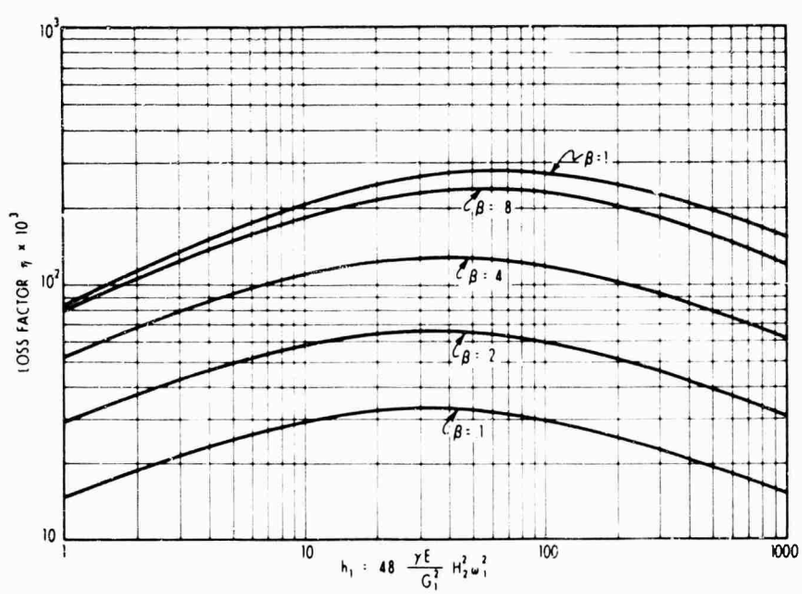

Fig. 3 - Generalized composite loss factor values for three-layer laminated beam

thickness, physical properties of the materials plus different end conditions, the problem is best handled on an individual need-to-solve basis.

From a design standpoint, the determination of the natural frequencies by solving a 12×12 determinant is too sophisticated and difficult to use. Therefore, a simplified approach has been recommended. This simplified method uses the frequency relation for a sandwich beam having a thin viscoelastic layer. The natural frequencies may be calculated from the expression

$$\omega_1^2 = \omega_{10}^2 [1 + 6\alpha] , \qquad (3)$$

in which ω_1 is the natural frequency of the composite sandwich beam having a thin viscoelastic layer, and ω_{10} is the natural frequency of one elastic layer carrying its own weight plus half of the weight of the viscoelastic layer, i.e.,

$$\omega_{10}^2 = \frac{a_n}{L^2} \left[\frac{EI}{\rho_e}\right]^{1/2} ,$$

where a_n is the mode number associated with the end conditions, L is the length of the beam, EI is the stiffness of one elastic layer, ρ_e is the mass/unit length of the elastic layer plus half the viscoelastic layer, and α is a shear parameter which varies with a_n or, in effect, ω_{10}. In particular,

$$\alpha = \frac{R_1 [\lambda_0 + R_1 S (1 + \beta_2)]}{\lambda_0^2 + 2\lambda_0 S R_1 + S^2 R_1^2 (1 + \beta_2)} , \qquad (4)$$

where

$$\lambda_0 = \frac{a_n}{L^2} ,$$

$$R_1 = \frac{G_1 b}{2H_2 K_1} ,$$

$$S = \frac{K_1 + K_3}{K_1} ,$$

and

$$K_i = Eb\, 2H_i , \quad i = 1, 3 .$$

It is to be noted that for a small a_n (low ω), α is approximately equal to 1/2 so that the factor $(1 + 6\alpha)$ equals 4. When this condition occurs, we have the case for both elastic layers acting together as a solid beam. As a_n becomes large (ω large), α approaches zero and each elastic layer vibrates, in effect, by itself as though it were completely isolated. Table 1 shows values of a_n for various end conditions. This table can be very helpful in predicting the natural frequency of a sandwich beam.

The results of the analytical work in this program places the designer in the position of being able to predict natural frequencies and associated composite loss factors for a sandwich beam having a thin viscoelastic layer. These predictions may be made if the cross-sectional geometry and physical properties of the elastic and viscoelastic materials are known. The curves shown herein and found in the references enable one to design highly damped laminates.

Equations are available for determining the natural frequencies and composite loss factors of various three-layer laminates, but the equations are complicated and require the use of a high-speed digital computer. A computer program is available, however, for predicting the loss factor as a function of frequency for laminated beams with up to 13 layers. Verification of the analytical predictions for damping of laminated beams have been successfully made by Douglas and Longley [6].

DYNAMIC SHEAR MODULUS MEASUREMENTS

Since the laminated materials considered for use are composed of layers of elastic and viscoelastic materials, the physical properties of these materials are important. Physical properties of elastic materials are well known for steel and aluminum, but are not well defined for viscoelastic materials. The nature of viscoelastic materials is such that the shear modulus, which is of interest in the flexural damping of laminates, is a function of temperature, time and/or frequency. From the vibratory damping standpoint, the shear modulus is considered a function of temperature and frequency and written in complex form by $G^* = G_1(1 + i\beta)$, where G_1 is the material loss factor β. To design laminates, the values of G_1 and β must be known for several temperatures and over a broad frequency range.

In the course of this program, it became apparent that measuring the shear modulus of viscoelastic materials was difficult. The extent of this difficulty was not known. Four laboratories actively determining the dynamic mechanical properties of viscoelastic materials were surveyed to ascertain the degree of

TABLE 1
Values of Mode Numbers Associated with End Condition

Beam Condition	Diagram	a_n [a]	
		General Relation	Specific Relation
Cantilever		$a_n \left(n - \frac{1}{2}\right)^2 \pi^2$ for $n \geq 2$	$a_1 = 3.52$ $a_2 = 22.0$ $a_3 = 61.7$ $a_4 = 121.0$ $a_5 = 200.0$
Simply supported	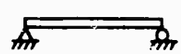	$a_n = (n\pi)^2$	$a_1 = 9.87$ $a_2 = 39.5$ $a_3 = 88.9$ $a_4 = 158.0$ $a_5 = 247.0$
Free-free		$a_n \left(n + \frac{1}{2}\right)^2 \pi^2$	$a_1 = 22.0$ $a_2 = 61.7$
Fixed-fixed	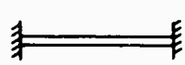	[same a_n for Free-free and fixed-fixed]	$a_3 = 121.0$ $a_4 = 200.0$ $a_5 = 298.2$
Fixed-pinned	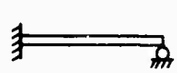	$a_n \left(n + \frac{1}{4}\right)^2 \pi^2$	$a_1 = 15.4$ $a_2 = 50.0$ $a_3 = 104.0$ $a_4 = 178.0$ $a_5 = 272.0$

[a] $\lambda_0 = \frac{a_n}{L^2}$.

agreement in measuring the shear moduli of two viscoelastic materials with good damping characteristics [7]. Figure 4 shows the materials used and the geometry required by two of the laboratories. The black material is a neoprene normally produced in sheets. The cylinder and block specimens were especially molded for two of the four participants. The white-appearing material is a filled polyvinyl chloride (PVC). Different apparatus was used by the four laboratories; two laboratories used the Fitzgerald apparatus, one used the flexometer developed by Painter, and the other used a torsional shear apparatus developed by Baltrukonis.

Fig. 4 - Viscoelastic materials used for dynamic tests in survey

Complete data were desired on the storage modulus and the loss modulus over a wide frequency and temperature range, but no participant was able to supply this. Typical reported data are shown in Figs. 5 and 6. Figure 5 presents results for the shear storage modulus of the PVC at 60°F. Three of the four participants reported, but the frequency coverage and agreement in results were limited. Results for the neoprene material were similar. Figure 6 shows typical results reported by all participants. Though the frequency coverage was improved, the differences in measured shear modulus values were large. One participant reported measurements which fluctuated widely over the frequency range. The dashed curve is an average of the points with an envelope showing the extent of fluctuations.

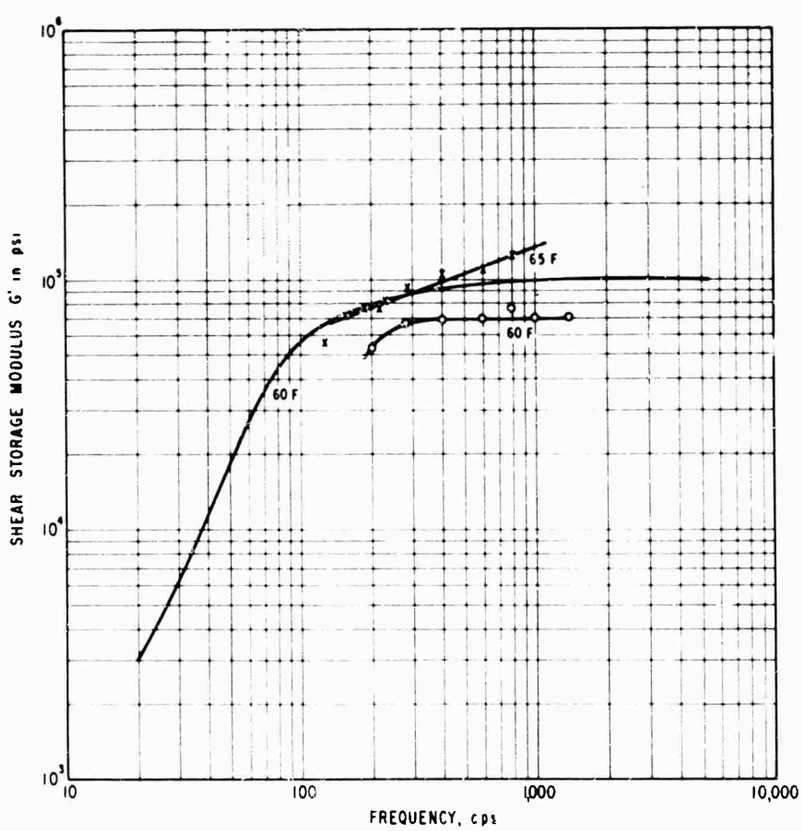

Fig. 5 - Comparison of shear storage modulus measurements for polyvinyl chloride damping material as measured by three activities

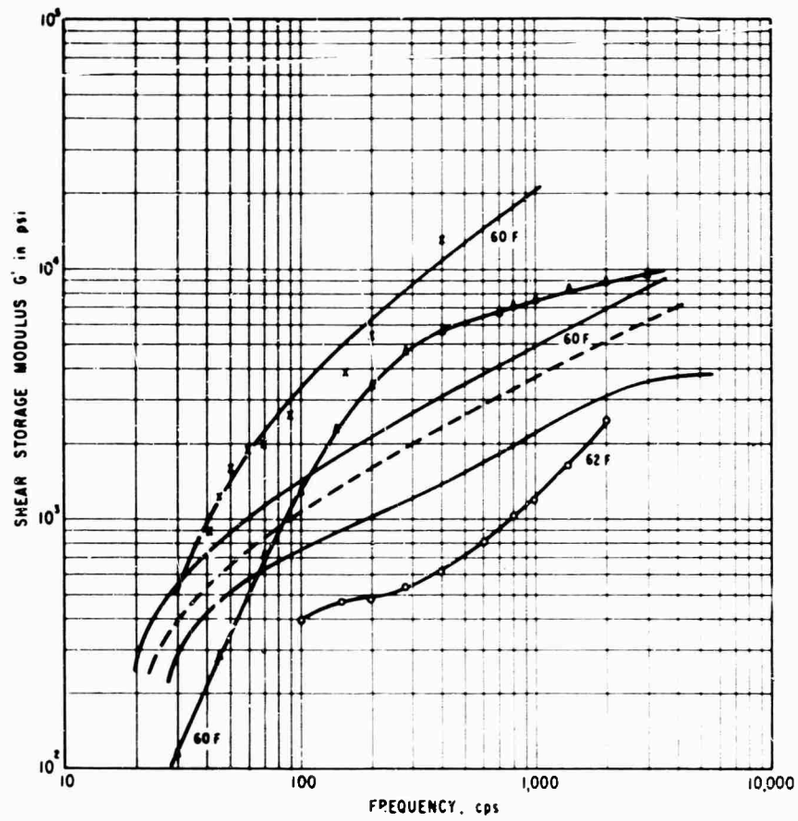

Fig. 6 - Comparison of shear storage modulus measurements for neoprene damping material as measured by four activities

The results of this survey indicated a degree of discrepancy in the measurement of the shear modulus of viscoelastic materials. Although the discrepancy may, in part, be attributed to differences in samples and strain amplitude, the survey strongly indicated that the apparatus and measuring techniques are the prime source of difficulty.

In view of the results obtained in the survey, a method was developed by Roscoe et al. [8] to measure the shear modulus and loss factor of viscoelastic materials using a three-layer laminated beam. The method utilizes the measured composite loss factor at resonant frequencies and the analytical relation derived by Kerwin et al. [2] for the damping of a sandwich beam. This method yielded repeatable and reliable measurements for the shear storage modulus from 100 to 40,000 psi and shear loss factor from 0.2 to 2.0 over a frequency range from 20 to 5000 Hz. Though this method has limitations, it offers a means of evaluating the damping material for the purpose of recommending cross-sectional changes of the composite and changes in the material dynamic properties.

FOUNDATION DESIGN AND TESTING

Concurrent with the analytical investigation and shear modulus tests, a major portion of the damping program was concerned with the design, fabrication and testing of representative machine foundation structures [9]. Figures 7 and 8 show solid steel and laminated foundation structures which were fabricated for a motor-pump. Laminated material which had shown excellent damping characteristics was employed in fabricating the damped foundation. Because of the low strength characteristic associated with highly damped laminates, 3/8-in. Huck bolts were placed on approximately 2-in. centers throughout the bedplates to add stiffness. The foundation legs were originally composed of several laminated members bolted together to gain required strength. Since it was impossible to weld this material, mounting the foundation for tests was accomplished by welding brackets to a test vessel hull to which the foundation was bolted. For comparison of vibration transmission losses, the solid steel foundation was mounted for test on the hull in the place where the laminated structure was tested.

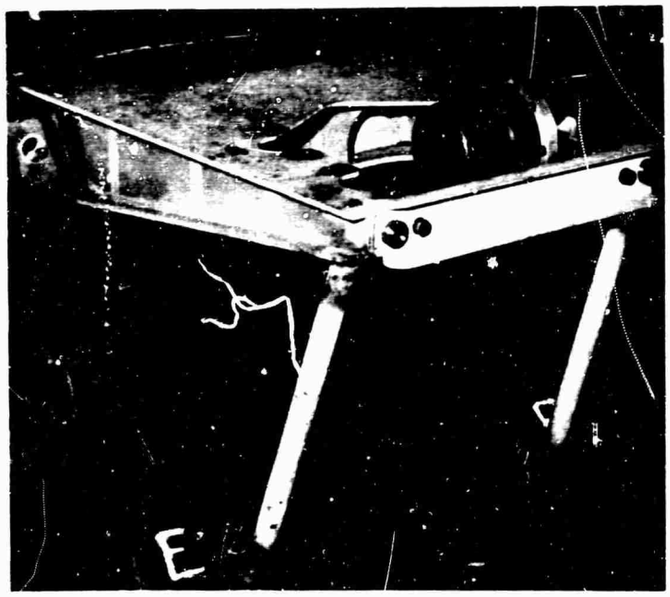

Fig. 7 - Solid steel machinery foundation

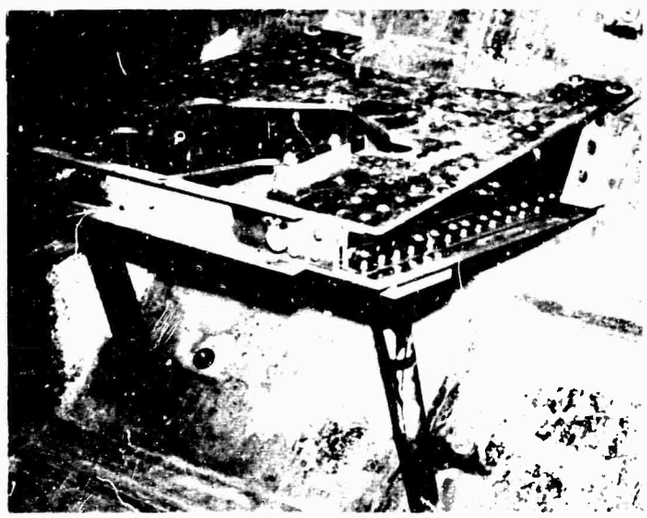

Fig. 8 - Laminated machinery foundation

Mechanical impedance tests were made on each foundation to determine the level of vibration transmitted to the hull, and overboard measurements were taken simultaneously to determine radiated noise. Results of these measurements showed that no reduction in radiated noise was accomplished with the laminated foundation. An analysis of the problem pointed to the laminated legs as a direct transmission path to the hull. The laminated legs were being excited axially, thereby producing no shear in the viscoelastic material. To compensate, the laminated legs were replaced by legs in the form of a pipe-within-a-pipe separated by a viscoelastic material (Fig. 8). Figure 9 shows the attenuation effects for this modification. It is seen that the use of damped pipe legs with the riveted foundation in place of the laminated ones resulted in negligible vibration transmission loss.

A further evaluation of the laminated foundation led to the conclusion that to gain substantial attenuation in vibration transmission

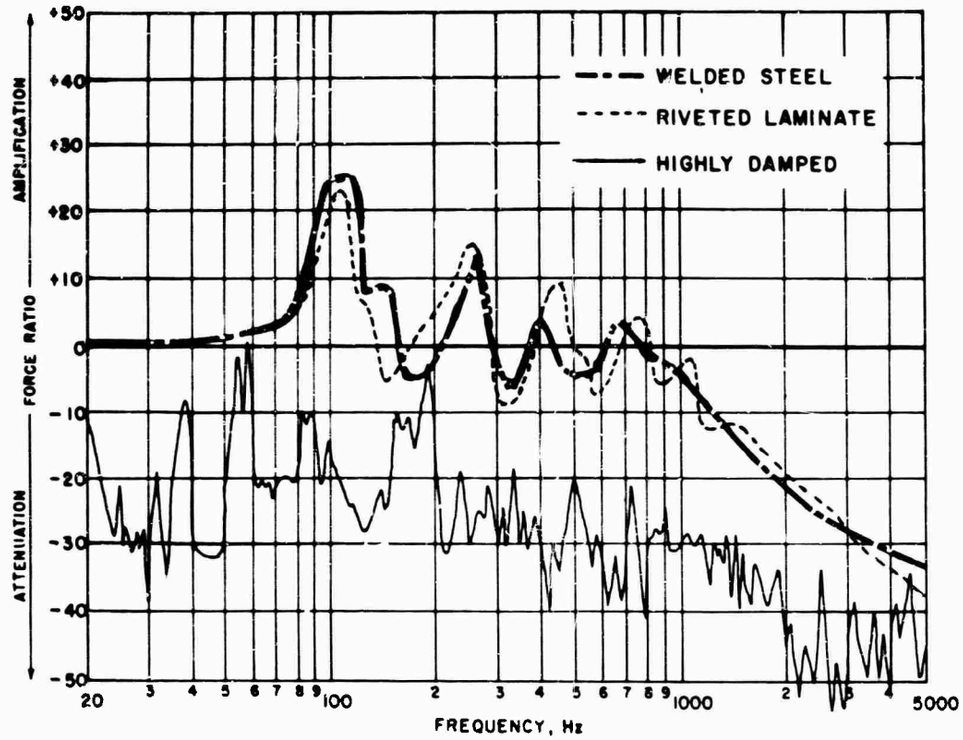

Fig. 9 - Comparison of damping effectiveness for machinery foundations

and a reduction in radiated noise, laminated materials must be used such that shearing of the viscoelastic material occurs. A completely redesigned motor-pump foundation (Fig. 10) was fabricated using pretwisted laminated beams. The damped pipe legs were also redesigned to provide a viscoelastic cushion at the bottom of the outer pipe which served as an isolation mount for the foundation. Brackets were used to attach the foundation to the hull, while the new design of the legs allowed them to be welded. An evaluation of this structure (Fig. 9) revealed that a substantial reduction in overboard noise had resulted. The application of laminated beams in present foundation designs appeared promising but limited, however, in machinery support structures. The length of the laminated members made the pretwisted foundation unacceptable for present use on operating vessels because of space limitation. This design, however, could be incorporated in future design of vessels so that the length of the laminated members is considered.

The damping obtained with the pipe-within-a-pipe configuration led to the fabrication of viscoelastic supported pipe-within-a-pipe portal frame foundations. Figure 11 shows a damped portal frame foundation (foreground) and an undamped one mounted for tests. Results of the tests are shown in Fig. 12. It is seen that, in general, a large reduction in overboard noise was obtained at the resonant frequencies with the damped pipe members. Because of the manner in which these foundations are designed, their application to immediate use on operating vessels seems practical.

The damping effectiveness of foundations are evaluated following the approach of Wright et al. [10] with several modifications. Evaluation follows the mobility matrix for three axis inputs and neglects rotational inputs. Experimental inverse mobilities are measured on a transfer basis from each input terminal to each output terminal. A combination of transfer inverse mobility with the termination mobility yields the insertion factor defined as

$$T_i^j = \frac{\text{transfer mobility with structure in place}}{\text{radiator mobility without structure in place}}$$

$$= \frac{V_{out}/F_{in}}{V_{out}/F_{out}} = \frac{F_{out}}{F_{in}} , \qquad (5)$$

where $i = 1, 2, 3, 4$, and $j = 1, 2, 3, 4$. Thus, the result of the experimental inverse mobility measurements is 16 insertion factors for each direction of input excitation. A total of 48

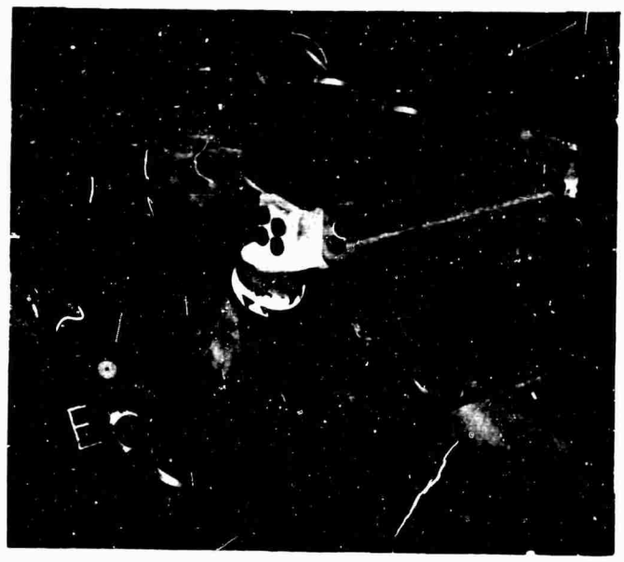

Fig. 10 - Highly damped machinery foundation

Fig. 11 - Damped portal frame foundation (foreground) and undamped portal frame foundation

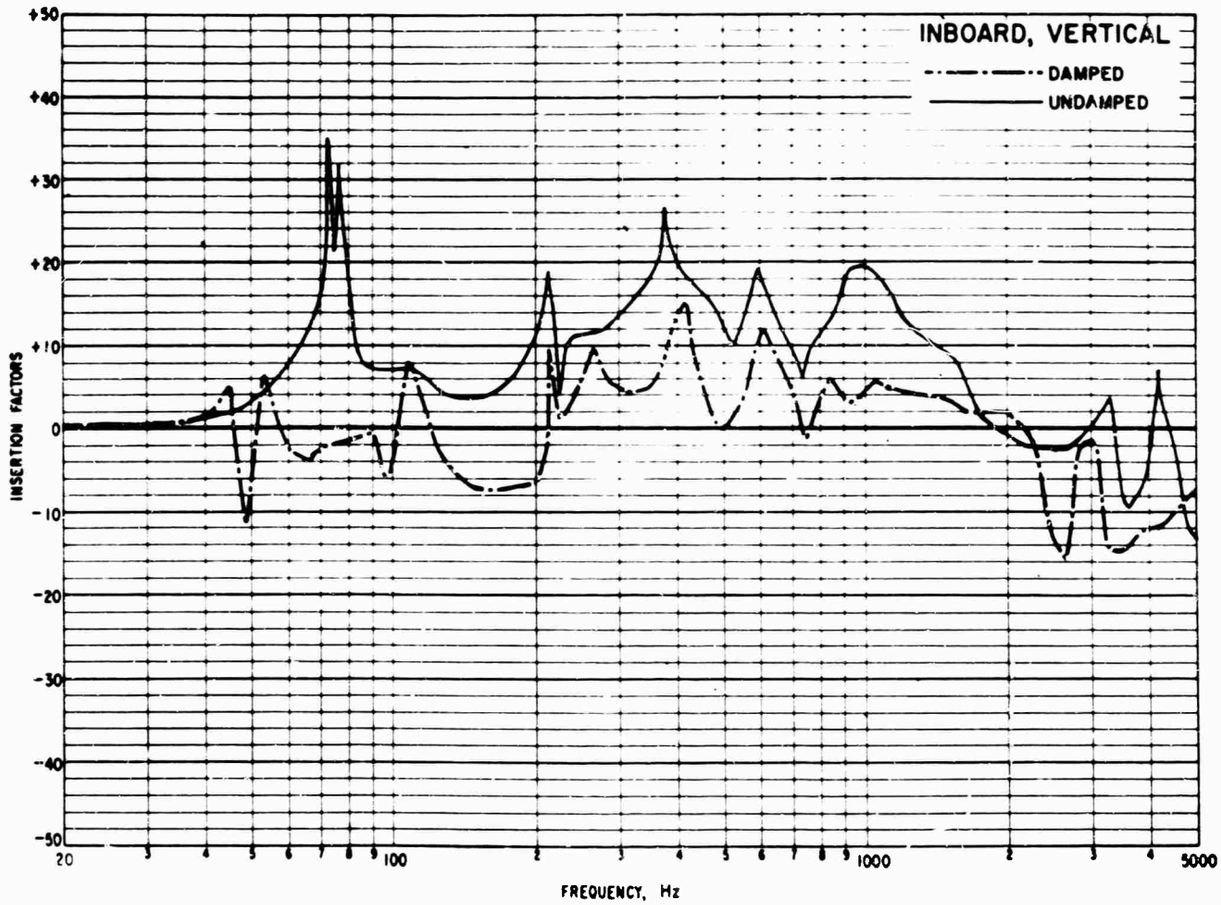

Fig. 12 - Comparison of damping effectiveness for damped and undamped portal frame foundations

insertion factor curves, therefore, are obtained with respect to frequency. The 16 insertion factor curves can be combined by power level summation and averaged to produce a force amplification ratio. This power level summation may be expressed as

$$T_n, \text{axis} = \sum_{i,j}^{\text{Power}} T_i^j - 10 \log i$$

and is easily handled graphically to solve the foundation transmission problem.

By using the radiated noise from the radiator structure as a check on the system approximation made through power level summation, it becomes apparent that the branch outputs are automatically vector summed by the radiator structure. The inputs can be summed using the same approach and approximations for pressure, i.e.,

$$P_j^i = \frac{\text{(output pressure in medium with structure in place input force with structure in place)}}{\text{(output pressure in medium without structure radiator input force)}} \tag{7}$$

or

$$P_j^i = \frac{F_{out}}{F_{in}} .$$

The four P_i^j for any single axis of excitation can be summed by the branched force technique.

The expression for pressure became

$$P_n, \text{axis} = \sum_{i,j}^{\text{Power}} P_i^j - 10 \log i . \tag{8}$$

Experimental agreement between T_n and P_n is normally within ±5 db.

Concurrent with the program to test and evaluate damped foundations, the development of instrumentation to measure force and velocity has been proceeding. As the level of the transmitted energy becomes smaller, accurate measurements become more difficult. To alleviate this problem, a three-channel automatic mechanical impedance plotting system was developed to increase the range, accuracy, and speed of data acquisition [11].

FUTURE CONSIDERATIONS

The analysis and testing of damped foundations and viscoelastic materials are continuing. Of future concern is the formulation of a viscoelastic material which can yield significant damping at 500°F and retain its other needed properties.

Analytical work will proceed to study the damping characteristics of the pipe-within-a-pipe damper to provide guidelines in the optimum design of this promising configuration.

Future experimental efforts will investigate spaced damping for large foundations in the design, fabrication, and evaluation of 13 different highly damped machinery foundations for vibration transmission, shock resistance and creep. Passing these laboratory examinations, the foundations will be installed in naval ships and retested at sea to determine total effectiveness.

REFERENCES

1. H. Oberst, "Über die Dämpfung der Biegeschwingungen dünner Bleche durch festhaltende Beläge," Acustica, Vol. 2, Akustische Beihefte, No. 4, pp. 181-194, 1952

2. Donald Ross, Eric E. Ungar, and E. M. Kerwin, Jr., "Damping of Flexural Vibrations by Means of Viscoelastic Laminae," Structural Damping, Section 3, Edited by J. E. Ruzicka, ASME, 1959

3. R. A. DiTaranto and W. Blasingame, "Composite Loss Factors of Selected Laminated Beams," J. Acoust. Soc. Am., Vol. 40, No. 1, pp. 187-194, July 1966

4. R. A. DiTaranto, "Theory of Vibratory Bending for Elastic and Viscoelastic Layered Finite Length Beams," J. Appl. Mech., Vol. 32, Dec. 1965

5. R. A. DiTaranto and W. Blasingame, "Effect of End Constraints on the Damping of Laminated Beams," J. Acoust. Soc. Am., Vol. 39, No. 2, pp. 405-407, Feb. 1966

6. B. Douglas and C. Longley, "The Critical Damping Calculator and the Evaluation Measuring Systems to Determine Damping Properties of Structures," MEL R&D Rept. 98/66, March 1966

7. W. Blasingame, "Comparison of Dynamic Shear Modulus Measurements on Two Damping Materials," MEL R&D Rept. 244/65, July 1965

8. A. J. Roscoe, E. V. Thomas, and W. Blasingame, "Measurement of Complex Shear Modulus of Viscoelastic Materials by Mechanical Impedance Methods," MEL R&D Rept. 238166, May 1966

9. E. V. Thomas, "Development of a Highly Damped Submarine Machinery Foundation," MEL Rept. 375165, Nov. 1965

10. D. V. Wright, et al., "Vibration Transmission and Impedance of Basic Foundation Structures," Westinghouse Res. Lab. Rept. 62-917-515-R1, Oct. 1962

11. E. V. Thomas and A. J. Roscoe, "Development of a Three Channel Mechanical Impedance and Phase Plotting System," MEL R&D Rept. 375/65, Oct. 1965

DISCUSSION

Mr. Ungar (Bolt Beranek and Newman): Were the tubes-within-tubes loaded in bending or torsion?

Mr. DiTaranto: The load was carried longitudinally from one tube through the viscoelastic material to the outside tube.

Mr. Ungar: This requires a different analysis.

Mr. DiTaranto: Yes. We have mentioned nothing here about the analysis; this is one of the things we are looking into right now.

Mr. Ungar: Have you done an analysis where the transfer is axial or torsional?

Mr. DiTaranto: No, this is a current program.

Mr. Ungar: Have you correlated theoretical and experimental multiple layer data?

Mr. DiTaranto: Yes, on simple beams, and the agreement between analysis and experiment is very good.

Mr. Plunkett: Didn't you publish the comparison between your experimental and theoretical results in the Journal of the Acoustical Society?

Mr. DiTaranto: Yes. We reported there the results of the experiment and theory that the composite loss factor versus natural frequency is independent of the mode shape and boundary conditions.

Mr. Plunkett: I was impressed by your experimental results for the highly damped structure. You had much detail in your spectrum, whereas you had relatively simple spectra for the less highly damped structures. Would you care to comment on that?

Mr. DiTaranto: I think maybe Mr. Thomas could comment on that. He had quite a bit to do with the testing.

Mr. Thomas: A lot of this was due to the measurement. We were getting exceptionally low levels on our hull structures, and we were picking up some waterborne excited noise.

* * *

DYNAMIC MECHANICAL STUDIES OF A COMPOSITE MATERIAL*

M. G. Sharma, M. Critchfield and W. F. St. Lawrence
The Pennsylvania State University
University Park, Pennsylvania

A study was made of the dynamic mechanical behavior of a composite material consisting of a soft substance interspersed with spherical particles of finely divided aluminum of prescribed volume concentrations. The study has been extended to frequencies between 300 and 1000 cps and to various temperatures below and above room temperature. An apparatus developed for the determination of the dynamic mechanical behavior of soft substances for this frequency range is described. The apparatus is provided with a thermal cabinet to study the effect of temperature on the dynamic mechanical behavior.

A theory that considers the composite material system to be made up of an elastic filler (aluminum) randomly dispersed in a matrix of a viscoelastic material (soft material) has been developed. The theory predicts the dynamic behavior of the material in terms of the creep properties of the constituent materials for uniaxial and volumetric compression loading.

An examination of the experimental data shows that the dynamic modulus and the damping properties of the material are considerably affected by the volume fraction of the filler substance in the bulk material. In addition, it is found that, by using the time-temperature shift principle, one reduced curve can be constructed for the complex dynamic modulus varying with the frequencies.

Finally, the theoretically predicted values are compared with the corresponding experimental results, and the comparisons are found to be reasonably good.

INTRODUCTION

In recent years great interest has been shown in the development of new materials that possess high strength as well as damping properties. This is due to the diverse use of engineering materials. For instance, the materials used in aerospace applications are not only subjected to extreme environmental conditions of temperature but also complex dynamic loading resulting from severe applications that occur during operation. For the effective design of structures for aerospace applications, it is very essential to determine the characteristic parameters that specify the mechanical behavior for all possible dynamic loading and temperature conditions.

Until recently, homogeneous (on macroscopic scale) high-strength materials with low damping properties were used for engineering structures. But with applications where materials are subjected to severe dynamic loads and high temperature, it has become necessary to select a material having both high strength and high damping properties to prolong the useful life of structural components. To achieve this purpose, new composite materials are developed. The composite materials usually consist of a combination of two or more materials, with one of the materials functioning as matrix to the remaining filler substances. The filler substances can be randomly dispersed or oriented in a particular direction in the bulk material. The mechanical behavior of such materials

*This paper was not presented at the Symposium.

depends on the type of the constituents, relative volume concentration of the matrix, the fillers and the geometry of the filler particles in the composite substance.

Over the past decade considerable effort has been directed towards the understanding of mechanical behavior of composite materials [1]. An examination of the literature indicates that most of the studies pertain to the behavior under static loading conditions. Very little work can be found on the dynamic mechanical behavior of composite materials [2].

This paper deals with an experimental program for the study of dynamic mechanical behavior of a viscoelastic material containing finely divided metallic substances of prescribed volume concentration. An apparatus specially developed for the purpose is described. Effect of temperature on the dynamic properties has been studied. Finally, an analytical procedure has been developed for the prediction of dynamic properties of composite material in terms of material properties of the constituents obtained from static loading conditions.

EXPERIMENTAL INVESTIGATION

Description of Apparatus

The dynamic mechanical behavior of a composite material was studied by developing an apparatus based on an experimental method originally conceived by Förster [3]. The specimen in the form of a cylindrical rod was subjected to longitudinal vibration. The frequency of vibration was varied continually so that the rod passes through various modes of vibration. The amplitude curves for resonant frequencies corresponding to various vibration modes were automatically recorded. The specimen was suspended by two fine silk threads from a rigid brass rod. A periodic force, approximately sinusoidal, was imposed on one end of the specimen by a coil and magnet arrangement. An identical arrangement picked up the response at the other end of the specimen. The entire driving and receiving system with the specimen was placed in a thermal cabinet designed for a temperature range of -40°F to 300°F. Figure 1 shows a block diagram for the experimental arrangement. The entire experimental setup is shown in Fig. 2.

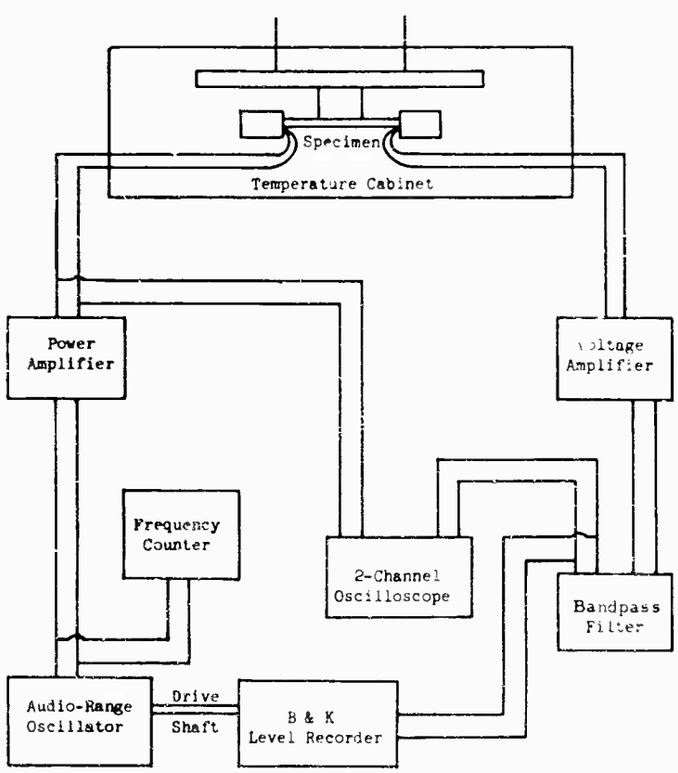

Fig. 1 - Diagram of experimental arrangement

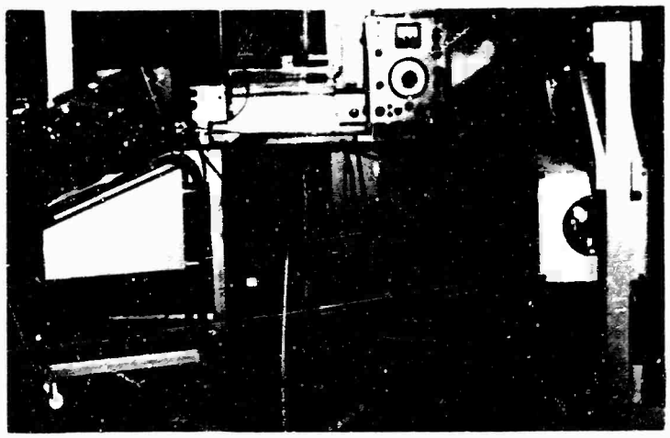

Fig. 2 - Experimental arrangement

Description of Driving and Pickup Systems

Figure 3 shows the location of the driving and pickup systems with respect to the specimen. The pickup and driving systems are made up of a solenoid coil and magnet assembly. The solenoid coils consisted of 70 turns of No. 38 enamel coated copper wire, wound in four layers. They were 1/4 in. in diameter and 3/32 in. long. Each layer was coated with epoxy during the winding process so that the coils would not unwind. Epoxy glue was used to secure the coils firmly to the ends of the specimens.

circular aperture of the front plate was 2000 gauss.

A periodic driving force (approximately sinusoidal) is imposed on the specimen when alternating current flows through the coil generating an alternating magnetic field that interacts with the steady-state magnetic field of the permanent magnet assembly. Precautions must be taken to center the driving coil properly within the aperture so that a uniform force is produced over the end face of the specimen. Otherwise, undesirable bending vibrations may be excited in the specimen. The resonant

Fig. 3 - Driving and pickup system specimen and suspension rod

Two identical magnet assemblies, one for each end of the specimen, were constructed. Figure 4 shows a cross section of the magnet assembly with a list of materials used in construction. After machining and cadmium plating, the components of the magnet assembly were assembled with epoxy glue and nonmagnetic bolts before magnetization. The magnet assembly was constructed in such a way as to produce a radially symmetric magnetic field. The estimated magnetic flux density in the

frequency of the driving coil was found to be approximately 110 cps. After running the setup at this frequency, the solenoid coils were found to be damaged. The uniform periodic driving force applied at the driving end of the specimen generates longitudinal vibrations in the specimen, causing a periodic displacement of the pickup solenoid coil within the steady magnet field of the magnet assembly at the pickup end of the specimen. As the moving coil cuts the lines of flux, an alternating voltage on the order of 1 mv

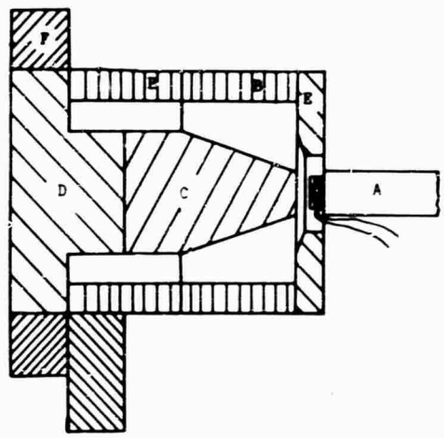

COMPONENTS AND MATERIALS:

A Specimen and Coil

B Permanent Ring Magnets
Cast Hyflux Alnico V
(Holding Force = 6 lb)

C Center Pole
Carpenter Covandar Magnetostrictive and High Saturation Alloy
(Cobalt, Vanadium Manganese, others)

D Back Plate
SAE 1020 Cold Rolled Steel

E Front Plate
SAE 1020 Cold Rolled Steel

F Assembly Mounting
Aluminum

Fig. 4 - Cross-sectional view of magnet assemblies

is induced in the coil. The magnet assemblies were mounted on a 30-in. long aluminum rod. This arrangement makes it possible to adjust the magnetic assemblies to accommodate any length of specimen.

Instrumentation

The instruments comprising the experimental arrangement are shown in Figs. 1 and 2. The arrangement consists of the driving and pickup circuits. In the driving circuit a 1-v signal generated by a B & K beat frequency oscillator is fed into a 32-w Knight power amplifier. The low 1-v output voltage was selected because it allowed a greater amplification of the signal without waveform distortion than did higher output voltages. The amplified signal is passed through both driving coil and one channel of a dual beam oscilloscope.

When the specimen vibrates, a 1-mv signal is generated in the pickup circuit. This signal is fed through a bandpass filter before entering the B & K recorder and the other channel of the oscilloscope. The dual beam oscilloscope is intended to monitor the input signal to the driving coil and the output signal from the pickup coil. The oscilloscope also gives the magnitude of the input and output voltages so that the sensitivity of the recorder may be regulated. The B & K recorder is a high-speed instrument for recording signal level variation with the frequency range of 20 to 200,000 cps. A special feature of the recorder is its provision to drive automatically the frequency dial on a B & K beat frequency oscillator.

Calibration

For the determination of dynamic behavior by the resonance method, the frequency values at the peaks of the recorded resonance curves and the bandwidth at the half-power points must be known. While passing through resonance, the frequency value corresponding to the peak amplitude may be accurately read directly from the electronic counter. However, reading the frequency values at the half-power points from the electronic counter is too difficult and inaccurate. This is because the half-power points cannot easily be detected when the recorder is quickly tracing a resonance curve. Therefore, the bandwidth has been obtained by a convenient and more accurate method [4]. The method determines $\Delta\omega/\omega_n$ where $\Delta\omega$ is the bandwidth and ω_n is the resonant frequency. Using this method, a calibration test was conducted leading to the following relation:

$$\frac{\Delta\omega}{\omega_n} = (4.9 \times 10^{-2})\,\Delta s\,, \qquad (1)$$

where Δs is the width of a recorded resonance curve (mm) at the half-power points, and ω_n is the resonant frequency (rad/sec).

Material Tested

The material used in the test program is Paracril RF-1 liquid polymer, a copolymer of butadiene and acrylic acid. The liquid polymer (63 percent by weight) was combined with a cross-linking agent, Epon 828 (27 percent by weight) and H-10 aluminum powder (10 percent

by weight; Valley Metallurgical Processing Co.) consisting of particles of 10 μ size. The material was cast in the form of cylindrical rods in cylindrical molds. The procedure for specimen preparation is described elsewhere [5].

EXPERIMENTAL PROCEDURE AND RESULTS

Longitudinal vibration experiments were conducted on specimens of the composite material in the frequency range of 300 to 1000 cps. The storage modulus and the loss modulus corresponding to eight resonant frequencies were obtained by vibrating four specimens of 9-, 8-, 7- and 6-in. lengths at their fundamental and first harmonics. The resonance curves for harmonics above the first were too low and broad for accurate measurements. The chart speed of 1 mm/sec and a drive shaft speed of 7.5 rpm were used in all four experiments. These speeds produced excellent resonance curves, in that the curves were relatively wide and sharp for accurate measurement. By adjusting the power amplifier setting and the sensitivity of the recorder, resonance curves with heights of approximately 65 mm were obtained. The ratio $\Delta\omega/\omega_n$ associated with each resonance curve was found by measuring Δs, the width of the resonance curve at the half-power points, and substituting in Eq. (1). The half-power points were determined by measuring down 3 db or 15 mm from the peak of a resonance curve. The resonant frequencies were determined with an accuracy of ±2 cps for the fundamental mode and ±3 cps for the first harmonics. To determine the resonant frequency of the specimen, the oscillator was switched from its automatic sweep mode to a manual sweep mode. The oscillator was then set at the frequency where a peak voltage was obtained from the output coil of the specimen. This peak voltage was then observed on the oscilloscope, and the corresponding frequency was read from the frequency counter. Using this procedure, the fundamental and first harmonic frequencies were easily obtained.

From the experimentally observed resonant frequencies and the width of resonance curves at half-power points, the dynamic properties of the composite material, specified in terms of the storage and loss modulus, were determined by using the following relations [6,7]:

$$E_1^*(\omega) = \frac{\ell^2 \rho \omega_n^2}{n^2 \pi^2} \tag{2}$$

and

$$E_2^*(\omega) = \frac{2\sqrt{3}}{\sqrt{3}}\left(\frac{\Delta\omega}{\omega_n}\right) E_1^*(\omega) . \tag{3}$$

where

$E_1^*(\omega)$ = storage modulus of composite material,

$E_2^*(\omega)$ = loss modulus of composite material,

ℓ = length of cylindrical specimen,

ρ = mass density of composite material, and

n = number of vibration mode.

Following the procedure described above, the storage and loss moduli were calculated from the vibration experiments conducted at various temperatures ranging from 22°F to 140°F. Figures 5 and 6 show the variations of $E_1^*(\omega)$ and $E_2^*(\omega)$ with frequency for various constant temperature values.

Using the time-temperature superposition principle [8], it was found that the curves in Figs. 5 and 6 could be expressed in terms of reduced storage and loss moduli curves as shown in Figs. 7 and 8. The shift factor required to construct the reduced curve is shown in Fig. 9, varying with temperature.

THEORETICAL CONSIDERATIONS

Following the procedure developed by Oldroyd [9] for an elastic solid with viscous inclusions, the response functions for the composite material consisting of a viscoelastic matrix with a small volume percentage of elastic filler can be shown to be

$$K^*(t) = \frac{[2K' + 4G(t)]K(t) + 4G(t)[K' - K(t)]c}{3K' + 4G(t) - 3[K' - K(t)]c} \tag{4}$$

and

$$G^*(t) = G(t)\left\{\frac{[9K(t)+8G(t)]G(t) + 6[K(t)+2G(t)]G' - [9K(t) + 8G(t)][G(t) - G']c}{[9K(t)+8G(t)]G(t)+6[K(t)+2G(t)]G' + 6[K(t) + 2G(t)][G(t) - G']c}\right\} \tag{5}$$

where

$K^*(t)$ = bulk modulus function for composite material,

$G^*(t)$ = shear modulus function for composite material,

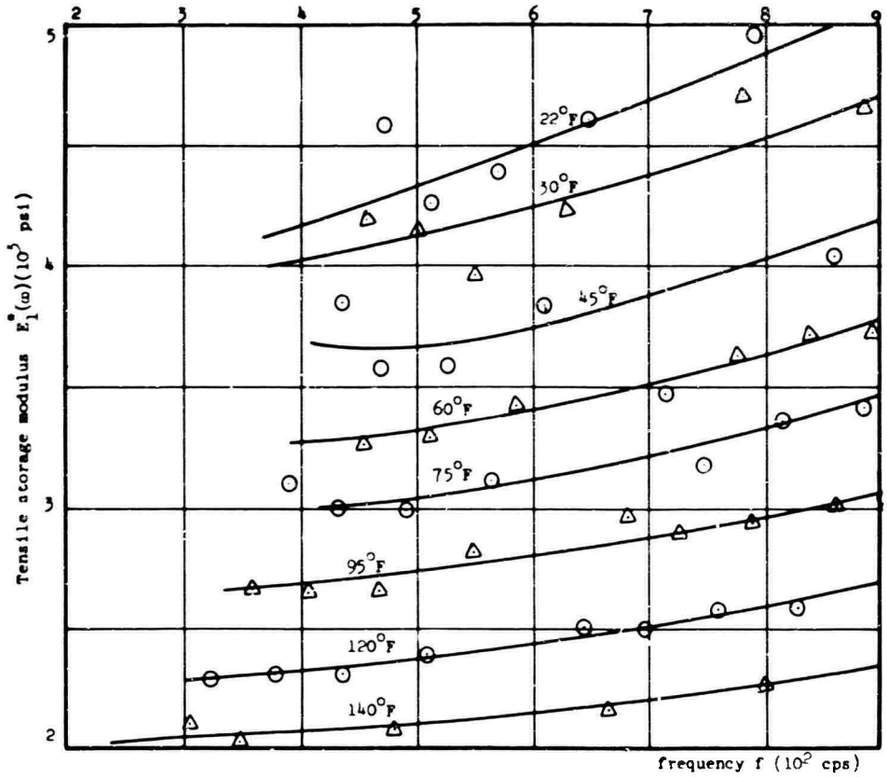

Fig. 5 - Variation of tensile modulus with frequency and temperature for composite material

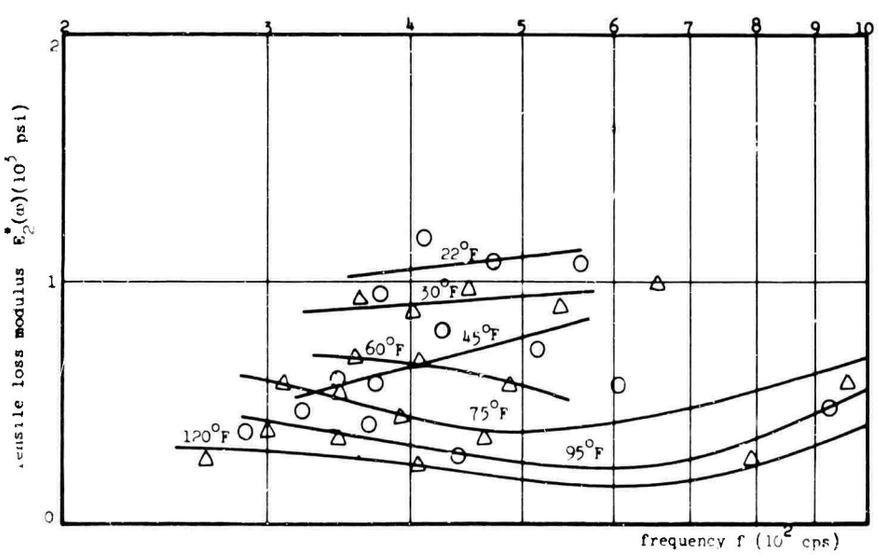

Fig. 6 - Variation of tensile loss modulus with frequency and temperature for composite material

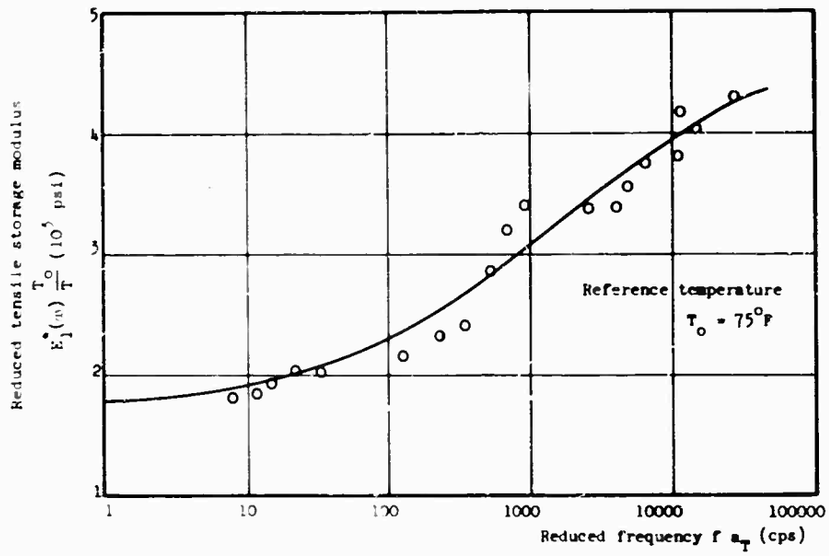

Fig. 7 - Reduced storage modulus curve for composite material

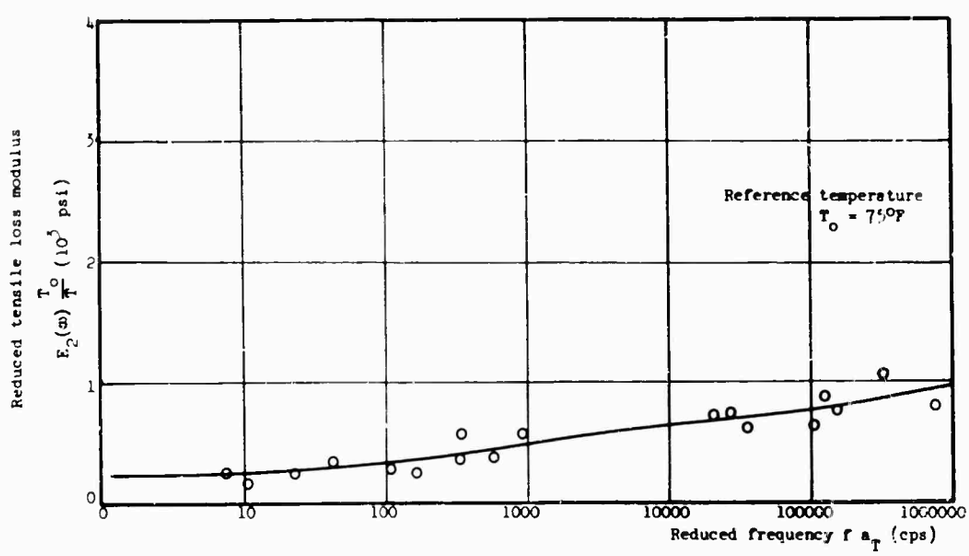

Fig. 8 - Reduced tensile loss modulus curve for composite material

$G(t)$ = shear modulus function for viscoelastic matrix,

$K(t)$ = bulk modulus function for viscoelastic matrix,

K', G' = bulk modulus and shear modulus for elastic filler substance,

c = volume concentration of filler in composite material, and

t = time.

For the composite viscoelastic material in a state of steady vibrations, the complex bulk and shear moduli are given by substituting $i\omega$ (where i is the imaginary number) for t in Eqs. (4) and (5). The justification for this procedure is given in the Appendix. Making the substitution for t with $i\omega$ in Eqs. (4) and (5) and separating the resulting complex function into real and imaginary parts, the following expressions are obtained:

$$K_1^*(\omega) = \frac{\alpha\gamma + \beta\delta}{\gamma^2 + \delta^2} \qquad (6) \text{ (Cont.)}$$

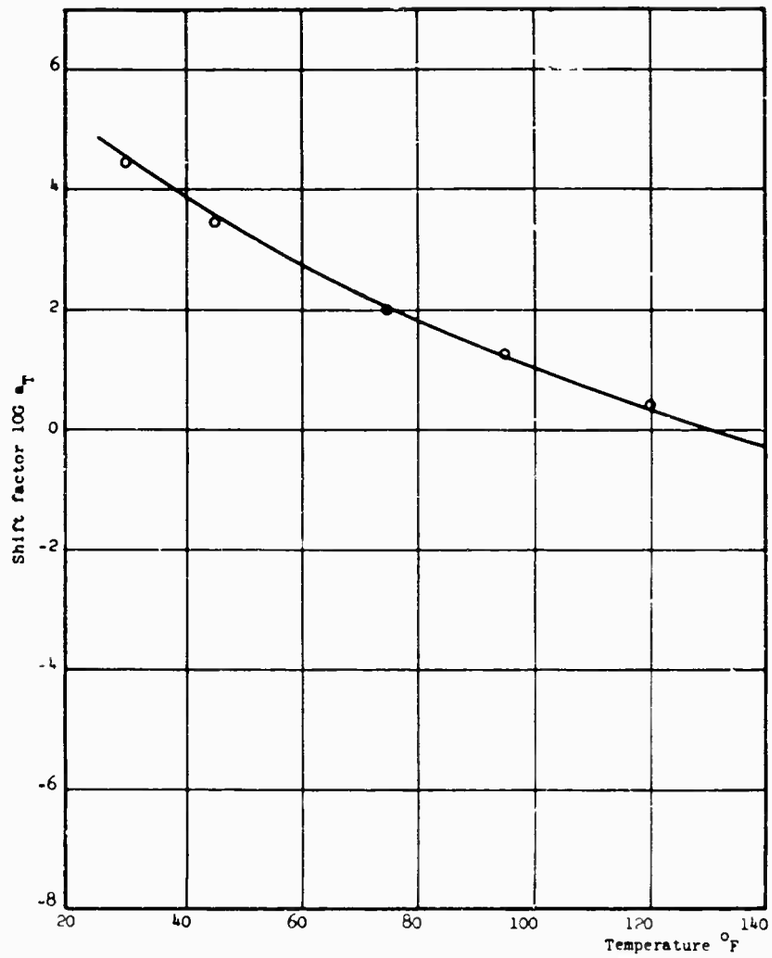

Fig. 9 - Variation of shift factor with temperature for composite material

and

$$K_2^*(\omega) = \frac{\beta\gamma - \alpha\delta}{\gamma^2 + \delta^2}, \qquad (6)$$

where

$$\alpha = \left\{K'[3K_1(\omega) + 4cG_1(\omega)] + 4[G_1(\omega)K_1(\omega) - G_2(\omega)K_2(\omega)](1-c)\right\};$$

$$\beta = \left\{K'[3K_2(\omega) + 4cG_2(\omega)] + 4[G_1(\omega)K_2(\omega) + G_2(\omega)K_1(\omega)](1-c)\right\};$$

$$\gamma = \left\{3K'(1-c) + [4G_1(\omega) + 3cK_1(\omega)]\right\};$$

$$\delta = \left\{4G_2(\omega) + 3cK_2(\omega)\right\};$$

$K_1(\omega), G_1(\omega)$ = storage bulk modulus and storage shear modulus, respectively, for viscoelastic matrix; and

$K_2(\omega), G_2(\omega)$ = loss bulk modulus and loss shear modulus, respectively, for viscoelastic matrix.

Similarly,

$$G_1^*(\omega) = \frac{\bar{\alpha}\bar{\gamma} + \bar{\beta}\bar{\delta}}{\bar{\gamma}^2 + \bar{\delta}^2}$$

and (7)

$$G_2^*(\omega) = \frac{\bar{\beta}\bar{\gamma} - \bar{\alpha}\bar{\delta}}{\bar{\gamma}^2 + \bar{\delta}^2},$$

where

$$\bar{\alpha} = [G_1(\omega)\bar{A} - G_2\bar{B}],$$

$$\bar{\beta} = [G_1\bar{B} + G_2\bar{A}],$$

$$\bar{A} = \left\{9[G_1(\omega)K_1(\omega) - G_2(\omega)K_2(\omega)](1-c) + G'[3K_1(\omega)(2+3c) + 4G_1(\omega)(3+2c)] + 8[(G_1(\omega))^2 - (G_2(\omega))^2](1-c)\right\},$$

$$\bar{B} = \Big\{9[G_1(\omega)K_2(\omega) + G_2(\omega)K_1(\omega)](1-c) + G'[3K_2(\omega)(2+3c) + 4G_2(\omega)(3+2c)] + 16G_1(\omega)\,G_2(\omega)(1-c)\Big\}.$$

$$\bar{\eta} = \Big\{3[G_1(\omega)K_1(\omega) - G_2(\omega)K_2(\omega)](3+2c) + 6G'[K_1(\omega) + 2G_1(\omega)](1-c) + 4[(G_1(\omega))^2 - (G_2(\omega))^2](2+3c)\Big\},$$

and

$$\bar{\xi} = \Big\{3[G_1(\omega)K_2(\omega) + G_2(\omega)K_1(\omega)](3+2c) + 6G'[K_2(\omega) + 2G_2(\omega)](1-c) + 8G_1(\omega)\,G_2(\omega)(2+3c)\Big\}.$$

Equations (6) and (7) are the expressions for the dynamic properties of the composite viscoelastic material in terms of the dynamic properties of the viscoelastic matrix, the material constants for the elastic filler, and the volume concentration of the filler.

CORRELATION OF THEORETICAL AND EXPERIMENTAL RESULTS

Creep tests in tension of the unfilled Paracril RF-1 gave the following expression for creep compliance function:

$$D(t) = D_o + D_1\left[1 - \exp\left(-\frac{t}{\lambda_D}\right)\right], \qquad (8)$$

where

$D_o = 60.45 \times 10^{-5}$ psi,

$D_1 = 22.20 \times 10^{-5}$ psi,

$\lambda_D = 33.6$ min, and

t = time (min).

In arriving at Eq. (8), it must be noted that linearization of the observed slight nonlinear behavior had been made.

Conducting volumetric creep experiments, it was noted that the bulk creep compliance function for the unfilled material is of the form

$$B(t) = B_o + B\left[1 - \exp\left(-\frac{t}{\lambda_B}\right)\right], \qquad (9)$$

where

$B_o = 2.58 \times 10^{-5}$ psi,

$B_1 = 1.59 \times 10^{-6}$ psi, and

$\lambda_B = 55$ min.

Using Eqs. (8) and (9), the storage and loss compliance functions can be evaluated and are given by [10]:

$$D_1(\omega) = D_o + D_1\left[\frac{1}{1+\omega^2\lambda_D^2}\right], \qquad (10)$$

$$D_2(\omega) = D_1\left[\frac{\omega\lambda_D}{1+\omega^2\lambda_D^2}\right], \qquad (11)$$

$$B_1(\omega) = B_o + B_1\left[\frac{1}{1+\omega^2\lambda_B^2}\right], \qquad (12)$$

and

$$B_2(\omega) = B_1\left[\frac{\omega\lambda_B}{1+\omega^2\lambda_B^2}\right], \qquad (13)$$

where $D_1(\omega), D_2(\omega)$ are storage and loss compliances in tension, respectively, and $B_1(\omega), B_2(\omega)$ are storage and loss bulk compliances, respectively. From Eqs. (10) through (13), the expressions for storage moduli can be determined as follows [10]:

$$E_1(\omega) = \frac{D_1(\omega)}{[D_1(\omega)]^2 + [D_2(\omega)]^2}, \qquad (14)$$

$$E_2(\omega) = \frac{D_2(\omega)}{[D_1(\omega)]^2 + [D_2(\omega)]^2},$$

$$K_1(\omega) = \frac{B_2(\omega)}{[B_1(\omega)]^2 + [B_2(\omega)]^2},$$

and (15)

$$K_2(\omega) = \frac{B_2(\omega)}{[B_1(\omega)]^2 + [B_2(\omega)]^2},$$

where $E_1(\omega)$ and $E_2(\omega)$ are the storage and loss modulus in tension, respectively. Equations (14) and (15) lead to the following expressions for storage and loss shear modulus:

$$G_1(\omega) \quad \frac{C_1C_3 + C_2C_4}{C_3^2 + C_4^2}$$

and (16)

$$G_2(\omega) = \frac{C_2C_3 - C_1C_4}{C_3^2 + C_4^2}.$$

where

$$C_1 = 3[E_1(\omega)K_1(\omega) - E_2(\omega)K_2(\omega)] ,$$

$$C_2 = 3[E_2(\omega)K_1(\omega) + E_1(\omega)K_2(\omega)] ,$$

$$C_3 = 9K_1(\omega) - E_1(\omega) ,$$

and

$$C_4 = 9K_2(\omega) - E_2(\omega) .$$

Substituting Eqs. (15) and (16) in Eqs. (6) and (7),

$$E^*(i\omega) = \frac{9G^*(i\omega)K^*(i\omega)}{3K^*(i\omega) + G^*(i\omega)} ,$$

where $E^*(i\omega)$ is the complex modulus in tension. The following expression for storage and loss tension modulus can be obtained after separating the real and imaginary parts in Eq. (17):

$$E_1^*(\omega) = \frac{\bar{C}_1\bar{C}_3 + \bar{C}_2\bar{C}_4}{\bar{C}_3^2 + \bar{C}_4^2}$$

and (18)

$$E_2^*(\omega) = \frac{\bar{C}_2\bar{C}_3 - \bar{C}_1\bar{C}_4}{\bar{C}_3^2 + \bar{C}_4^2} ,$$

where

$$\bar{C}_1 = 9[G_1^*(\omega)K_1^*(\omega) - G_2^*(\omega)K_2^*(\omega)]$$

$$\bar{C}_2 = G_2^*(\omega)K_1^*(\omega) + G_1^*(\omega)K_2^*(\omega) ,$$

$$\bar{C}_3 = 3K_1^*(\omega) + G_1^*(\omega) ,$$

and

$$C_4 = 3K_2^*(\omega) + G_2^*(\omega) .$$

Using Eq. (18) and the material constants for the unfilled Paracril RF-1, as given by Eqs. (8) and (9), the theoretical values of storage and loss modulus for various frequencies were calculated for a filler (aluminum) concentration of 10 percent. Table 1 compares the theoretically predicted and experimentally determined values.

DISCUSSION

The apparatus described here is very suitable for studying the dynamic mechanical behavior of materials. Since the test material was soft, the frequency range for which the dynamic properties were evaluated was small — 300 to 1000 cps. This is in part due to the limited number of resonant modes that can be produced because of large damping occurring in the material. A stiffer material would have given a greater number of resonant modes and thus would have increased the range of frequencies. An extension of the present investigation indicates that the increase of percentage of filler in the bulk material would stiffen the

TABLE 1
Theoretically Predicted vs Experimental Values for Composite Material

Frequency (cps)	Theoretical Values		Experimental Values		
	$E_1(\omega)$	$E_2(\omega)$	$E_1(\omega)$	$E_2(\omega)$	$\tan\theta$ [a]
300	2053	2.854×10^{-6}	2925	590	0.180
375	2053	2.29×10^{-6}	3025	480	0.167
450	2053	1.903×10^{-6}	3080	390	0.122
525	2053	1.631×10^{-6}	3150	390	0.140
600	2053	1.4270×10^{-6}	3200	410	0.215
675	2053	1.270×10^{-6}	3250	460	0.283
750	2053	1.141×10^{-6}	3310	510	0.272
825	2053	1.038×10^{-6}	3350	510	0.240
900	2053	9.513×10^{-7}	3400	610	0.197
975	2053	8.787×10^{-7}	3450	660	0.170

[a] $\tan\theta = E_2/E_1$.

material further, leading to an increase in frequency range for which the dynamic properties can be evaluated.

The dynamic properties of the material, specified in terms of the storage modulus and the loss modulus, are very much dependent on the frequency of excitation and the operating temperature. This can be easily seen from Figs. 5 and 6. It is interesting to note that the time-temperature shift hypothesis makes it possible to construct reduced modulus curves covering a frequency range of 10 to 10^4 cps (Figs. 7 and 8).

The dynamic properties of the composite material have been predicted from the static creep properties of the viscoelastic matrix and the elastic constants of the filler. The comparison between theoretical and experimental values is shown in Table 1. The theoretical value for storage modulus remains constant for the range of frequencies studied, and the value checks better for lower frequencies than for higher frequencies. The constancy of theoretical value for storage modulus is due to the second term in Eqs. (10) and (12) becoming small, resulting in constant values of $D_1(\omega)$ and $B_1(\omega)$. The discrepancy between the theoretical and experimental values of loss modulus is much greater. This can be explained as follows. The creep data used for prediction were obtained for time scales much larger than those of the dynamic experiments, since it is extremely difficult to obtain accurate creep data for the small time scale in the dynamic experiments. It can be argued that one may get better correlation if one can obtain accurate creep data for times on the order of milliseconds.

ACKNOWLEDGMENTS

The content of this article is part of the investigation sponsored by the Army Research Office, Durham, under Project No. 20010501B-700. The authors are grateful to Indiana General Corp., Valparaiso, Ind., and Carpenter Steel Co., Reading, Pa., for donating the materials for the magnet assembly.

REFERENCES

1. D. Cratchley, "Experimental Aspects of Fibre Reinforced Metals," Metallurgical Reviews, Vol. 10, No. 37, 1965

2. L. E. Nielsen, Mechanical Properties of Polymers, pp. 138-201. Reinhold Publishing Corp., New York, 1962

3. F. Z. Förster, "Ein neues Messverfahren zur Bestimmung des Elazitamoduls und der Dampfung," Zeits. Metalkunde, Vol. 29, p. 109, 1937

4. D. E. Kline, "A Recording Apparatus for Measuring the Dynamic Mechanical Properties of Polymers," J. Polymer Sci., Vol. 22, p. 449, 1956

5. M. G. Sharma and C. K. Lim, "Investigations on the Biaxial Stress-Strain and Fracture Behavior of a Solid Fuel Propellant Material," Pennsylvania State Univ. Tech. Rept. No. 3; submitted to Jet Propulsion Lab., May 1966

6. N. W. McLachlan, Theory of Vibrations. Dover, New York, 1951

7. H. A. Stuart, Die Physik der Hochpolymeren, pp. 88-89. Springer-Verlag, Berlin, 1956

8. J. D. Ferry, Viscoelastic Properties of Polymers, pp. 201-247. John Wiley and Sons, New York, 1961

9. J. G. Oldroyd, "The Effect of Small Viscous Inclusions on the Mechanical Properties of an Elastic Solid," Deformation and Flow of Solids, pp. 304-313. Springer-Verlag, Berlin, Germany, 1956

10. J. V. Schmitz, Testing of Polymers, Vol. 1, pp. 147-199. Interscience Publishers, New York, 1965

Appendix

TRANSFORMATION OF TIME-DEPENDENT TO FREQUENCY-DEPENDENT RESPONSE FUNCTIONS

The justification for substitution of $(i\omega)$ for in Eqs. (4) and (5) to obtain the complex moduli for the composite material can be established as follows. Suppose a linear

viscoelastic material is subjected to a steady vibration as expressed by

$$\sigma(t) = \sigma_o e^{i\omega t}, \qquad \text{(A-1)}$$

where $\sigma(t)$ is the time-dependent stress and σ_o is the amplitude of stress. The resulting strain can be shown to be

$$\epsilon(t) = \sigma_o e^{i(\omega t - \delta)}, \qquad \text{(A-2)}$$

where

$\epsilon(t)$ = time-dependent strain,

ϵ_o = strain amplitude,

δ = phase angle, and

$i = \sqrt{-1}$, imaginary number.

The stress-strain law for a linear viscoelastic material can be expressed in general form as

$$P\,\sigma(t) = Q\,\epsilon(t), \qquad \text{(A-3)}$$

where

$$P = \frac{\partial^n}{\partial t^n} + p_{n-1}\frac{\partial^{n-1}}{\partial t^{n-1}} + \cdots + p_o$$

and

$$Q = q_m \frac{\partial^m}{\partial t^m} + q_{m-1}\frac{\partial^{m-1}}{\partial t^{m-1}} + \cdots + q_o.$$

Substituting Eqs. (A-1) and (A-2) into Eq. (A-3) yields

$$\left[(i\omega)^n + p_{n-1}(i\omega)^{n-1} + \cdots + p_o\right]\sigma_o e^{i\omega t} = \left[q_m(i\omega)^m + q_{m-1}(i\omega)^{m-1} + \cdots + q_o\right]\epsilon_o e^{i(\omega t - \delta)}. \qquad \text{(A-4)}$$

By definition,

$$\frac{\sigma(t)}{\epsilon(t)} = \frac{\sigma_o e^{i\omega\delta}}{\epsilon_o} = E^*(i\omega). \qquad \text{(A-5)}$$

That is,

$$E^*(i\omega) = \frac{\left[q_m(i\omega)^m + q_{m-1}(i\omega)^{m-1} + \cdots + q_o\right]}{\left[(i\omega)^n + p_{m-1}(i\omega)^{n-1} + \cdots + p_o\right]}. \qquad \text{(A-6)}$$

If $\sigma(t)$ and $\epsilon(t)$ in Eq. (A-3) apply to a relaxation test, the following relation holds good:

$$\frac{\sigma(t)}{\epsilon_o} = \left(\frac{Q}{P}\right) = E(t), \qquad \text{(A-7)}$$

where ϵ_o is the constant value of strain in a relaxation test. The correspondence between Eqs. (A-6) and (A-7) is immediate.

* * *

DISTRIBUTION

Aberdeen Proving Ground, Md.
Att: Ballistic Research Lab. 1
Att: Development & Proof Services 1
Att: Physical Test Lab. 1

Air Defense Command, Ent AFB
Att: ADIRP 1

Air Force Academy, Colo.
Att: Dept. Mech. DFME (U) 1

Air Force Headquarters, DC
Att: Operations Analysis Off., Off. Vice Chief of Staff, Library 2
Att: AFDRD-GW 1

Air Force Missile Development Center, Holloman AFB
Att: RRRT/Miss R. Porter 1
Att: MDS/Dr. M. G. Jaenke 1
Att: MDSSS/Mr. G. R. Moser 1

Air Force Missile Test Center, Patrick AFB
Att: MT LLL-3 (Classified Material) 2
Att: MU-135, Technical Library (U) 1

Air Force Office of Scientific Research, DC
Att: Library (U) 1

Air Force Packaging Evaluation Agency, Brookley AFB
Att: MOSPR 1
Att: MONE 1

Air Force Regional Civil Engineer
Att: North Atlantic Region, AFRCE-NA-A 1

Air Force Rocket Propulsion Lab., Calif.
Att: Mr. A. J. Davies (RPFDE) 1

Air Force Systems Command, Andrews AFB
Att: Technical Library 2

Air Force Weapons Laboratory, Kirtland AFB
Att: Development Test Division 1
Att: Dr. W. E. Fisher, WLRS 1
Att: SWOI 631-276 1

Air Proving Ground Center, Eglin AFB
Att: PGTRI, Technical Library 1

Army Edgewood Arsenal, Maryland
Att: Library 1

Army Electronics Command, Phila. 1

Army Electronics Command, Ft. Monmouth
Att: Mr. J. J. Oliveri 1

Army Engineer R&D Laboratories, Ft. Belvoir
Att: Package Development Branch 1
Att: Director of Research 1
Att: Chief, Spec. Proj. Branch 4

Army Engineer Waterways Experiment Station, Vicksburg
Att: Library 1

Army Frankford Arsenal, Phila.
Att: Library Branch, CC 0270/40 1
Att: Mr. David Askin, Q6200 1

Army Materials Research Agency, Watertown
Att: Dr. Reinier Beeuwkes, Jr. 2

Army Materiel Command, DC
Att: AMCRD-R 1

Army Missile Command, Redstone Arsenal
Att: AMSMI-RB 1
Att: AMSMI-RG 1
Att: AMSMI-RL 1
Att: AMSMI-RS 1
Att: AMSMI-RT 1
Att: AMSMI-RTR, Mr. J. M. Taylor 1
Att: AMSMI-RSM, Mr. E. J. Wheelahan 1

Army Mobility Command, Centerline
Att: Mr. Otto Renius 1

Army Natick Laboratories, Mass.
Att: Technical Library 2
Att: Mr. W. B. Brierly 1
Att: Chief, Container Div. 1

Army, Office Chief of Engineers, DC
Att: ENGMC-EM 2

Army, Office Chief of R&D, DC
Att: Scientific & Tech. Information Div. 1

Army, Office Chief of Staff, Logistics
Att: Director of Transportation Engrg. 1

Army Tank-Automotive Center, Warren
Att: SMOTA-RRS, Tech. Library 1
Att: SMOTA-RCE, Mr. D. J. Hackenbruch 1
Att: SMOTA-RRC 1

Army Transportation Engineering Agency, Ft. Eustis
Att: Library 1
Att: Mr. L. J. Pursifull 1

Army Transportation Research Command, Ft. Eustis
Att: Dr. R. L. Echols, Physical Sci. Res. Group 1